The ESCRT Machinery regulates Retromer dependent Transcytosis of Septate Junction Components in *Drosophila*

Inaugural-Dissertation

zur Erlangung des Doktorgrades
der Mathematisch-Naturwissenschaftlichen Fakultät
der Heinrich-Heine-Universität Düsseldorf

vorgelegt von

Hendrik Pannen
aus Düsseldorf

Düsseldorf, Oktober 2020

aus dem Institut für Genetik
der Heinrich-Heine-Universität Düsseldorf

Gedruckt mit der Genehmigung der Mathematisch-Naturwissenschaftlichen Fakultät der Heinrich-Heine-Universität Düsseldorf

Berichterstatter:
1. Prof. Dr. Thomas Klein

2. Jun.-Prof. Dr. Mathias Beller

Tag der mündlichen Prüfung: 23.11.2020

“Knowledge speaks, but wisdom listens”

-Jimi Hendrix

Table of Contents

1 Introduction 3
1.1 Epithelial Organisation and Polarity 3
1.2 Occluding junctions of *Drosophila* and mammalian epithelia 5
1.2.1 The Septate Junction (SJ) of *Drosophila* 5
1.2.2 The Mammalian Paranodal Septate Junction (PSJ) 10
1.2.3 The Mammalian Tight Junction (TJ) 11
1.3 The Endosomal System 12
1.3.1 The Retromer Complex 13
1.3.2 The Endosomal Sorting Complex Required for Transport (ESCRT) 15
1.4 The function of *Drosophila* ESCRT in maintenance of epithelial organization 17
1.5 Aims of this thesis 19
2 Manuscript 20
2.1 Introduction 21
2.2 Results 25
2.3 Discussion 44
2.4 Materials and Methods 49
2.5 Acknowledgements 54
2.6 Additional Information 55
2.7 Funding 55
2.8 Competing Interests 55
2.9 References 55
2.10 Supplementary Information 60
2.11 Author contributions to the manuscript 79
3 Additional Experimental Data 80
3.1 Comparative trafficking analysis of the Claudins Mega and Kune 80

3.2 Requirement for Rab7 activity in Retromer dependent junctional delivery of Mega 83

3.3 The function of Vps34/PI3K in transport of Mega 85

3.4 Small-scale RNAi screen to find novel factors implicated in SJ delivery of Mega .. 88

4 Concluding Remarks 92

5 Summary 94

6 Zusammenfassung 95

7 References 96

8 List of Abbreviations 104

9 Acknowledgements 105

10 Eidesstattliche Erklärung 106

1 Introduction

The emergence of epithelial tissues provided early multicellular organisms with new functional and mechanical properties that were crucial in driving the evolution of metazoan life. Two key features of epithelia, cellular adhesion and diffusion barrier function, cooperatively fueled the development of complex organisms. While adhesion-mediated coupling of cells enabled the formation of intricate tissue shapes such as spheres or tubes, epithelial barrier function laid the foundation for metabolic homeostasis.

Epithelia fulfill a plethora of functions in higher species and disruption of their organization is associated with diseases such as cancer. Carcinomas, tumors of epithelial origin, account for the majority of cancers in human. Thus, understanding the complex processes involved in epithelial tissue homeostasis is of significant clinical importance.

1.1 Epithelial Organisation and Polarity

Two major hallmarks define the epithelial tissue type: The existence of apicobasal cell polarity and intercellular adhesion. While the former was introduced with the emergence of a highly complex protein network containing the ancient transmembrane protein Crumbs (Crb) and several cytoplasmic proteins (polarity cues), adhesion became prominent with the appearance of the Cadherin / Catenin complex (Nichols et al., 2012). Although still under debate, it is believed that the Crb and Cadherin complexes evolved approximately in parallel, with Crb aiding the formation and localization of Cadherin complexes to specific membrane domains, the adherens junctions (AJs) (Le Bivic, 2013).

While epithelial Cadherin (E-cad) established itself as the major adhesive molecule throughout metazoan epithelia evolution, Crb is also potent to mediate adhesion by homophilic interactions of its extracellular domains (Thompson et al., 2013). Nevertheless, the prominent roles of Crb in establishing cell polarity and regulating cellular signaling depend on its short and highly conserved intracellular domain (Pocha and Knust, 2013). During early *Drosophila* embryonic development, the primary epithelium forms by cellularization and subsequent polarization of the syncytial blastoderm. Crb is a key factor during the polarization process as it determines the apical subdomain of the newly formed membrane, thereby providing the spatial cue necessary for concentrating early E-cad based focal adhesions into functional AJ (Grawe et al., 1996; Tepass, 1996; Wodarz et al., 1995). While Crb-complex dependent polarization is specific to epithelial tissues, several conserved cytoplasmic factors globally control apical identity in all

types of polarized cells. Among these, the atypical protein kinase C (aPKC) complex, cell division control protein 42 (Cdc42) and proteins of the partitioning defective (PAR) family constitute the major agents (Assemat et al., 2008; Goldstein and Macara, 2007). The requirement for these factors in establishing apicobasal polarity is particularly evident in *bazooka* (*baz*, the Drosophila PAR-3 homologue) mutant fly embryos, which fail to polarize the blastoderm epithelium and do not form AJ (Muller and Wieschaus, 1996). Additionally, *baz* mutant embryos establish a disorganized multilayered tissue instead of the primary epithelium, underscoring the importance of cell polarity cues in maintaining integrity of single layer epithelial sheets (Muller and Wieschaus, 1996).

The activity of apical cues is opposed by the function of basolateral cell polarity factors, namely components of the Scribble (Scrib) / Discslarge (Dlg) / Lethal giant larvae (Lgl) complex (Bilder et al., 2000; Bilder and Perrimon, 2000). In contrast to AJ associated apical cues, these proteins localize at the cytoplasmic side of the membrane basal to the AJ, thereby defining the so-called basolateral domain (Bilder et al., 2000; Bilder and Perrimon, 2000). They are closely associated with the Septate Junction (SJ), which mediates diffusion barrier function in arthropod epithelia (see section 1.2 below). Importantly, formation of the SJ in embryonic and imaginal disc epithelia depends on the basolateral polarity factors Dlg and Scrib (Woods et al., 1996; Zeitler et al., 2004). In addition, the basolateral polarity cues are required to locally restrict the activity of the apical cues at the lateral membrane, thereby preventing apicalization of the epithelium (Bilder and Perrimon, 2000). Similarly, apical polarity cues are required for local suppression of basolateral membrane identity (Bilder et al., 2003; Tanentzapf and Tepass, 2003). Thus, a mechanism based on mutual inhibition of apical and basolateral polarity factors is at work in epithelia to maintain polarity and integrity of the tissue.

Equally paramount to epithelial integrity is the AJ protein E-cad, encoded by the *shotgun* (*shg*) gene in *Drosophila* (Tepass et al., 1996). E-cad is a single-pass transmembrane protein containing Cadherin repeats in its extracellular domain that engage in calcium ion dependent homophilic interaction in the intercellular space, thereby providing adhesion between cells within the epithelial layer (Oda and Takeichi, 2011). At the cytoplasmic side, α- and β-Catenin connect E-cad intracellular domains with the cortical actin cytoskeleton (Yamada et al., 2005). This provides mechanical coupling of individual cells to a functional unit and lays the foundation for morphogenetic remodeling of the epithelium.

1.2 Occluding junctions of *Drosophila* and mammalian epithelia

While E-Cad based AJ establish and regulate the mechanical properties of the epithelium, a second type of junction is indispensable for epithelial function: the occluding junction. The purpose of this cell-cell contact structure is the tight sealing of the intercellular space, thereby preventing unchecked paracellular (in between cells) diffusion of molecules across epithelial sheets. Two major types of occluding junctions, septate junctions (SJ) and tight junctions (TJ), mediate barrier function in metazoan species. They are easily distinguished by their appearance in transmission electron micrographs of juxtaposed epithelial membranes.

While SJ are characterized by interspaced electron-dense septa in the intermembrane space, TJ based cell-cell contacts seal neighboring membranes by forming 'kissing points' (Fig. 1 and (Furuse and Tsukita, 2006)). SJ mediate membrane occlusion in protostomes whilst TJ seem to exist only in chordates (Ganot et al., 2015). Occluding junctions of early metazoans such as *Hydra* or cnidarian species resemble arthropod SJ, suggesting that SJ-like structures provided the archetype of occluding junctions in animalia evolution (Filshie and Flower, 1977; Green and Flower, 1980; Wood, 1959). The different types of occluding junctions in arthropods and mammals are depicted in Figure 1.

1.2.1 The Septate Junction (SJ) of *Drosophila*

Research conducted in *Drosophila melanogaster* paved the way to understanding structure, function and establishment of arthropod SJ. During *Drosophila* embryogenesis, SJ initially appear in the ectoderm after the emergence of AJ (Eichenberger-Glinz, 1979). In arthropod species, two different types of SJ exist that differ in composition, structure and localization along the apicobasal axis of juxtaposed membranes. While pleated SJ (pSJ) are found in ectodermally derived epithelia (e.g. epidermis, imaginal discs) basal to the AJ belt, smooth SJ (sSJ) exist only in epithelia with mesoderm origin (e.g. midgut), in which they localize apically of the AJ (Tepass and Hartenstein, 1994). This organization with occluding sSJ being apical of the AJ is analogous to the TJ / AJ configuration in mammalian epithelia. Strikingly, cell polarity in the sSJ containing *Drosophila* midgut epithelium depends on Integrin and does not require classical polarity cues (Dlg, aPKC, Crb, Baz), akin to mammalian epithelia (Chen et al., 2018). Surprisingly, while apical polarity factors Crb and Baz are not detectably expressed in the midgut, basolateral cues Dlg / Scrib / Lgl localize at the basolateral membrane corresponding to the sSJ, despite being dispensable for epithelial polarity and integrity (Chen et al., 2018). This is consistent with sSJ and pSJ sharing a subset of cytoplasmic scaffolding factors, despite

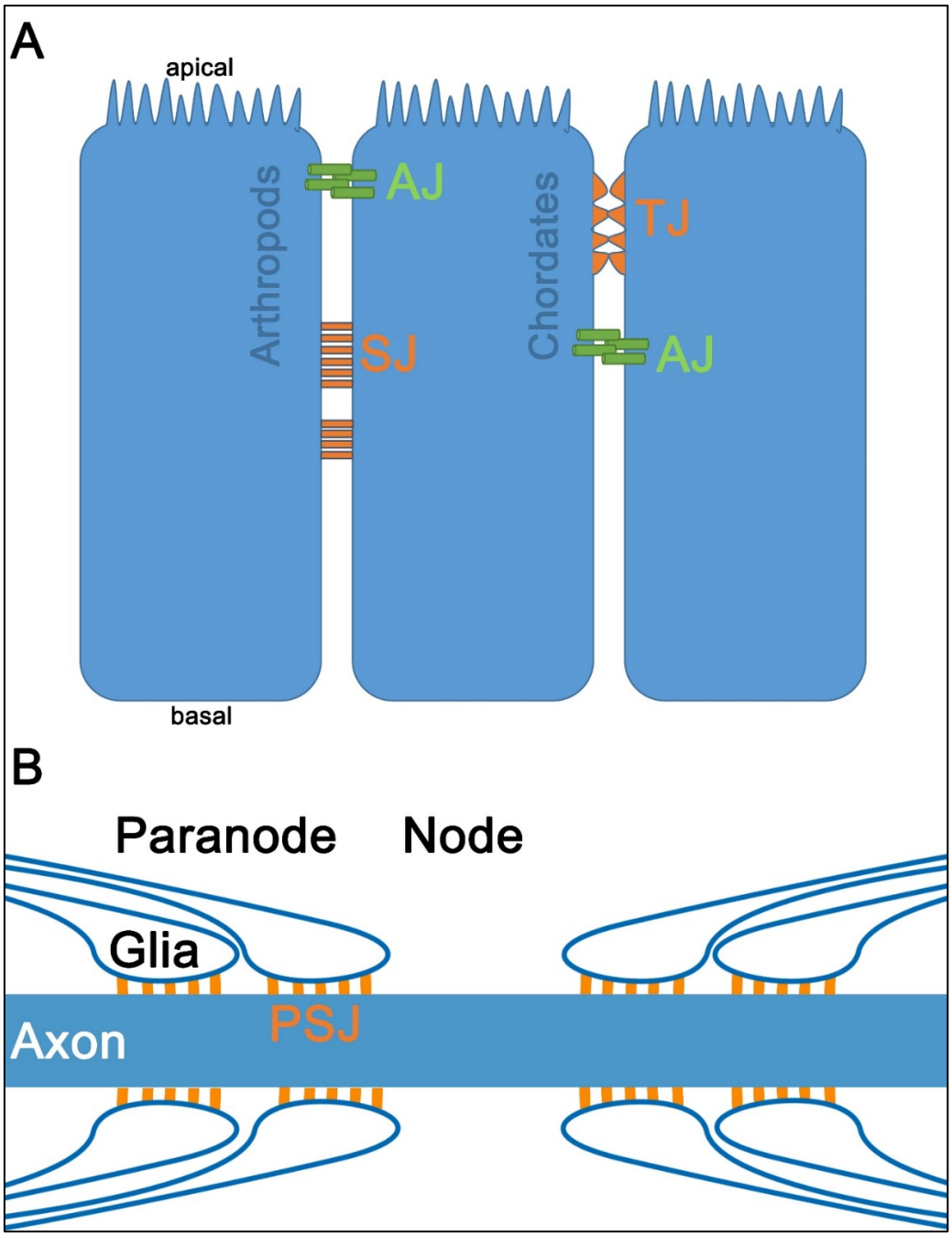

Figure 1. Types of occluding junctions in *Drosophila* and mammals. (**A**) In arthropods such as *Drosophila*, E-cad based AJ (green) are found in the apical region of the basolateral membrane of epithelial cells. The individual occluding septa of SJ (orange) line the juxtaposed basolateral membranes basal to the AJ. In contrast, in chordates such as mammals, the occluding TJ (orange) lies apical to the AJ. Unlike the SJ with its ladder-like appearance, the TJ is characterized by opposing membranes meeting each other in 'kissing points'. (**B**) The paranodal SJ (PSJ, orange) in mammals is structurally and functionally similar to the *Drosophila* SJ, with individual interspaced septa lining the intercellular space of juxtaposed Axon/Glia membranes in the paranode region.

differing drastically in their structural composition. Specifically, only three sSJ specific components (Snakeskin, Mesh and Tetraspanin 2A) have been described thus far while well

over 20 proteins have been associated with pSJ (Izumi et al., 2016; Izumi et al., 2012; Yanagihashi et al., 2012).

The vast amount of different structural components of pSJ support the image of a complex, convoluted multiprotein network required for junction formation and function. The initially characterized components of *Drosophila* pSJ were the single-pass transmembrane protein Neurexin IV (Nrx-IV) and the cytoplasmic scaffolding protein Coracle (Cora) (Baumgartner et al., 1996; Fehon et al., 1994). Epithelia of *cora* mutant embryos do not have defects in apicobasal polarity but fail to form functional pSJ, indicated by lack of septa in the intermembrane space and penetration of a diffusible dye across epithelial layers (Lamb et al., 1998). Similarly, *nrxIV* mutants fail to form pSJ (Baumgartner et al., 1996). Cora directly binds the cytoplasmic domain of NrxIV and this interaction is interdependent, as *cora* and *nrxIV* deficient epithelia fail to localize the respective interaction partner to the pSJ (Lamb et al., 1998; Ward et al., 1998).

Subsequently, further transmembrane proteins constituting structural pSJ components were identified. Among them, Neuroglian (Nrg), as well as the Na+/K+ ATPase subunits ATPα and Nervana2 (Nrv2), which are required for both barrier function and SJ formation (Genova and Fehon, 2003; Paul et al., 2003). Studies with the homologs of Nrg and NrxIV in mammalian paranodal SJ (see also section 1.2.2) suggest that these proteins interact with their extracellular domains *in trans* at juxtaposed membranes of the axoglial junction (Charles et al., 2002). This seems to hold true in *Drosophila* pSJ, as wildtype cells fail to localize Nrx or Cora to pSJ at the interface of wildtype and *cora* mutant imaginal disc tissue (Genova and Fehon, 2003). Additionally, biochemical data suggest that Cora, NrxIV, Nrv2, ATPα and Nrg form a stable protein complex, with lack of any complex component leading to loss of the interaction partners from the SJ (Genova and Fehon, 2003). However, the protein levels of these pSJ components are largely unaffected upon loss of individual complex components, suggesting that proteins are not degraded when complex assembly is impaired (Genova and Fehon, 2003). The existence of a stable pSJ core complex is further supported by Fluorescence Recovery after Photobleaching (FRAP) experiments, which revealed virtually indistinguishable kinetics for fluorescently tagged Nrg, Nrv2, ATPα and Cora (Oshima and Fehon, 2011). The observed slow FRAP rates support the existence of a relatively stable and immobile pSJ core complex with little protein turnover. In contrast, the pSJ associated cytoplasmic polarity protein Dlg is not part of the core complex as it rapidly recovers its pSJ association following photobleaching (Oshima and Fehon, 2011). This finding corroborates the functional independence of basolateral cell polarity cues and pSJ components, despite their close association at the

junctional membrane. Another pSJ associated component which is not structural part of the core complex is the transmembrane protein FasciclinIII (FasIII), a homophilic adhesion molecule localized at the lateral membrane and the pSJ in a Dlg dependent manner (Snow et al., 1989; Woods et al., 1996). Similarly to Dlg, FasIII levels at the pSJ are not affected in clonal tissue mutant for a pSJ core component, indicating that certain pSJ associated transmembrane proteins are not necessarily structural components of the core junction complex (Genova and Fehon, 2003).

The discovery of *Drosophila* Claudins expanded the functional and structural similarity of pSJ with mammalian TJ, since Claudins constitute the major agents in providing barrier function and modulation within TJ (Gunzel and Yu, 2013). While the Claudin family comprises 27 members in mammals, only three *Drosophila* Claudins have been characterized: Megatrachea (Mega), Sinuous (Sinu) and Kune-Kune (Kune) (Behr et al., 2003; Nelson et al., 2010; Tsukita et al., 2019; Wu et al., 2004). All Claudins share a conserved topology consisting of four transmembrane domains, two differently sized extracellular loops and cytoplasmic N- and C-termini (Krause et al., 2008). Experimental data primarily from mammalian cell culture systems has established the engagement of the Claudin extracellular loops in homo- and heterophilic interactions (*cis* and *trans*) in the paracellular space, thereby establishing epithelial barrier function (Gunzel and Yu, 2013). Consistently, loss of any of the three *Drosophila* Claudins abolishes epithelial barrier function, visualized by dye penetration across epithelial layers in mutant embryos (Behr et al., 2003; Nelson et al., 2010; Wu et al., 2004).
Initially found in a screen for factors affecting tracheal morphology, *mega* mutant embryos were shown to display a characteristic tube elongation phenotype, which motivated the naming of the gene (Behr et al., 2003). Mega localization to the pSJ depends on *cora* and *NrxIV* and is independent of *FasIII*, in line with Mega being a structural component of pSJ (Behr et al., 2003). In *cora* and *nrxIV* mutant embryos, Mega is spread along the entire lateral membrane of the hindgut epithelium instead of being enriched specifically at pSJ, a phenotype that is commonly observed with pSJ core components upon loss of individual complex members (Behr et al., 2003; Paul et al., 2003). Consistent with Mega being a core component of the pSJ, mass spectrometry based analysis of the Mega interactome recovered most pSJ components and FRAP rates of GFP-tagged Nrv2 and ATPα were drastically increased in *mega* embryos, indicating destabilization of the immobile core complex in the mutant situation (Jaspers et al., 2012; Oshima and Fehon, 2011). The elongated tube phenotype of *mega* is supposedly caused by hypertrophy of the apical domain upon loss of this basolaterally localized pSJ protein, as has

been shown for mutants of other pSJ components (Behr et al., 2003; Beitel and Krasnow, 2000; Hemphala et al., 2003). In support of this model based on apical / basolateral imbalance, reducing the amount of the apical polarity protein Crb can suppress tracheal elongation phenotypes in the *Drosophila* embryo (Dong et al., 2014).

The tracheal elongation phenotype, characterized by a wavy dorsal trunk, also explains the naming of the gene *sinuous*, which encodes for another *Drosophila* Claudin (Beitel and Krasnow, 2000; Wu et al., 2004). Sinu localizes to pSJ of embryonic epithelia and this localization depends on core pSJ components, as Sinu spreads along the entire lateral membrane in *cora*, *nrv2* or *NrxIV* mutant embryos (Wu et al., 2004). Similar to *mega* mutant embryos, epithelial barrier function and organization of pSJ is disturbed in *sinu* animals (Wu et al., 2004). However, in contrast to *mega* mutant embryos which lack detectable junctional septa, *sinu* mutants still occasionally form ladder-like pSJ but the overall density of septa seems to be reduced (Behr et al., 2003; Wu et al., 2004). It also appears that in certain tissues such as the embryonic hindgut, *sinu* is required for the expression level of pSJ proteins, although this has not been tested biochemically (Wu et al., 2004). The authors concluded that while certain aspects are shared among the *sinu* and *mega* phenotypes, the functions of the individual Claudins differ.

The third *Drosophila* Claudin, Kune-kune (Kune), was identified due to its homologies with Mega/Sinu and subsequently characterized (Nelson et al., 2010). Similarly to the aforementioned Claudins, *kune* obtained its name due to the elongated wavy trachea phenotype of mutant embryos (kune-kune: Japanese for “wiggling like a snake”) (Nelson et al., 2010). Akin to Mega and Sinu, Kune localization to the junction requires pSJ core components and *kune* embryos display leaky epithelial barrier function (Nelson et al., 2010). Additionally, in *kune* mutants, pSJ components Cora, ATPα, Mega, Sinu and Dlg show reduced levels and spreading along the lateral membrane (Nelson et al., 2010). Interestingly, in a direct comparison of *mega*, *sinu* and *kune* mutants, loss of *kune* led to Cora spreading along the lateral membrane and also seemed to reduce overall Cora levels in the tissue. In contrast, Cora levels appeared wildtype in *mega* embryos but the protein was still found spreading along the lateral membrane (Nelson et al., 2010). Finally, Cora levels were reduced in *sinu* animals but it was still enriched at the pSJ (Nelson et al., 2010). Albeit lacking quantitative evidence, these data suggest that the roles of Mega, Sinu and Kune in pSJ formation differ substantially, with loss of *kune* representing the most severe phenotype concerning Cora subcellular localization.

In addition to aforementioned cytoplasmic and transmembrane pSJ components, several GPI-anchored proteins are required for junction formation and / or structure. Among them are the

homophilic adhesion molecule Lachesin (Lac), the NrxIV and Nrg interaction partner Contactin, the Lymphocyte Antigen 6 (Ly-6) superfamily members Crooked, Coiled, Crimpled, Boudin as well as the proteins Undicht and Melanotransferrin (Faivre-Sarrailh et al., 2004; Hijazi et al., 2009; Jaspers et al., 2012; Llimargas et al., 2004; Nilton et al., 2010; Petri et al., 2019; Tiklova et al., 2010). Interestingly, while most of these proteins are pSJ localized, some (e.g. Crooked and Coiled) do not associate with the junction, suggesting that they are not structural components of the pSJ, but aid in formation and / or transport of the junctional complex (Nilton et al., 2010).

Despite the vast amount of studies on pSJ components, relatively little is known about junction assembly and maintenance. During pSJ formation in the embryo, pSJ components initially localize evenly distributed at the lateral membrane in embryonic stage 13 and become concentrated in the junctional region by stage 15 via a process requiring endocytosis (Tiklova et al., 2010). The finding that Clathrin, Dynamin and the endosomal GTPases Rab5 and Rab11 are required for this transcytosis-like process suggests that endosomal trafficking of pSJ complexes is essential for junction formation (Tiklova et al., 2010). Consistently, pSJ components were detected in endosomal compartments (Nilton et al., 2010; Tiklova et al., 2010). Clathrin heavy chain (Chc) was found in a proteomic analysis of the Mega protein complex and a putative Chc sorting motif within the Mega intracellular domain supports a potential interaction of this pSJ component with Clathrin (Jaspers et al., 2012). Recent studies have established that biosynthetic supply of pSJ components is achieved by integration into the junction from the apical side in a ‘conveyor belt’ like fashion (Babatz et al., 2018; Daniel et al., 2018). Interestingly, in subperineurial glia cells undergoing extensive cellular growth during larval development, pSJs are established as highly folded strands which unfold during cell growth, thereby maintaining barrier function (Babatz et al., 2018). While these results give insight into pSJ maintenance in a tissue undergoing extensive cellular growth, the understanding of pSJ maintenance in highly proliferative tissues such as imaginal discs remains unknown.

1.2.2 The Mammalian Paranodal Septate Junction (PSJ)

Structurally related to the arthropod SJ is the paranodal septate junction (PSJ) of mammalian nerve tissue, which is characterized by individual interspaced septa connecting the axonal membrane with the myelin sheath in vicinity of the node of Ranvier (Rosenbluth, 2009). The molecular basis of this intercellular contact is established by a tripartite protein complex

consisting of the proteins Contactin, Contactin-associated protein (CNTNAP/Caspr) and Neurofascin-155 (NF155), which are homologs of the *Drosophila* pSJ components Contactin (Cont), NrxIV and Nrg, respectively (Boyle et al., 2001; Einheber et al., 1997; Menegoz et al., 1997; Peles et al., 1997; Tait et al., 2000). CNTNAP engages in *cis* interactions with Contactin and this interaction is believed to be required for PSJ complex formation at the paranodal axon membrane, as Contactin deficient mice lack CNTNAP at the PSJ (Boyle et al., 2001; Peles et al., 1997). This is paralleled by the finding that in *Drosophila cont* deficient embryos, NrxIV fails to accumulate at the pSJ (Faivre-Sarrailh et al., 2004). Opposing the axonal CNTNAP/Contactin complex is the paranodal myelin membrane enriched in NF155, which can bind Contactin *in trans* (Tait et al., 2000; Volkmer et al., 1998). Thus, a complex comprising the mammalian homologs of *Drosophila* NrxIV, Cont and Nrg constitutes the junctional core network of PSJ. Additionally, protein 4.1, which is homolog to *Drosophila* Cora, associates with the cytoplasmic tail of CNTNAP in a similar fashion as Cora associates with the intracellular domain of NrxIV (Denisenko-Nehrbass et al., 2003; Menegoz et al., 1997; Ward et al., 1998). The conserved proteins and interactions of mammalian PSJ and *Drosophila* pSJ complexes suggest that PSJ might reflect an adaptation of an ancient protein network with occluding properties to support the evolution of myelinated axons, which are vertebrate specific (Hildebrand et al., 1993).

While PNS provide a biochemical and electrical barrier during saltatory propagation of action potentials within myelinated nerves, a different type of occluding junction mediates barrier formation predominantly in mammalian epithelia.

1.2.3 The Mammalian Tight Junction (TJ)

Diffusion barrier function of mammalian epithelia is mediated by the Tight Junction (TJ), another occluding cell-cell-contact structure with functional homology to *Drosophila* SJ. Unlike SJ, TJ do not form interspaced septa but are characterized by ‘kissing points’ of juxtaposed membranes in electron micrographs (see. Fig. 1) (Farquhar and Palade, 1963). TJ are positioned apical to AJs, which is the inverted configuration of the AJ / pSJ setup in *Drosophila* ectodermal epithelia. While TJ and pSJ significantly differ in their structure, they share a set of conserved components which mediate barrier formation, most notably proteins of the Claudin family (Zihni et al., 2016). The mammalian Claudin family comprises 27 members, which are differentially expressed in various tissue types and not only mediate barrier function but also selective permeability (Tsukita et al., 2019). An example of the latter is the formation

of paracellular channels by Claudin-2, which increase selective paracellular permeability across epithelial layers (Furuse et al., 2001; Weber et al., 2015). Thus, Claudins do not only perform static sealing functions within TJ but also finely modulate the permeability properties of individual TJ strands. Besides Claudins, another type of four-pass transmembrane protein is required for mammalian TJ integrity: Occludin (Cummins, 2012). Unlike the Claudins, this protein does not possess arthropod homologs with high similarity. The cytoplasmic face of Occludin interacts with the scaffolding factors Zonula Occludens 1, 2 and 3 (ZO-1, ZO-2, ZO-3), providing a link to the actin cytoskeleton (Furuse et al., 1994; Haskins et al., 1998; Itoh et al., 1999). Although not strongly conserved between *Drosophila* and mammals, these proteins belong to the MAGUK (Membrane-Associated GUanylate Kinase) family of proteins with a common domain composition (Funke et al., 2005). Members of this family are pSJ scaffolding factors such as Dlg and Vari or the AJ associated Polychaetoid, which shares the highest homologies with mammalian ZO proteins (Bachmann et al., 2008; Djiane et al., 2011; Moyer and Jacobs, 2008; Woods and Bryant, 1991; Wu et al., 2007). Thus, although differing substantially in their molecular composition (with exception of Claudins), a shared feature of TJ and *Drosophila* pSJ is the connection of the occluding structure with the actin cytoskeleton via adaptor proteins that form a junctional scaffold.

1.3 The Endosomal System

Intracellular trafficking, degradation and recycling of transmembrane proteins, such as junctional components, is governed by a highly complex system of dynamic endosomal compartments. Cargo can enter the endosomal system by endocytosis, a membrane internalization process often depending on Clathrin coat scaffolding and vesicle stalk abscission by the GTPase Dynamin, encoded by the gene *shibire* (*shi*) in Drosophila (Mettlen et al., 2009; van der Bliek and Meyerowitz, 1991). Endocytic vesicles may undergo homotypic fusion to form early endosomal compartments. This process depends on the early endosomal GTPase Rab5, a master regulator of endosome biogenesis (Wandinger-Ness and Zerial, 2014). When activated by GDP/GTP cycling, Rab5 localizes to the vesicle membrane where it recruits effectors such as phosphoinositide-3-kinase (PI3K) and early-endosomal autoantigen (EEA1), which mediate the generation of endosome specific lipids (Phosphatidylinositol-3-phosphates / PIP3) in the outer membrane leaflet and homotypic fusion, respectively (Christoforidis et al., 1999; Marat and Haucke, 2016; Simonsen et al., 1998). Rab5 positive early endosomes continue to accumulate cargo proteins at their limiting membrane while undergoing maturation, a process

defined by generation of intraluminal vesicles (ILV) and progressive acidification of the endosomal lumen (Huotari and Helenius, 2011). A hallmark of endosome maturation is the 'Rab-Conversion', an exchange of early endosomal Rab5 with Rab7, mediated by the Rab7 Guanine nucleotide exchange factor (GEF) Dmon1 in *Drosophila* (Rink et al., 2005; Yousefian et al., 2013). Rab7 governs endosomal maturation by coordinating cargo recycling, endosome mobility and endosome-lysosome fusion along the degradative route (Guerra and Bucci, 2016). The fusion of ILV containing mature endosomes (termed multivesicular bodies / MVB) with the lysosome terminates the life cycle of the endosome and serves to degrade the cargo proteins contained within the MVB lumen (Luzio et al., 2007). Figure 2 provides an overview on the endosomal system and its associated sorting machineries.

1.3.1 The Retromer Complex

Cargo proteins within the endosomal system can escape lysosomal degradation by undergoing recycling, which is performed by one of several specialized machineries. The Retromer complex, which was initially characterized as a regulator of cargo retrieval from endosomes to the Golgi in yeast, has emerged as a central conductor of recycling from maturing endosomes (Horazdovsky et al., 1997; Seaman, 2012; Seaman et al., 1997). Retromer dependent recycling is characterized by sorting of cargo into tubular endosomal domains which eventually abscise to form recycling carriers (Cullen and Steinberg, 2018). Two Retromer subcomplexes, the cargo selective complex (CSC) and the SNX-BAR (Sorting Nexin-Bin/Amphyphysin/Rvs) complex have been initially described to mediate cargo recognition and membrane tubulation, respectively (Horazdovsky et al., 1997; Nothwehr and Hindes, 1997; Seaman et al., 1997). The CSC is an ancient and stable heterotrimeric complex containing the proteins Vps26, Vps29 and Vps35, which localize to the mammalian maturing endosome / MVB in a Rab7 dependent manner and are able to bind cargo proteins (Rojas et al., 2008; Seaman, 2004; Seaman et al., 2009). Specifically, Vps26 and Vps35 recognize distinct sorting motifs within cytoplasmic tails of cargo proteins, which serve to cluster CSC with its cargo at the endosomal membrane (Fjorback et al., 2012; Lucas et al., 2016; Suzuki et al., 2019). Vps35 is the centerpiece of the CSC, with its elongated alpha-solenoid / horseshoe shape bringing together Vps26 and Vps29, which associate with the opposing ends of Vps35 (Fig. 2 and (Hierro et al., 2007; Lucas et al., 2016)). The mammalian CSC was shown to form multiple oligomers, thereby providing an adaptable endosomal scaffold, which may be modulated by cooperation with one of several Retromer associated SNX proteins (Kendall et al., 2020). This is consistent with the CSC

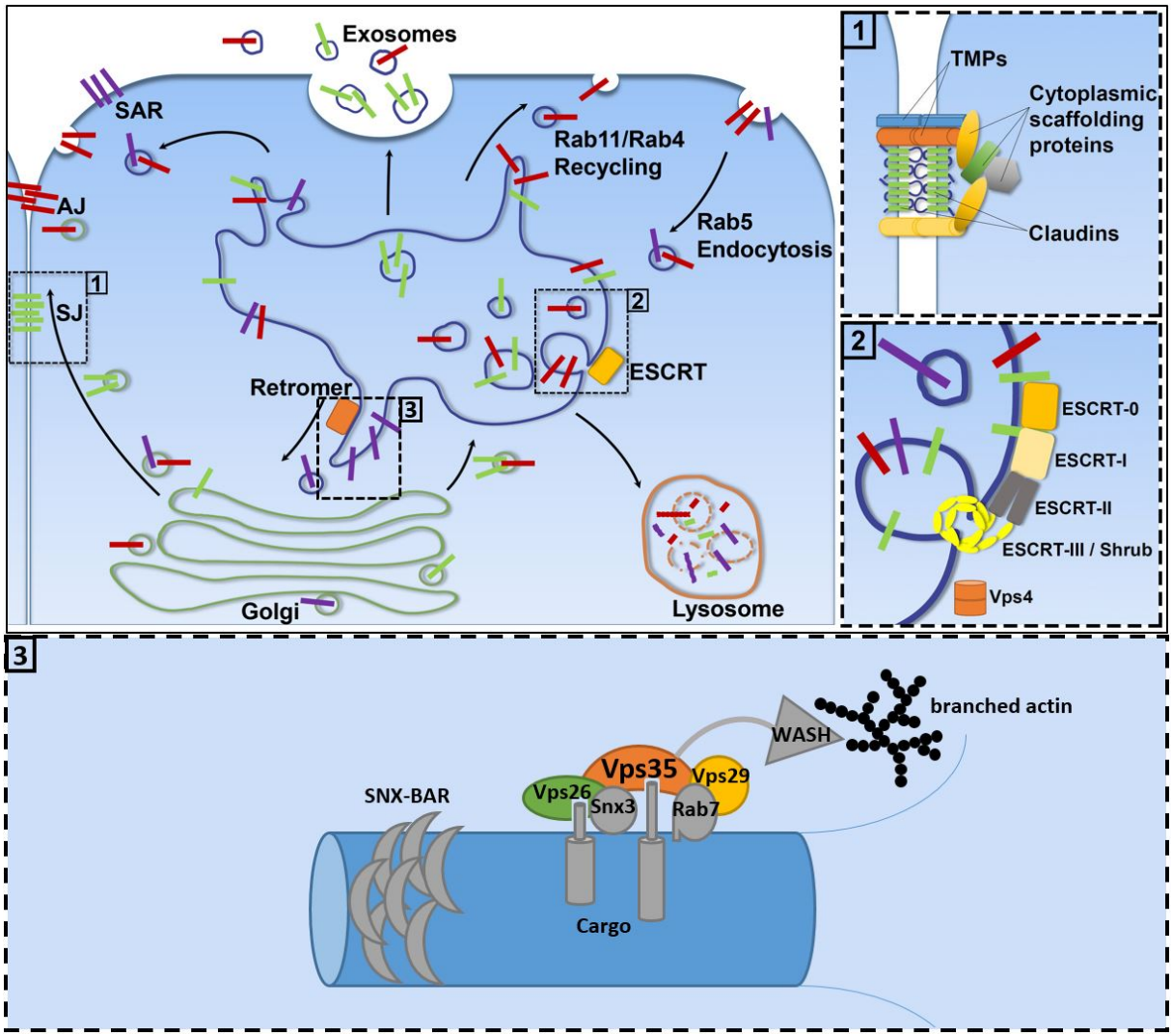

Figure 2. The endosomal system. The maturing endosome coordinates endocytic uptake (e.g. Rab5 dependent), recycling to the plasma membrane or the Golgi (e.g. Rab4, Rab11 or Retromer dependent) and packaging into ILV (e.g. ESCRT dependent) of transmembrane proteins (TMPs), such as SJ components (**1**). MVBs may also fuse with the plasma membrane to release ILVs as exosomes. (**2**) Organization of the heterooligomeric ESCRT-machinery, required for ILV generation at the limiting membrane of maturing endosomes. The ESCRT-III component Shrub (bright yellow) forms long helical polymers, thereby mediating ILV neck constriction and abscission. (**3**) Retromer CSC (coloured) and associated (grey) proteins. The CSC binds cargo via Vps35 and Vps26. Vps26 is able to bind Snx3, which is required for a subset of CSC dependent sorting events. Rab7 binds to the CSC and its activity is regulated by Vps29. Vps35 binds the WASH-complex component Fam21, linking the CSC to branched filamentous actin patches. SNX-BAR proteins mediate endosomal tubulation and may act in CSC dependent or independent cargo retrieval.

governing several different retrieval pathways, dependent on its cooperation with a variety of specialized sorting nexins, which are characterized by the phospholipid-binding PX (phox homology) domain (Cullen and Korswagen, 2011). Via Vps35 binding to the tail of Fam21, a WASH (Wiskott-Aldrich Syndrome Protein and SCAR Homolog) complex component, the

CSC is linked to this regulator of branched filamentous actin (Gomez and Billadeau, 2009). It is believed that patches of endosomally localized branched actin governed by the WASH complex may help stabilize retrieval subdomains and possibly even tubule generation and abscission (Wang et al., 2018).

While cooperation of the CSC with the membrane deforming SNX-BAR factors Vps5p and Vps17p represents the classical yeast Retromer pathway, the situation is more complex in metazoans (Horazdovsky et al., 1997). Specifically, the sorting nexins SNX3 and SNX27 (both lacking the membrane sensing BAR domain) emerged as regulators of alternative CSC dependent retrieval routes (Lauffer et al., 2010; Lucas et al., 2016; Strochlic et al., 2007; Temkin et al., 2011; Xu et al., 2001). While SNX3 cooperating with the CSC can mediate endosome-to-Golgi retrieval, SNX27 has been shown to recycle its specific cargo to the plasma membrane (Harterink et al., 2011; Lauffer et al., 2010; Temkin et al., 2011; Zhang et al., 2011). This supports the notion that depending on its SNX cofactors, the CSC is able to coordinate a variety of retrieval routes. However, the finding that SNX-BAR proteins can also mediate CSC independent cargo recognition and retrieval challenges the universal role of the CSC in endosomal recycling (Kvainickas et al., 2017; Yong et al., 2020). Nevertheless, among the hundreds of cargos requiring CSC for their correct subcellular localization are proteins such as Wntless (an essential regulator of Wnt trafficking), Rhodopsin, the apical cell polarity determinant Crumbs and the planar polarity proteins Flamingo and Strabismus (Pocha et al., 2011; Steinberg et al., 2013; Strutt et al., 2019; Wang et al., 2014).

Diverse physiological functions of Retromer are also reflected in humans, where it regulates amyloid precursor protein (APP) and cathepsin D trafficking, which has implications in Alzheimer and Parkinson diseases, respectively (Fjorback et al., 2012; Muhammad et al., 2008; Small and Petsko, 2015; Vilarino-Guell et al., 2011; Zimprich et al., 2011).

1.3.2 The Endosomal Sorting Complex Required for Transport (ESCRT)

Cargo within the endosomal system that does not undergo recycling to the Golgi or the plasma membrane may become target of lysosomal degradation. An important prerequisite to endosomal cargo breakdown in the lysosome is its packaging into ILV, which requires the canonical function of the ESCRT machinery, an endosomal multiprotein sorting complex conserved throughout all eukaryote species (Williams and Urbe, 2007). Four in sequence acting ESCRT complexes (ESCRT-0/ESCRT-I/ESCRT-II/ESCRT-III) cooperating with the ATPase Vps4 mediate cargo sorting and ILV formation (Teis et al., 2009).

The ESCRT pathway is initiated by recognition of ubiquitinated endosomal cargo proteins by the ESCRT-0 complex components Hrs and STAM (Bilodeau et al., 2002; Takahashi et al., 2015). The ESCRT-0 components possess ubiquitin interacting motifs (UIM) mediating cargo binding and FYVE domains, which interact with the PIP3 lipids of endosomes, thereby targeting ESCRT-0 to the endosomal membrane (Hofmann and Falquet, 2001; Misra and Hurley, 1999; Raiborg et al., 2001b; Shih et al., 2002). Besides binding and clustering ubiquitinated cargo, Hrs also recruits Clathrin to the endosomal membrane, which supports the formation of a degradative endosomal subdomain (Raiborg et al., 2001a; Sachse et al., 2002). Endosomally localized ESCRT-0 is required for recruitment of the next in sequence acting complex, ESCRT-I, which physically binds Hrs and similarly recognizes ubiquitinated cargo (Katzmann et al., 2001; Katzmann et al., 2003).

ESCRT-I is a heterotetramer with stalk-like shape that cooperates with ESCRT-0 in sorting of ubiquitinated proteins (Bilodeau et al., 2003; Kostelansky et al., 2007; Kostelansky et al., 2006). Among the four ESCRT-I components is yeast Vps23, encoded by the gene *TSG101* (tumor susceptibility gene 101) in humans and *Drosophila* (Garrus et al., 2001; Li and Cohen, 1996; Moberg et al., 2005). ESCRT-I directly interacts with ESCRT-II, another ubiquitin binding and PIP3 interacting complex that contains three components (Babst et al., 2002; Teo et al., 2006). ESCRT-II consists of the components Vps36, Vps21 and Vps25, that exist in a 1:1:2 stoichiometry, with two Vps25 molecules extending from a Vps36/Vps21 stalk, thereby forming a ‘Y’ shape (Hierro et al., 2004; Teo et al., 2004).

ESCRT-II serves as the platform for ESCRT-III filament generation, which supplies the crucial membrane deforming activity required for ILV formation and abscission (Henne et al., 2012; Im et al., 2009; Teis et al., 2010; Teo et al., 2004). Unlike the upstream ESCRT complexes, ESCRT-III components only transiently form a complex at the endosomal membrane, where they can generate long helical filaments that drive membrane deformation (McCullough et al., 2018). Specifically, the role of the ESCRT-III component Vps32 (Snf7 in Yeast / Chmp4 in mammals / Shrub in *Drosophila*) in generation of membrane deforming polymers is well established (Saksena et al., 2009; Schoneberg et al., 2018; Teis et al., 2008). While ESCRT-III activity provides the necessary force for budding of ILVs that contain the ubiquitinated cargo, ATP-dependent cooperation with the ATPase Vps4 is required for abscission and release of the nascent ILV (Lata et al., 2008; Schoneberg et al., 2018). Another function of Vps4 is the disassembly of ESCRT-III polymers, which is the final step of the ILV/MVB pathway and releases ESCRT-III components from the membrane into the cytosol, where they are made

available for subsequent rounds of ILV formation (Babst et al., 1998; Lata et al., 2008; Scott et al., 2005).

While ILV formation is the well-characterized canonical function of the ESCRT machinery, a variety of other cellular processes have been described to require activity of this ancient multiprotein complex (all of which depend on ESCRT-III membrane deforming activity). Among those are RNA virus budding, cytokinetic abscission and nuclear envelope repair (Carlton et al., 2012; Guizetti et al., 2011; Morita and Sundquist, 2004; Raab et al., 2016).

1.4 The function of *Drosophila* ESCRT in maintenance of epithelial organization

Loss of ESCRT function is associated with the formation of aberrant, swollen endosomal compartments in yeast and mammalian cells that fail to degrade and recycle cargo (Doyotte et al., 2005; Raymond et al., 1992; Rieder et al., 1996). This global effect on endosomal trafficking of transmembrane proteins has impacts on a multitude of cellular events such as signaling homeostasis, which is particularly evident in *Drosophila* imaginal disc tissue. Here, loss of ESCRT function disrupts signaling pathways such as Notch, Decapentaplegic (Dpp), Jun-Kinase (JNK) and Hippo signaling; resulting in apoptosis, overproliferation and neoplastic transformation of the tissue (Herz et al., 2006; Moberg et al., 2005; Thompson et al., 2005; Vaccari and Bilder, 2005; Woodfield et al., 2013). The latter describes the process of an aberrant change in tissue properties and growth, often associated with oncogenesis. In epithelial tissues, neoplastic transformation typically occurs by conversion of the epithelial layer(s) containing polarized cells into multilayered tumorous masses comprised of non-polar mesenchymal-like cells (epithelial to mesenchymal transition – EMT).

One aspect of the neoplastic phenotype induced by loss of ESCRT function in *Drosophila* imaginal discs is mislocalization of cell polarity cues within the tissue, suggesting that epithelial properties are at least partially lost (Woodfield et al., 2013). Additionally, ESCRT deficient imaginal discs highly express Matrix metalloprotease (Mmp), which is able to cleave extracellular matrix components, thereby facilitating invasive tissue behavior and metastasis (Beaucher et al., 2007; Woodfield et al., 2013). Importantly, in eye imaginal discs, curbing ectopic JAK/STAT signaling induced by ESCRT loss of function partially rescues neoplastic transformation of the tissue (Woodfield et al., 2013).

Neoplastic transformation induced by ESCRT loss in *Drosophila* imaginal disc tissue resembles epithelial tumorigenesis with EMT-like character (Vaccari and Bilder, 2009). A hallmark of EMT is the downregulation of E-cad, which results in AJ disassembly and increased cell

motility / migratory behavior (Loh et al., 2019). This suggests that ESCRT deficient *Drosophila* imaginal disc tissue may have compromised junctional integrity, supporting its EMT-like transformation. Indeed, junctional molecules such as E-cad and cell polarity factors such aPKC and Dlg appear to partially lose their cortical subcellular localization in ESCRT deficient imaginal disc tissue (Vaccari and Bilder, 2005).

However, since ultrastructural data is lacking, whether cell-cell-junction integrity relies on ESCRT function in imaginal disc epithelia remains obscure. Additionally, previous studies employed genetic methods for induction of large ESCRT mutant clones within wildtypic imaginal disc tissue to analyze the neoplastic phenotype. These clones appear as highly disorganized and overproliferated tumorous masses within the tissue, hampering analysis. Importantly, this phenotype represents a relatively late stage of ESCRT induced epithelial neoplasia and does not permit analysis of early cellular events occurring within the ESCRT deficient tissue prior to neoplastic transformation.

To circumvent this problem, an RNAi based approach was used to spatiotemporally deplete wing imaginal discs of the ESCRT-III core component Shrub in experiments preceding this work (unpublished data, Master´s thesis Hendrik Pannen). This allowed the generation of wing discs representing different stages of ESCRT induced neoplasia, thus enabling a chronological dissection of the events ultimately leading to neoplastic tissue transformation. One of the findings was that upon Shrub depletion, Notch signaling is ectopically activated already at a very early stage, prior to tissue overproliferation and neoplasia. Additionally, an ultrastructure analysis revealed that SJ density within Shrub depleted wing disc tissue is significantly reduced at the late neoplastic stage and the Claudin Mega required Shrub for its localization at the SJ already at pre-neoplastic stages (unpublished data, Master´s thesis Hendrik Pannen).

These data suggest that ESCRT has a critical function in maintenance of SJ in the proliferative wing disc epithelium, likely by regulating the intracellular transport of Mega and possibly other SJ components.

While these initial data reveal a novel and unprecedented role for ESCRT in epithelial homeostasis of *Drosophila* wing imaginal discs, they do not explain how the degradative ESCRT machinery regulates SJ directed trafficking of an essential junction core component. The work presented here therefore aims to unravel the mechanisms behind ESCRT mediated regulation of SJ integrity.

1.5 Aims of this thesis

The ESCRT-III core component Shrub was previously shown to be required for maintenance of SJ density in *Drosophila* wing imaginal discs as well as for delivery of the SJ core component Mega to the junctional membrane (unpublished data, Master´s thesis Hendrik Pannen).
These initial findings raise plenty of important questions about this novel ESCRT function which include, but are not limited to the following:

How does the ESCRT machinery, whose canonical function is degradative protein trafficking, regulate delivery of Mega to the SJ?

Does ESCRT possibly regulate the function of endocytic factors involved in export / recycling of transmembrane proteins from maturing endosomes?

Is ESCRT generally required for anterograde transport of SJ components or is its function limited to Mega or a small subset of SJ proteins?

Does reduction of SJ density following Shrub depletion correlate with a diminished epithelial barrier function?

What occurs first during progression of Shrub depleted tissue towards neoplasia, the reduction in SJ density or neoplastic transformation / multilayering of the epithelial tissue?

To address these questions, a combination of molecular and genetic methods along with fluorescent and transmission electron microscopy will be used in this study. Ultimately, the aim of this work is to deepen understanding about the multiple functions of ESCRT in a *Drosophila* epithelium and to unravel its novel role in regulating the integrity of a critical epithelial structure, the SJ.

2 Manuscript

The ESCRT Machinery regulates Retromer dependent Transcytosis of Septate Junction Components in *Drosophila*

Hendrik Pannen[1], Tim Rapp[1] and Thomas Klein[1*]

[1]Institute of Genetics, Heinrich-Heine-Universität Düsseldorf, Düsseldorf, Germany

[*]Author for correspondence (Thomas.klein@hhu.de)

Abstract

Loss of ESCRT function in *Drosophila* imaginal discs is known to cause neoplastic overgrowth fuelled by mis-regulation of signalling pathways. Its impact on junctional integrity, however, remains obscure. To dissect the events leading to neoplasia, we used transmission electron microscopy (TEM) on wing imaginal discs temporally depleted of the ESCRT-III core component Shrub. We find a specific requirement for Shrub in maintaining Septate Junction (SJ) integrity by transporting the Claudin Megatrachea (Mega) to the SJ. In absence of Shrub function, Mega is lost from the SJ and becomes trapped on endosomes coated with the endosomal retrieval machinery Retromer. We show that ESCRT function is required for apical localization and mobility of Retromer positive carrier vesicles, which mediate the biosynthetic delivery of Mega to the SJ. Accordingly, loss of Retromer function impairs the anterograde transport of several SJ core components, revealing a novel physiological role for this ancient endosomal agent.

2.1 Introduction

Developmental and physiological function of epithelia rely on a set of cellular junctions, linking cells within the tissue to a functional unit. While E-cadherin based adherens junctions (AJs) provide adhesion and mechanical properties, formation of the paracellular diffusion barrier depends on tight junctions (TJs). Proteins of the conserved Claudin family play a key role in establishing and regulating TJ permeability in the intercellular space by homo- and heterophilic interactions with Claudins of neighbouring cells (Gunzel and Yu, 2013). Arthropods, such as *Drosophila*, do not possess TJs but a functionally similar structure in ectodermally derived epithelia termed pleated Septate Junction (pSJ, SJ hereafter), characterized by protein dense septa lining the intercellular space in electron micrographs (Gilula et al., 1970). Structure and function of *Drosophila* SJs depends on a convoluted multiprotein complex containing at least a dozen components. Three Claudins, among them Megatrachea (Mega), have been shown to be required for SJ formation and barrier function in flies (Behr et al., 2003; Nelson et al., 2010; Wu et al., 2004). Besides Claudins, several transmembrane proteins (TMPs) such as Neurexin-IV (NrxIV), Neuroglian (Nrg) or ATPα contribute to the formation of the stable SJ core complex, which is characterized by low mobility within the membrane (Baumgartner et al., 1996; Genova and Fehon, 2003; Oshima and Fehon, 2011). At the intracellular side of the junction, cytoplasmic proteins such as Coracle (Cora), Varicose (Vari) and Discs large (Dlg) associate with the transmembrane components, contributing to the formation of a stable fence-like scaffold (Bachmann et al., 2008; Lamb et al., 1998; Laval et al., 2008; Woods and Bryant, 1991; Wu et al., 2007). While junction formation during embryogenesis requires the SJ localized cytoplasmic protein Dlg, this basolateral cell polarity factor is not a structural part of the immobile junction core complex (Oshima and Fehon, 2011; Woods et al., 1996). This explains the functional separation of barrier formation and apicobasal polarity despite the close association of Dlg-complex components with the SJ. Albeit growing knowledge about the structural composition of SJs, the intracellular events required for assembly and maintenance of SJ complexes remain largely unknown. Specifically, how proliferative tissues, such as the imaginal disc epithelium, maintain SJ integrity is not well established.

It was recently shown that newly synthesized SJ components integrate into the junction from the apical side (in between AJ and SJ) in a ‘conveyor belt-like’ fashion (Babatz et al., 2018; Daniel et al., 2018). In addition, SJ components are frequently associated with endosomal compartments, suggesting a role for the endosomal system in coordinating transport and turnover of SJ complexes (Nilton et al., 2010; Tempesta et al., 2017; Tiklova et al., 2010).

Consistently, endocytosis is required to concentrate SJ components at the junctional region during embryogenesis (Tiklova et al., 2010). This suggests that passage through the endosomal system is a necessity for SJ components to form a stable junctional complex, with the underlying mechanisms remaining poorly characterized.

The endosomal system fulfils a plethora of physiological functions by tightly regulating the intracellular transport of TMPs within the cell. Following endocytosis from the plasma membrane, TMPs enter the endosomal system where they undergo cargo specific sorting. This process provides separation of proteins destined for degradation from those that exit the endosomal system to be recycled. Two evolutionary conserved endosomal sorting machineries, the Endosomal Sorting Complex Required for Transport (ESCRT) and the Retromer complex, mediate cargo sorting into the degradative and recycling pathway, respectively (Cullen and Steinberg, 2018). To coordinate these opposing transport activities, the endosomal system comprises a highly dynamic membrane network governing Retromer dependent tubulation for recycling and ESCRT mediated generation of intraluminal vesicles (ILV) for degradation.

Endocytosed proteins can evade ESCRT dependent packaging into ILVs by exiting the maturing endosome (ME) through tubular retrieval domains induced by specialized recycling machineries such as Retromer. Initially characterized as a regulator of endosome to Golgi cargo retrieval in yeast, this endosomal agent comprises two subcomplexes that cooperatively drive cargo sorting into tubular recycling carriers (Carlton et al., 2004; Horazdovsky et al., 1997; Seaman et al., 1997). Similar to the ESCRT machinery, cargo clustering and membrane deformation is performed by distinct functional units within the Retromer pathway. Motif based cargo recognition and aggregation is mediated by the endosomally localized Vps26:Vps29:Vps35 complex, which has been termed cargo-selective complex (CSC) (Lucas et al., 2016; Nothwehr et al., 2000; Seaman et al., 1997).

Since the ancient CSC does not possess membrane bending activity, cooperation with tubulating factors such as proteins of the SNX-BAR (Sorting Nexin-Bin/Amphiphysin/Rvs) family is required for recycling carrier generation (Cullen, 2008). Proteins containing the curved BAR-domain can assemble into regular helical coats on endosomes, thereby inducing cytoplasm faced tubulation (Frost et al., 2009). Concerted action of CSC stably complexed with SNX-BAR proteins to retrieve endosomal cargo was initially characterized as the classical Retromer pathway in yeast (Horazdovsky et al., 1997; Seaman et al., 1998). In metazoans however, Retromer function is not restricted to SNX-BAR dependent pathways. Specifically, cooperation of CSC with SNX3 or SNX27 (both lacking BAR domains) emerged as alternative routes for endosomal retrieval (Harterink et al., 2011; Lauffer et al., 2010; Steinberg et al.,

2013). Proteomic data from mammalian cells suggest that surface levels of well over 100 TMPs depend on Retromer and many of these proteins seemingly interact with CSC or SNX27 (Steinberg et al., 2013). Recently, *Drosophila* has proven invaluable for assessing and confirming the physiological relevance of some of these putative Retromer cargos *in vivo* (Strutt et al., 2019).

Cargo proteins within the endosomal system that do not undergo recycling can enter the degradative trafficking route starting with their sorting into ILVs. Generation of ILVs at the limiting membrane of MEs requires the canonical ESCRT function, which is performed by four in sequence acting complexes (ESCRT-0, -I, -II, III) and the ATPase Vps4 (Babst et al., 2002a; Babst et al., 2002b; Babst et al., 1998; Bilodeau et al., 2002; Katzmann et al., 2001). Ubiquitination of TMPs serves as the primary degradative sorting signal and sequestration of TMPs into ILVs is an essential prerequisite to complete lysosomal degradation. Several ESCRT components such as Vps27/Hrs (ESCRT-0) and Vps23/TSG101 (ESCRT-I) possess Ubiquitin interacting motifs, which allow them to bind and cluster ubiquitinated TMPs (Bilodeau et al., 2002; Katzmann et al., 2001; Shih et al., 2002). Consequently, local concentration of ubiquitinated cargo by ESCRT complexes establishes a degradative subdomain at the endosomal membrane that is spatially separated from the retrieval subdomain (Norris et al., 2017; Raiborg et al., 2002; Raiborg et al., 2001).

While ESCRT-0-II complexes provide cargo recognition and clustering, the membrane deforming activity required to bud and abscise ILVs into the endosomal lumen depends on ESCRT-III components, which polymerize into helical arrays at the endosomal membrane (Hanson et al., 2008; Saksena et al., 2009). The most abundant ESCRT-III component is the highly conserved yeast Snf7/Vps32, encoded by the gene *shrub* (*shrb*) in *Drosophila* (Sweeney et al., 2006; Teis et al., 2008). Unlike upstream ESCRT components, ESCRT-III proteins only transiently assemble into a heterooligomeric complex at the endosomal membrane (Teis et al., 2008; Wollert et al., 2009). As a consequence of ESCRT activity, the maturing endosome accumulates cargo-containing ILVs and can be recognised in electron micrographs as a multivesicular body (MVB). The ESCRT/ MVB pathway ends with Vps4 dependent dissociation of ESCRT-III components from the endosomal membrane. This step is required for the release of the nascent ILV and subsequent rounds of ILV formation (Babst et al., 1998; Wollert et al., 2009). Loss of ESCRT function was initially studied in yeast cells in which it led to the emergence of an aberrant pre-vacuolar endosomal organelle, termed class E compartment (Raymond et al., 1992). This defective endosomal structure is characterized by accumulation

of degradative cargo and a failure to fuse with the vacuole / lysosome (Doyotte et al., 2005; Raymond et al., 1992).

The physiological relevance of ESCRT mediated degradative TMP trafficking is particularly evident in *Drosophila* imaginal disc tissue. Here, loss of ESCRT function induces severe overgrowth, multilayering, apoptosis and invasive behaviour of the tissue; a phenotype attributed to mis-regulation of cellular signalling pathways, such as the Jak/Stat-, Jun-Kinase- and Notch pathways (Herz et al., 2006; Moberg et al., 2005; Thompson et al., 2005; Vaccari and Bilder, 2005). Consequently, ESCRT components were classified as endocytic neoplastic tumour suppressor genes (nTSG) in *Drosophila* (Hariharan and Bilder, 2006). While induction of over-proliferation and apoptosis in nTSG mutants have been extensively characterized, the events leading to loss of cell polarity and ultimately neoplastic transformation of the tissue remain poorly understood.

Here, we have analysed the integrity of cellular junctions in an ESCRT depleted wing imaginal disc epithelium to gain insight into the initial events leading to neoplastic transformation. To our surprise, preceding neoplastic overgrowth, we found a strong and specific reduction in the density of SJ. We show that ESCRT and Retromer functions are required for anterograde transport of SJ components. By dissecting the intracellular trafficking itinerary of the Claudin Megatrachea, we reveal that biosynthetic delivery of this core SJ component depends on a complex basal to apical transcytosis route relying on ESCRT and Retromer functions.

2.2 Results

ESCRT knockdown specifically affects SJ integrity

To analyse the impact of ESCRT loss of function on junctional integrity, transmission electron microscopy (TEM) was used on wing imaginal discs that have been depleted of ESCRT function. We devised an RNAi based approach allowing spatiotemporal knockdown of the ESCRT-III component Shrub. By using *hh*Gal4 and the temperature sensitive Gal4 Repressor (*tub*Gal80^{ts}), we specifically inhibited Shrub protein expression in the posterior compartment by expressing a UAS-*shrub*-RNAi construct (Sweeney et al., 2006) for specified durations. After 32h of RNAi expression, Shrub protein was effectively reduced in the posterior compartment as visualized by antibody staining (Fig.1A). ESCRT loss of function is known to induce high levels of apoptosis in imaginal disc tissue (Herz et al., 2006; Thompson et al., 2005; Vaccari and Bilder, 2005). Since apoptotic cells disassemble their junctions prior to extrusion from the tissue (Brancolini et al., 1997; Steinhusen et al., 2001), we co-expressed the viral caspase inhibitor p35 (Hay et al., 1994) with *shrub*-RNAi to preserve tissue integrity and allow unambiguous analysis of junctional structures. Interestingly, while 48h expression of *p35* + *shrub*-RNAi yielded discs with no apparent morphological defects seen in a thin section (Fig.1B), discs after 65h of expression were disorganized and multi-layered in the posterior compartment as reported for *shrub* null mutant clonal eye disc tissue (Fig.1C; (Vaccari et al., 2009)). This indicates that our assay is able to reproduce the hallmarks of ESCRT mediated neoplasia.

We used the 48h stage to analyse junctions by TEM prior to neoplasia. In the wildtype anterior control compartment, the membrane basal to the AJ was lined with the ladder-like electron dense structures that represent the SJ (Fig. 1E, arrow). In the posterior (*shrub*-RNAi) compartment however, only few electron dense structures basally to the AJ were detected and an obvious ladder pattern was rarely seen (Fig. 1E´). Interestingly, we did not find AJ appearance to differ noticeably between wildtype and *shrub*-RNAi compartments (Fig. 1E/E´). We sought to quantify SJ integrity by measuring the total length of electron dense structures basally to the AJ in a region of interest (ROI) with specified length of 2µm. In anterior control compartments, roughly 32% of membrane within ROIs was lined with SJ (Fig. 1D). This value decreased to about 15% in posterior compartments, indicating that 48h expression of *p35* + *shrub*-RNAi reduces SJ density in wing discs by more than 50% (Fig. 1D). Due to the lack of apparent neoplastic transformation at the 48h stage, we conclude that reduction in SJ density

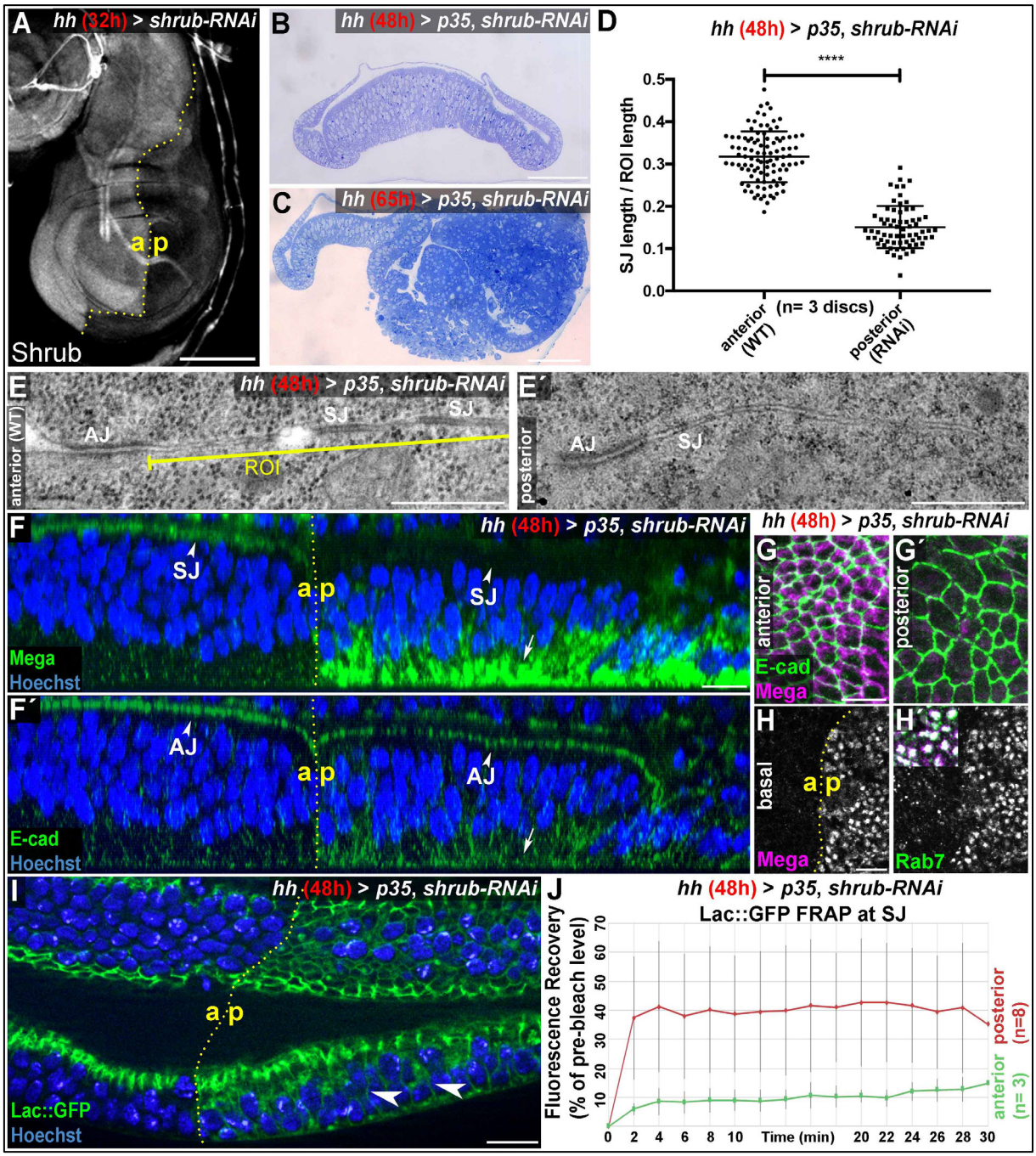

Figure 1. The ESCRT-III component Shrub is required for SJ integrity. (**A**) 32h expression of *shrub-RNAi* under the control of *hhGal4* effectively depletes Shrub levels in the posterior compartment of wing imaginal discs. (**B-C**) Thin sections of wing discs co-expressing *shrub-RNAi* and *p35* for either 48h (**B**) or 65h (**C**). Note the intact epithelial monolayer at the 48h stage (**B**) vs. posterior neoplastic overgrowth after 65h (**C**). (**D**) Quantification of electron-dense SJ in TEM sections reveals a ~50% reduction of SJ strands within Shrub depleted compartments (48h) compared to control. Each data point represents a single junctional region of interest (ROI) of 2µm length as defined in **(E**) A two-tailed t-test was used for statistical analysis with the significance level **** representing a p-value < 0.0001. Representative ROIs of control (**E**) and Shrub depleted compartments (**E´**) visualize the reduction in electron dense SJ. (**F**) Optical section of a wing disc after 48h of Shrub depletion in the posterior compartment. The claudin Mega is lost from the apical SJ (compare arrowheads) and accumulates basal to the nuclei (arrow). In contrast, E-cad localization to AJ between the anterior control and the posterior compartment is

largely unaffected (compare arrowheads in **F´**) while only little accumulation is seen at the basal pole (arrow). (**G**) Projections of the junctional area show the close association of E-cad with Mega in anterior control compartments (**G**) and apparent lack of junctional Mega in the Shrub depleted tissue (**G´**). In basal planes, intracellular accumulation of Mega within the *shrub-RNAi* compartment is evident as a punctate pattern, colocalizing with the endosomal marker Rab7 (**H**). Subcellular localization of the SJ component Lachesin::GFP is restricted to SJ in anterior control compartments while showing extensive spread along the entire lateral membrane in Shrub depleted cells (arrowheads in **I**). (**J**) Fluorescence recovery after photobleaching (FRAP) analysis of Lac::GFP at the SJ reveals increased mobility in *shrub-RNAi* tissue, indicating defective fence function of SJ. a: anterior / p:posterior. Scale bar in (**A**) 100µm, (**B-C**) 50µm, (**E**) 0.5µm and all other panels 10µm.

does not reflect indirect effects resulting from ESCRT induced epithelial to mesenchymal transition (EMT), but rather suggests a direct involvement of ESCRT in maintaining SJ density in wing imaginal discs.

We turned to fluorescence microscopy to analyse the subcellular localization of junctional proteins upon Shrub depletion. Again, we used depletion for 48h, which does not show apparent neoplastic overgrowth and thus preserves epithelial monolayer organization. We used antibodies against E-Cadherin and the Claudin Mega to reveal AJ and SJ, respectively. Both proteins localised almost exclusively at the apical membrane in wildtype cells of the anterior compartment of the disc (Fig.1F, left arrowheads). However, in the Shrub depleted posterior compartment, Mega was not detected at the SJs, while E-cad showed wildtype AJ localisation (Fig.1F, right arrowheads). The absence of Mega from SJs is also visible in maximum intensity projections of the junctional region (Fig. 1G). Importantly, Mega accumulated in vesicle like structures at the basal side of the cells, suggesting that it might be trapped in intracellular compartments (Fig. 1F, arrow). This basal fraction of Mega was strongly labelled with the endosomal marker Rab7, suggesting that Mega was trapped within maturing endosomes (Fig. 1H).

We reasoned that junctional loss of Mega together with the decreased SJ density revealed by TEM analysis point towards defects in SJ integrity / function in *shrub*-RNAi tissue. Indeed, dye exclusion experiments suggest that the barrier function is compromised in *shrub*-RNAi expressing wing discs (Figure S1). Support for this notion comes also from another experiment. The GPI-anchored SJ protein Lachesin (Lac) is required for barrier function and localized at the outer membrane leaflet (Llimargas et al., 2004). We visualized endogenous Lac localisation by using a GFP protein trap line in *p35* + *shrub*-RNAi expressing discs. While Lac::GFP was restricted to SJ in the anterior control compartment, the protein spread more laterally in *shrub*-RNAi tissue (Fig. 1I, arrowheads). Interestingly, this phenotype resembles mis-localisation of

SJ proteins in mutants of individual complex components during junction formation in the embryo. For example, in *mega* deficient embryos, NrxIV fails to concentrate at the SJ and localizes along the entire lateral membrane (Behr et al., 2003). We conclude that Shrub function maintains integrity of the SJ complex required for containment of Lac within the junction of the wing disc epithelium. The lateral spreading also suggests that Lac::GFP mobility within the membrane is increased in Shrub depleted tissue. We measured fluorescence recovery after photobleaching (FRAP) of Lac::GFP to test this hypothesis. Consistent with a very stable and immobile SJ complex (Oshima and Fehon, 2011), Lac::GFP fluorescence recovery at the junction was low in the anterior control compartment, with GFP signal intensities barely reaching 20% of the pre-bleach levels half an hour after photobleaching (Fig. 1I, yellow graph). In the *shrub*-RNAi compartment however, Lac::GFP fluorescence recovery was quick and reached a plateau at roughly 40% of pre-bleach levels after a few minutes. This suggests that a fraction of Lac::GFP molecules shows increased mobility within the junctional membrane region in *shrub*-RNAi expressing cells, in line with a defective barrier / fence function of the SJ complex.

Altogether, these results indicate that SJ integrity critically depends on ESCRT function and suggest that Shrub is required for intracellular transport of Mega from an endosomal compartment towards the junction.

The Retromer CSC regulates membrane levels of SJ core components

The loss of Mega from the SJ and concomitant accumulation in basal aggregates cannot easily be explained with a role of Shrub in Mega degradative trafficking but rather suggest that its export from the endosomal system might be impaired in Shrub depleted tissue. Consistent with a non-degradative ESCRT role in transport of Mega, we did not find Mega to accumulate intracellularly when we interfered with endosomal maturation or prevented endolysosomal fusion downstream of ESCRT function, in contrast to the canonical ESCRT cargo Notch (Fig. S2). These results suggest that Mega undergoes very little (if any) lysosomal turnover in wing imaginal discs and point towards an ESCRT function that is distinct from the degradative MVB pathway in trafficking of Mega.

We hypothesized that biosynthetic delivery of Mega to the SJ might require an endosomal recycling pathway depending on ESCRT for its proper function. To test this idea, we depleted imaginal discs of proteins known to regulate endosomal recycling and analysed the impact on junctional Mega levels. We found that expression of an RNAi construct targeting the Retromer

CSC component Vps35 led to a significant reduction of Mega at the SJ (Fig. S2C), which led us to investigate the function of Retromer in transport of SJ components. We generated null mutant clones of the Retromer core component *Vps35* (*Vps35^{MH20}*, (Franch-Marro et al., 2008) in wing discs and analysed the subcellular distribution of junctional proteins. While Mega membrane levels at the SJ were reduced in *Vps35^{MH20}* tissue, junctional E-cad levels were unaffected (Fig. 2A). This result is analogous to the phenotype seen upon *shrub*-RNAi expression (Fig. 1).

We also found reduced membrane levels of the SJ core components ATPα, NrxIV and Nrg in *Vps35^{MH20}* clones, visualized by using endogenously tagged GFP protein trap lines (Fig. 2B-D). These data suggest that Retromer has a general function in SJ protein trafficking that is not restricted to Mega. In line with this, quantification of junctional signal revealed that all tested SJ core components show similarly reduced levels in *Vps35^{MH20}* tissue (roughly 50% compared to wildtype, Fig. 2H). Additionally, we found *Vps35* to be required for membrane levels of SJ components in several tissues, such as eye / leg imaginal discs and pupal wings, pointing to a general requirement of the Retromer pathway for SJ protein transport (Fig. S3). Surprisingly, loss of NrxIV::GFP from the SJ membrane in *Vps35^{MH20}* mutant pupal wing tissue was more severe compared to the phenotype seen in third instar wing discs, suggesting that SJs within tissues that actively remodel junctions and do not strongly proliferate might be even more sensitive towards loss of Retromer function (Fig. S3).

Clones mutant for the Vps35 interaction partner *Vps26* phenocopied *Vps35^{MH20}* tissue with regard to Mega membrane levels, supporting a general function of the CSC in transport of SJ components (Fig. 2E). Interestingly, in contrast to these structural SJ core components, the levels of the associated cytoplasmic scaffolding proteins Dlg and Cora were unaffected in *Vps35^{MH20}* mutant tissues (Fig. 2F, G). This is consistent with *Vps35^{MH20}* clones maintaining intact apicobasal polarity and supports a role of Retromer in trafficking specific structural components of SJs. Nevertheless, our extended analysis with further SJ components revealed that the GPI-anchored proteins Lachesin, Contactin, as well as the cytoplasmic Varicose, show reduced SJ levels in *Vps35^{MH20}* clones (Fig. S4). This indicates that the Retromer CSC regulates apical levels of a large subset of SJ components.

Next, we quantified SJ density detected by TEM in wing discs depleted of Vps26 and found a reduction of electron dense septa by about 60% (Fig. S5). Consistent with compromised SJ integrity, a diffusible dye readily infiltrated Vps26 depleted tissue, indicating defective barrier function (Fig. S1). We conclude that the Retromer CSC regulates membrane levels of many SJ core components, thereby contributing to junction integrity and function.

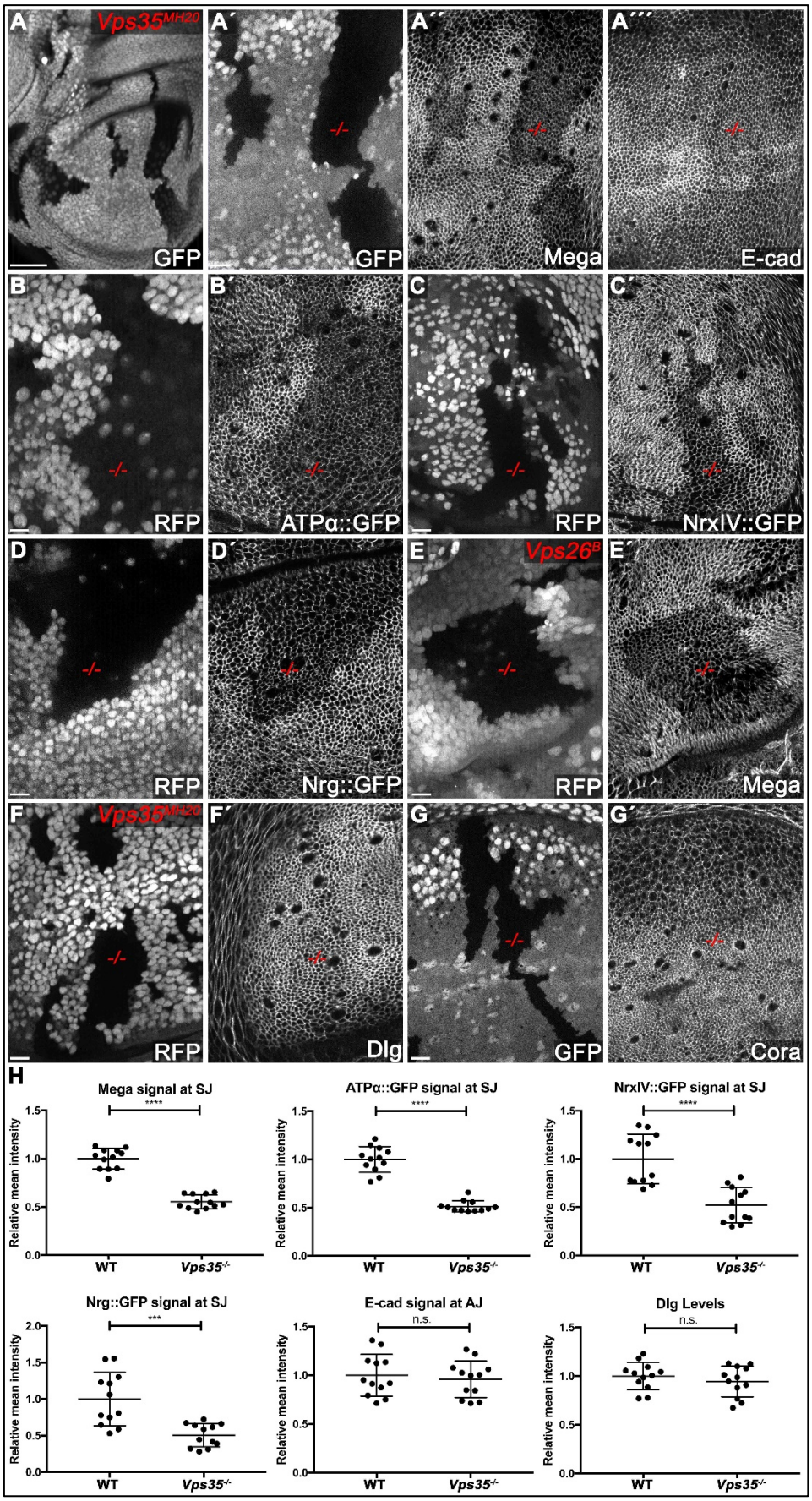

Figure 2. The Retromer CSC regulates membrane levels of SJ core components. (**A**) Null mutant clones of the Retromer component *Vps35* were generated in wing discs. Mutant tissue (-/-) is marked by absence of either

GFP or RFP. Mega signal at the SJ is reduced in *Vps35*^{MH20} tissue (**A´´**), while apical E-cad levels are unaffected (**A´´´**). (**B-D**) Endogenously tagged SJ core components ATPα (**B**), NrxIV (**C**) and Nrg (**D**) show reduced membrane levels in *Vps35*^{MH20} tissue. (**E**) *Vps26* clones phenocopy *Vps35* clones with respect to junctional localization of Mega (compare **E´** with **A´´**). (**F-G**) Junctional localizations of SJ associated cytoplasmic proteins Dlg and Cora are unaffected in *Vps35*^{MH20} cells. (**H**) Quantification of junctional membrane levels of indicated proteins in wildtype and *Vps35*^{MH20} tissue. Each dot represents fluorescence intensity of a junctional region in either clonal (*Vps35*^{MH20}) or surrounding wildtype tissue. n=4 discs for each component. A two-tailed t-test was used for statistical analysis with the significance levels **** representing a p-value of < 0.0001, ***: < 0.001 and n.s. (not significant): ≥ 0.05. Note that the transmembrane SJ components Mega, ATPα, NrxIV and Nrg are similarly affected, showing reduced levels at the SJ within *Vps35*^{MH20} tissue by ~50%, while E-cad and Dlg apical levels do not significantly differ between wildtype and *Vps35*^{MH20} tissue. Scale bar in (**A**) 50µm, in all other panels 10µm.

In optical sections of *Vps35*^{MH20} clones, endogenously tagged Mega::YFP protein shows reduced overall levels throughout the mutant tissue (Fig. S4 A, G). This suggests that misrouting of Mega into the degradative pathway may occur upon loss of *Vps35* function, as has been shown for many Retromer cargos (Franch-Marro et al., 2008; Harterink et al., 2011; Pocha et al., 2011). Consistently, when Retromer function and endo-lysosomal fusion are simultaneously impaired, Mega::YFP shows reduced SJ levels and accumulates in intracellular vesicles, hinting at a failure to be degraded (Fig. S2). This result supports that misrouting of Mega into the degradation pathway occurs when CSC function is compromised. We conclude that Mega behaves like a *bona fide* Retromer cargo.

To gain further insight into the CSC dependent pathway required for SJ delivery of Mega, we investigated null mutant clones of known Retromer associated factors (SNX-BAR, Snx3, Snx27 and the WASH-complex component Fam21). Surprisingly, we failed to find any of these proteins to be required for the regulation of Mega membrane levels, raising questions on the mechanism governing CSC dependent transport of Mega (Fig. S6). Nevertheless, based on above findings, we propose a novel function of the Retromer CSC in delivery of SJ core components to the junction, thereby contributing to SJ homeostasis.

ESCRT regulates subcellular localization and mobility of the Retromer CSC

The above results indicate that Retromer is required for regulating membrane levels of Mega and other SJ components. Therefore, trapping of Mega in basally localized endosomal compartments upon *shrub*-RNAi expression could be a consequence of defective Retromer dependent endosomal export in this ESCRT deficient situation. We reasoned that loss of

ESCRT function might alter organization and function of Retromer dependent carrier vesicles, thereby affecting cargo flux. To test this, we analysed the subcellular distribution of Retromer components in Shrub depleted cells. We visualized the Retromer CSC by using an endogenously tagged Vps35 (Vps35::RFP, (Koles et al., 2015)). In anterior control compartments, Vps35::RFP was found in vesicular structures throughout the cell, but with significantly higher abundance in the apical cytoplasm (Fig. 3A-D, arrows). Interestingly, this polarized apical localization is consistent with an apical transport hub at the junction level in wing disc cells that is characterized by enrichment of more than half of the *Drosophila* Rab GTPases (Dunst et al., 2015). In contrast to its concentration within the apical hub, little Vps35::RFP was detected in the basal cytoplasm of wildtype tissue (Fig. 1A´). Upon *shrub*-RNAi expression however, Vps35::RFP strongly accumulated basally (Fig. 1A´, arrowhead) while apical hub localization was almost completely abolished (Fig. 1A). Therefore, loss of Shrub function appears to re-distribute Vps35::RFP positive vesicles from the apical hub into the basal cytoplasm where they accumulate. This apical to basal shift of Retromer CSC positive vesicles is also evident in optical cross sections of wing discs expressing RNAi constructs for several ESCRT components (Fig. 3B-D, compare arrows with arrowheads). Importantly, RNAi directed against the ESCRT-I component TSG101 or Vps4, but not ESCRT-0, phenocopied *shrub*-RNAi expression with regard to Vps35::RFP subcellular localization (Fig. 3B-D, Fig. S7). This indicates that several ESCRT complexes are required for maintaining apical hub localization of the CSC in the wing disc epithelium.

We found strong colocalization of Mega and Vps35::RFP on basal endosomal aggregates of *shrub*-RNAi expressing cells (Fig. S8). This is in line with Mega being trapped in aberrant Rab7 and CSC positive endosomal compartments residing in the basal cytoplasm of ESCRT deficient cells. Our analysis of these basal aggregates revealed that besides containing Mega, they are enriched in ubiquitinated cargo and are coated with Retromer components, Hrs and endosomal GTPases Rab5 and Rab7 (Fig. S8). We conclude that these aggregates likely represent *Drosophila* ‘class E-like’ compartments, which is supported by TEM analysis of basally localized endosomal structures within *shrub*-RNAi expressing wing disc tissue (Fig. S9). While the regularly shaped and sized MVBs of wildtype cells were absent Shrub depleted cells, we found a variety of enlarged, abnormal membranous compartments that are reminiscent of class E compartments in mammalian cells (Doyotte et al., 2005; Stuffers et al., 2009).

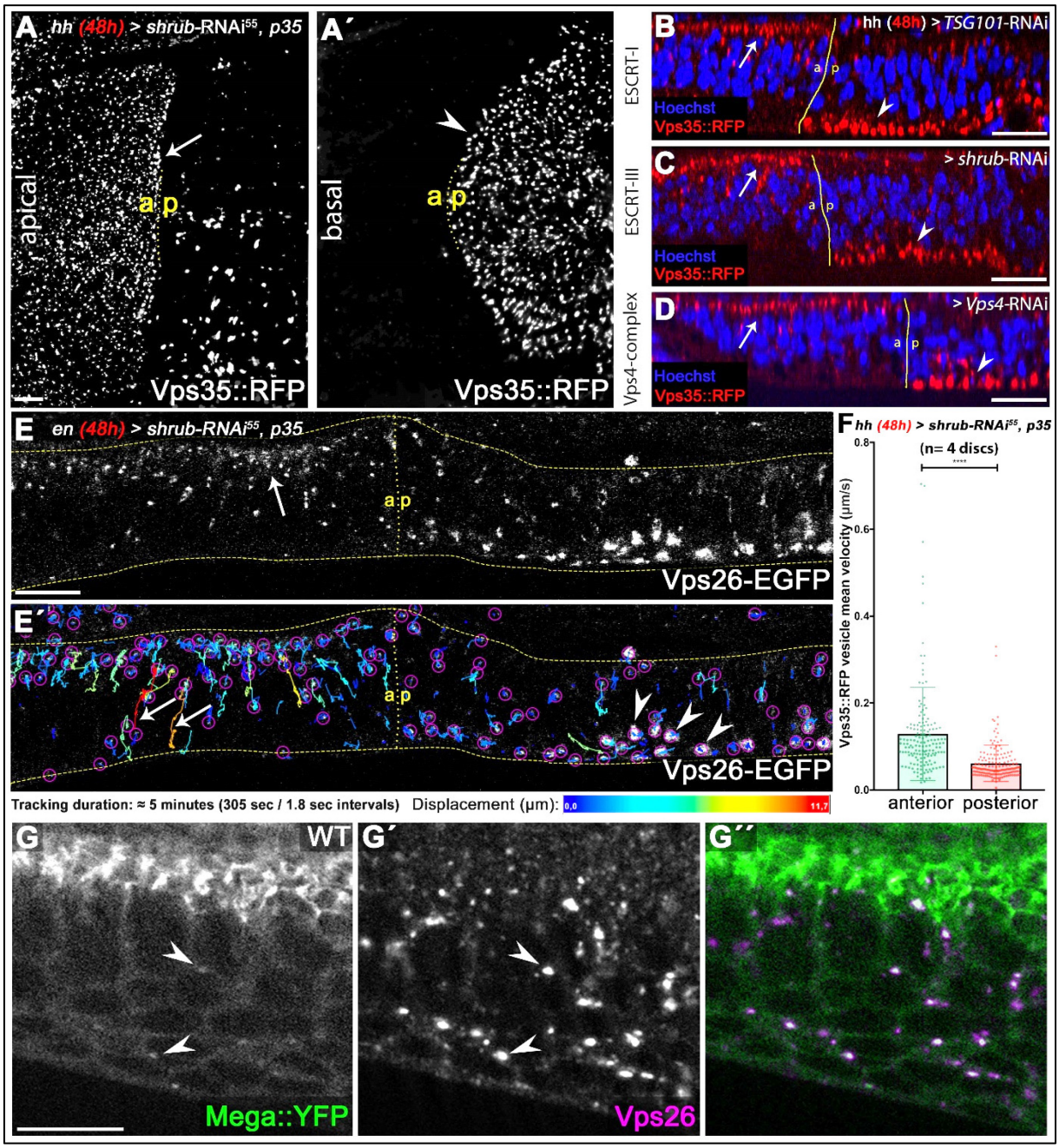

Figure 3. ESCRT function is required for CSC Retromer subcellular localization and mobility. (**A**) Endogenously tagged Vps35::RFP localizes in a vesicular pattern within the apical hub in wildtype control compartments (arrow). After 48h of Shrub depletion, Vps35::RFP apical hub localization is largely abolished and basal accumulation is seen (arrowhead in **A´**). Basally accumulated Mega (see also Figure 1) colocalizes with Vps35::RFP in aberrant endosomal compartments within *shrub-RNAi* tissue (inset in **A´**). (**B-D**) The shift in subcellular localization of Vps35::RFP from the apical hub (wildtype, arrows) to basal aggregates (ESCRT-depleted compartment, arrowheads) is detected upon knockdown of ESCRT components TSG101, Shrub as well as Vps4. This indicates that regulation of Retromer subcellular localization is a general ESCRT function in wing discs. (**E**) Live-imaging and vesicle tracking of a genomic Vps26-EGFP construct at the anterior/posterior boundary of a wing disc expressing *shrub-RNAi* for 48h in the posterior compartment under control of *en*Gal4. Note the apical hub in the anterior control compartment and the large basally localized Vps26-EGFP aggregates

in the posterior Shrub depleted compartment (compare with Vps35::RFP in **C**). (**E´**) Individual vesicle trajectories visualize Vps26-EGFP movement within the tissue after a 5min imaging acquisition. Note the high mobility of several vesicles along the apicobasal axis in the anterior control compartment (arrows). In contrast to long distance shuttling of Vps26-EGFP in the control tissue, basal Vps26-EGFP aggregates (arrowheads) in the Shrub depleted posterior compartment are largely static and overall vesicle dynamic is reduced. (**F**) Quantification of Vps35::RFP mobility in wildtype (anterior) and Shrub depleted (posterior) tissue. Each dot represents mean velocity of a single tracked vesicle. Note the reduced mean velocity of Vps35::RFP and the high ratio of low mobility vesicles within Shrub depleted compartments. A two-tailed t-test was used for statistical analysis with the significance level **** representing a p-value < 0.0001. (**G**) Endogenously tagged Mega::YFP colocalizes with Vps26 in vesicular structures residing in the apical as well as basal cytoplasm (arrowheads). Scale bars in all panels represent 10µm.

We speculate that these irregular compartments aberrantly cluster endosomal machineries and cargos, thereby interfering with endosome function. Consequently, the SJ phenotype seen in *shrub*-RNAi tissue (Fig. 1) could be explained by basal displacement of Retromer dependent carriers, which are required for targeting SJ components to the junctional region.

The apical bias of Vps35::RFP positive vesicles in wildtype cells suggests a polarized movement of CSC carriers along the apicobasal axis with relatively long dwell times at the apical hub. We reasoned that in wing discs, a majority of CSC dependent cargo might be released preferentially at the apical pole of the cells. We turned to live imaging to study movement of CSC positive vesicles in wildtype and Shrub depleted cells. We visualized CSC using Vps35::RFP or a transgene encompassing the genomic region of *Vps26* fused to a C-terminal EGFP-tag (Wang et al., 2014). In anterior control compartments, Vps26-EGFP localised in a vesicular pattern throughout the cells with increased abundance at the apical hub (Fig. 3E, arrow). In the posterior Shrub depleted cells however, Vps26-EGFP localization at the apical hub was reduced and basal accumulation was evident (Fig. 3E). Therefore, live imaging of Vps26-EGFP recapitulates the apical to basal shift of Vps35::RFP in ESCRT depleted fixed tissue (Fig. 3B). We used Vps35::RFP / Vps26-EGFP to record time series of CSC positive carrier vesicles within wildtype and Shrub depleted tissue. We applied the Fiji plugin TrackMate (Tinevez et al., 2017) to map individual trajectories of Vps35::RFP / Vps26-EGFP vesicles over a timeframe of 5 minutes (Fig. 3E´). The results clearly show that the CSC carriers in anterior control cells were highly mobile along the apicobasal axis with a subset of vesicles moving rapidly and relatively long distances between the apical and basal poles (Fig. 3E´, arrows). This suggests that CSC carriers, although preferentially residing at the apical hub, are highly mobile and occasionally shuttle between the apical and basal poles of wing disc cells. In contrast, long distance movement of Vps35::RFP / Vps26-EGFP vesicles was severely

reduced in the posterior Shrub depleted compartment (Fig. 3E´ and F). Importantly, the basal CSC aggregates were mostly immobile, showing no apparent movement along the apicobasal axis (Fig. 3E´, arrowheads). These results indicate that ESCRT function is required for the mobility of CSC positive endosomes.

We hypothesized that certain Retromer cargos might rely on CSC shuttling between the apical and basal poles for efficient transport. Mega::YFP vesicular structures colocalized extensively with Vps26 not only at the junctional level but also in vesicles with close proximity to the basal pole of the cells (arrowheads in Fig. 3G). This suggests that Mega and possibly other SJ components shuttle along the apicobasal axis in CSC positive carrier vesicles. We confirmed this by live imaging of Mega::YFP together with Vps35::RFP (Video S1). While the majority of Mega::YFP signal represented the SJ pool, the few mobile vesicles that we detected were associated with Vps35::RFP. Thus, Mega is moving along the apicobasal axis in CSC decorated vesicles.

Together, the results reveal that ESCRT function regulates the mobility and apical hub localization of Retromer CSC positive endosomes. We conclude that by trapping CSC on aberrant endosomal compartments, loss of ESCRT function impairs Retromer dependent export of Mega from the endosome, consequently depleting the SJ pool in wing disc cells.

Mega undergoes basal to apical transcytosis prior to reaching the SJ

Endosomal trafficking by Retromer could occur via several different pathways. While certain Retromer cargos are transported directly from endosomes to the plasma membrane, the classical Retromer route involves cargo recycling in a detour via the Golgi. Besides these two endosomal recycling pathways, Retromer has also been shown to regulate transcytosis from one membrane domain to another (Verges et al., 2004). Prior to all Retromer and ESCRT dependent trafficking events, endocytosis of cargo is required for subsequent sorting within the endosomal system. We reasoned that blocking endocytosis of Mega might reveal the membrane domain from which it is internalized into the endosomal system and aid in understanding how the Retromer pathway is involved in its trafficking.

We suppressed Clathrin-mediated endocytosis by RNAi mediated depletion of Clathrin heavy chain (Chc) for 32h in the posterior compartment. While depletion of Chc did not have an apparent effect on junctional E-cad levels (Fig. 4A´), Mega::YFP was strongly reduced at the SJ (Fig. 4A´´). Since membrane proteins accumulate at their site of endocytosis when the

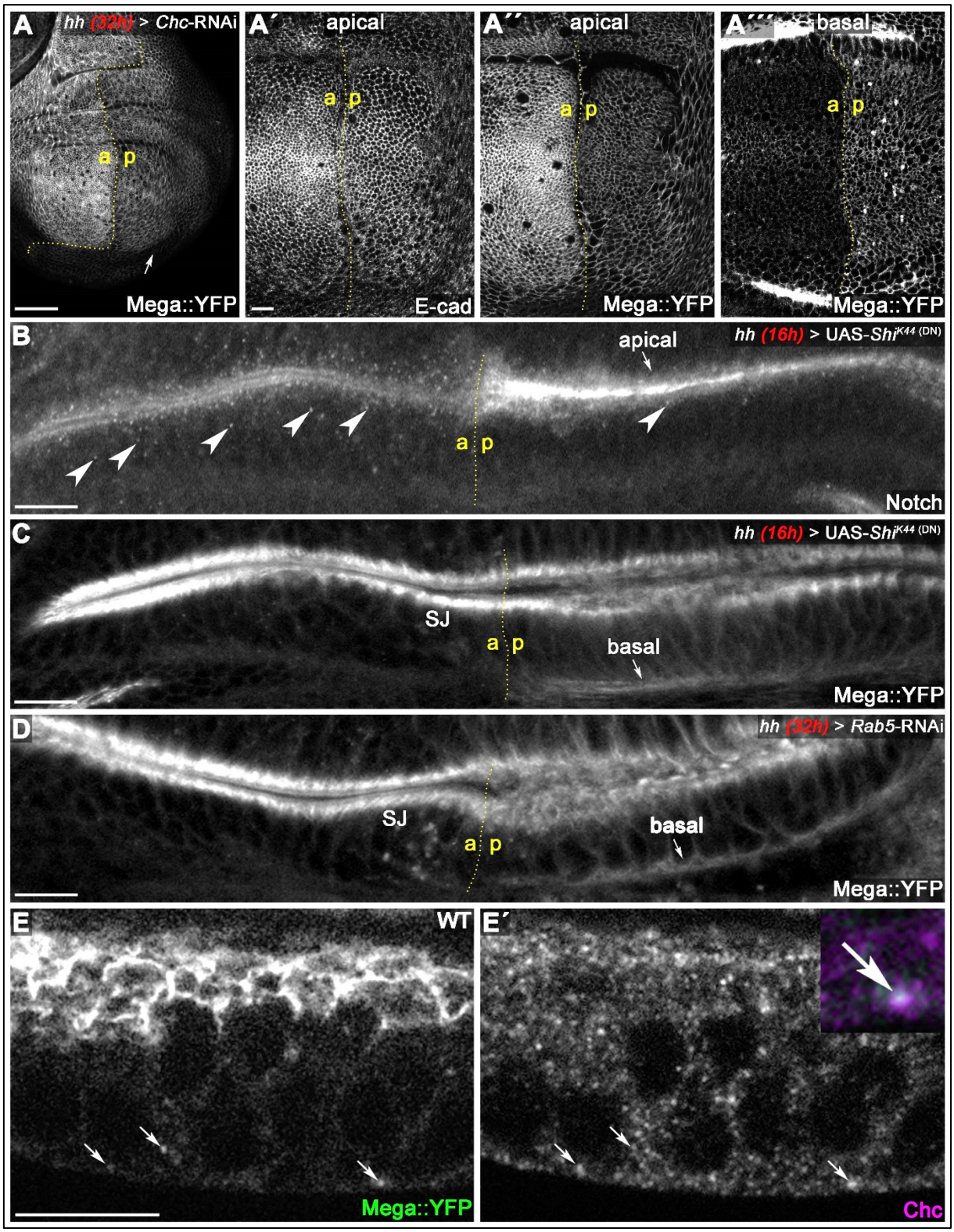

Figure 4. Mega is endocytosed at the basodistal membrane. (**A**) Depletion of Clathrin via *Chc-RNAi* expression for 32h in the posterior compartment reduces apical membrane levels of Mega::YFP. While E-cad based AJ appear unaffected following Chc depletion (**A´**), the junctional Mega::YFP pool is reduced (**A´´**). In a basal focal plane, Mega::YFP is seen accumulating in the basodistal part of the lateral membrane in the *Chc-RNAi* expressing posterior compartment. (**B-C**) Expression of a dominant negative Dynamin construct (Shi^{K44}) leads to apical accumulation of Notch within an epithelial fold of the hinge region (arrow in **B**) and reduces the amount of Notch

positive vesicles (arrowheads). In contrast, posterior Mega::YFP signal at the SJ is reduced and a basal pool is visible (arrow in **C**). (**D**) Depleting Rab5 in the posterior compartment yields a similar Mega::YFP phenotype with respect to junctional levels and basal accumulation (arrow in **D**). (**E**) In line with internalization from the basodistal membrane, Mega::YFP colocalizes with Clathrin at vesicular structures near the basal cell pole (arrows in **E** and **E´**). Scale bars in all panels represent 10µm except for (**A**)**,** in which it represents 50µm.

internalization process is inhibited, this result argues against Mega undergoing Clathrin-dependent endocytosis at the apical membrane. Importantly, we found Mega::YFP accumulating at the most basal region of the lateral membrane (Fig. 4A´´´), suggesting that Mega is continuously removed from a basal membrane pool by endocytosis. These results also suggest that Mega, prior to accumulating at the SJ, undergoes Clathrin-mediated endocytosis at the most basal section of the basolateral membrane (for the sake of simplicity, we will refer to this as the basodistal membrane).

Next, we interfered with Dynamin-dependent endocytosis by expressing a dominant negative version of Shibire, the *Drosophila* Dynamin homolog (UAS-*Shi*^{K44}, (Moline et al., 1999)) under the control of *hh*Gal4. An expression of Shi^{K44} for 16h was sufficient to cause strong accumulation of Notch at the apical membrane, indicating that Dynamin-dependent endocytosis of apically internalized membrane proteins is effectively impaired (Fig. 4B). In line with diminished uptake of Notch into the endosomal system, we found reduced abundance of intracellular Notch vesicles in the posterior compartment (Fig. 4B, arrowheads). In contrast to apically endocytosed Notch, Mega::YFP seemed to be reduced at the SJ level upon 16h of Shi^{K44} expression (Fig. 4C). Instead, it accumulated at the basal pole of the cells (Fig. 4C, arrow). Reduced SJ levels accompanied by basodistal accumulation of Mega::YFP were also found upon depleting the tissue of Rab5 by RNAi expression (Fig. 4D). This common phenotype suggests that a critical step in SJ supply of Mega is its internalization from the basodistal membrane, hinting at a transcytosis-like mechanism in basal to apical direction. We confirmed the close association of Mega with Chc in wing imaginal discs by detecting colocalisation of Mega::YFP and Chc in vesicular structures in wildtype tissue (Fig. 4E), which is consistent with Chc being part of the Mega proteome in *Drosophila* embryos (Jaspers et al., 2012). Importantly, Mega::YFP vesicles in proximity to the basodistal membrane were Chc positive, in line with Mega being endocytosed basally (Fig. 4E, arrows).

Together, these data support a transcytosis-like mechanism from the basodistal domain of the lateral membrane to the SJ, which is required to supply the junction with newly synthesized Mega. This process depends on the endocytic and early endosomal machinery as interference

with Dynamin, Clathrin and Rab5 function leads to reduced SJ levels of Mega accompanied by its accumulation at the basodistal membrane. The results suggest that Mega needs to traverse through the endosomal system prior to reaching the SJ and argue against a conventional recycling function of Retromer in this process. This notion is further supported by our comparative analysis of Mega trafficking to that of Crumbs (Crb), an established Retromer recycling cargo in wing discs (Pocha et al., 2011). It revealed distinct phenotypes upon Vps35 loss or inhibition of endocytosis, suggesting that these proteins do not undergo a common Retromer dependent pathway (Fig. S10).

We conclude that Mega is not undergoing apical recycling but requires basal to apical transcytosis for junctional delivery. Thus, our data suggest that transcytosis of SJ components is not limited to initial SJ formation in the embryo (Tiklova et al., 2010), but is also required in a proliferative epithelium to maintain the junctional pool of Mega.

Basal to apical transcytosis of Mega depends on ESCRT and Retromer function

The complex anterograde trafficking of Mega to the SJ prompted us to investigate it in more detail. We generated an HA-tagged UAS-Mega construct, allowing us to analyse its delivery to SJ upon over-expression. Continuous expression of UAS-HA-Mega led to its integration into SJ, which we confirmed by colocalization with Lac::GFP (Fig. 5A´´). Interestingly, in contrast to endogenous Mega, we detected a fraction of HA-Mega at the most basal part of the epithelium (Fig. 5A). This suggests that the basodistal membrane pool of Mega that we observed upon endocytosis block is also detectable upon Mega overexpression. We also found increased abundance of intracellular vesicles, consistent with elevated trafficking of Mega within the cells (Fig. 5B). HA-Mega colocalized with Vps35::RFP on vesicles (Fig. 5B, arrows), reminiscent of endogenous Mega shuttling in CSC dependent endosomal carriers. Hence, we conclude that over-expression of UAS-HA-Mega recapitulates the hallmarks of Mega intracellular transport.

While the majority of HA-Mega signal upon continuous overexpression was detected at the SJ level (Fig. 5C, arrowhead), HA-Mega was also found in lateral and basal membrane regions (Fig. 5C, arrow). Strikingly, the basodistal pool of HA-Mega was characterized by an intense membrane localization pattern resembling the staining of the junctional region (Fig. 5C´).

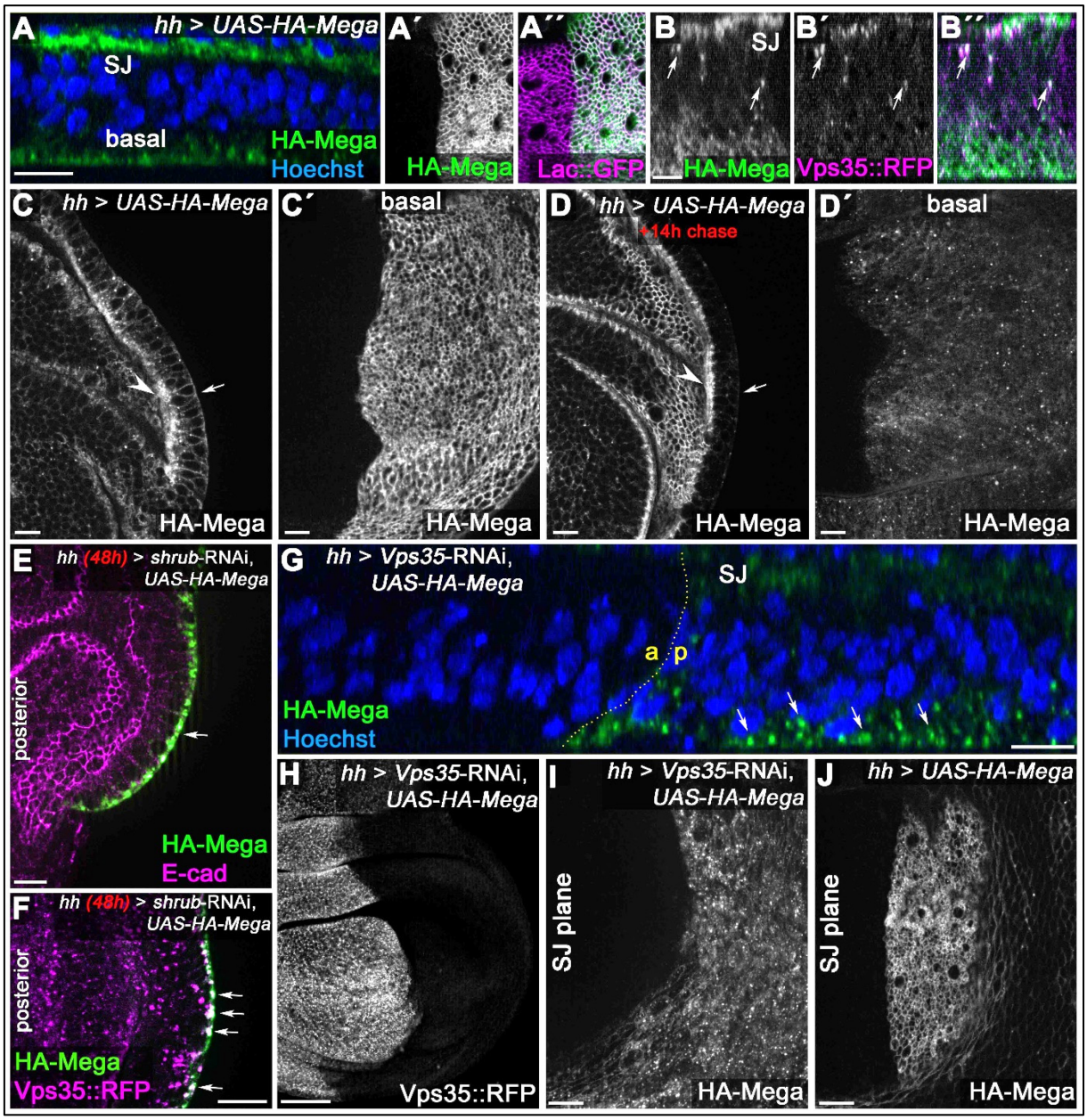

Figure 5. Basal to apical transcytosis of Mega requires ESCRT and Retromer function. (**A**) UAS-driven overexpression of HA-tagged Mega reveals a basal pool opposing the apical SJ fraction. Similarly to endogenously tagged Mega::YFP (see Fig. **3G**), HA-Mega colocalizes with the CSC along the apicobasal axis (arrows in **B**). (**C**) Continuous overexpression of HA-Mega yields a strong SJ signal (arrowhead) as well as lateral and basal (arrow) staining of HA-Mega. (**C´**) In a basal focal plane, the strong accumulation of HA-Mega in a junction like fashion at the basodistal membrane is seen. (**D**) Following a 14h chase at 18°C to halt further expression, HA-Mega signal is almost exclusively confined to the SJ (arrowhead) with very little basal staining (arrow). (**D´**) The basodistal membrane pool of HA-Mega (compare with C´) vanished after 14h chase, in line with a transient localization of HA-Mega at this membrane domain. (**E**) In Shrub depleted tissue, overexpressed HA-Mega does not reach the SJ and is found exclusively in large basal aggregates (arrow). (**F**) These basal aggregates are positive for Vps35::RFP (arrows). (**G**) Similarly, in Vps35 depleted tissue, apical SJ signal of HA-Mega is faint and vesicular accumulation in the basal cytoplasm is seen (arrows). (**H**) Knockdown efficiency of the *Vps35*-RNAi. (**I**) No distinct membrane

staining of HA-Mega is visible in the SJ plane of Vps35 depleted tissue, in contrast to HA-Mega junctional localization in wildtype tissue (**J**). Scale bar in (**B**) represents 5µm, in (**G**): 50µm and in all other panels: 10µm.

The previous experiments suggested that Mega is continuously endocytosed from the basodistal membrane to supply the SJ pool. We therefore reasoned that basodistal membrane accumulation is a short-lived intermediate step in Mega transport towards the SJ. To proof this assumption, we conducted a pulse-chase experiment using the Gal4/Galt80ts system and found that HA-Mega localization was much more confined to the SJ (similar to endogenous Mega localization) when its expression was halted for 14h after continuous expression (Fig. 5D). After this chase, the basodistal membrane pool was almost completely diminished (Fig. 5D). This is consistent with a transient localization of Mega at the basodistal membrane prior to endocytosis and subsequent targeting to SJ.

Next, we investigated the roles of ESCRT and Retromer in HA-Mega trafficking. When we expressed HA-Mega in *shrub*-RNAi tissue, it failed to reach the SJ altogether and instead was trapped within aberrant endosomal compartments in the basal cytoplasm (Fig. 5E, arrow). Colocalization with Vps35::RFP confirmed that HA-Mega accumulated in basal Retromer CSC positive compartments (Fig. 5F, arrows), consistent with the results obtained from endogenous Mega staining in *shrub*-RNAi tissue (Fig. S8F-G). When we expressed HA-Mega in CSC depleted tissue (*Vps35*-RNAi), a similar, albeit weaker trapping of HA-Mega in basally localized vesicular compartments was observed (Fig. 5G, arrows). In contrast to exclusive localization of HA-Mega in basal aggregates upon *shrub*-RNAi expression (Fig. 5F, arrows), we also detected a pool of HA-Mega at the SJ level (Fig. 5I). However, imaging the SJ plane revealed that apical HA-Mega was mostly vesicular with no apparent membrane staining (Fig. 5I). This is in strong contrast to HA-Mega localization in wildtype tissue, characterized by a distinct junctional honeycomb pattern in both the disc proper and the overlaying peripodial disc cells (Fig. 5J). This suggests that HA-Mega fails to integrate into the SJ in Retromer or ESCRT depleted wing disc cells.

Recognition of proteins by the ESCRT machinery requires cargo ubiquitination, serving as a sorting signal for the ILV pathway (Bilodeau et al., 2002; Katzmann et al., 2001; Shih et al., 2002). To test whether HA-Mega requires ubiquitination for its integration into SJ, we devised a UAS-HA-Mega construct in which all intracellular lysines (K) were changed to arginines (R) (UAS HA-Mega^{K2R}). This construct should be devoid of any potential ubiquitination, thereby preventing a possible recognition by ESCRT and sorting into the ILV pathway. However, upon expression in wing disc cells, HA-Mega^{K2R} targeting to the junctional membrane was not

impaired and the subcellular localization of the construct was indistinguishable from wildtype HA-Mega (Fig. S11). This result suggests that Mega transcytosis and SJ integration does not require ubiquitination and that direct interaction with ESCRT components and sorting into ILVs is not required during anterograde transport of Mega. The data are compatible with a model of indirect regulation of Mega trafficking by ESCRT that is based on the requirement for ESCRT function in maintaining apical localization and mobility of the Retromer CSC.

Based on above findings, we conclude that a functional endosomal system is critically required for Mega transcytosis from the basodistal to the apical membrane, which is an essential prerequisite for its delivery to the SJ. Importantly, our data indicate a crucial role for ESCRT and Retromer in a pathway that regulates anterograde trafficking of an apically localized membrane protein.

Mega translation and subsequent exit from the Golgi occurs in the basal cytoplasm

The previous experiments suggested that Mega, despite residing in apical SJs, requires crucial trafficking steps at the basodistal plasma membrane prior to its integration into the junction. We therefore wondered whether locally restricted synthesis of Mega in the basal part of the cell might account for the transient pool at the basal plasma membrane observed upon endocytosis block or Mega overexpression.

We used RNA fluorescence in situ hybridization to reveal the subcellular localization of Mega transcripts. To verify RNA probe specificity, we expressed UAS-HA-Mega using *hh*Gal4, which should strongly increase transcript abundance and consequently fluorescence signal intensity in the posterior compartment. Consistently, we found intense Mega RNA staining in the posterior compartment, confirming the specificity of our probe (Fig. 6A). We also detected some apical fluorescence signal that is notably visible in the epithelial fold of the hinge region (Fig. 6A, B, asterisk). Very likely, this fraction represents an unspecific signal from fluorophores accumulating in the extracellular space between the peripodial membrane and the disc proper, since the signal intensity did not differ between the wildtype anterior and the HA-Mega overexpressing posterior compartment (Fig. 6B, asterisk). In contrast, the specific intracellular signal representing Mega transcript was markedly increased in the posterior compartment (Fig. 6B). Strikingly, endogenous, as well as overexpressed Mega RNA, was almost exclusively detected in dotted structures residing in the basal cytoplasm (Fig. 6B, arrows and arrowheads, respectively).

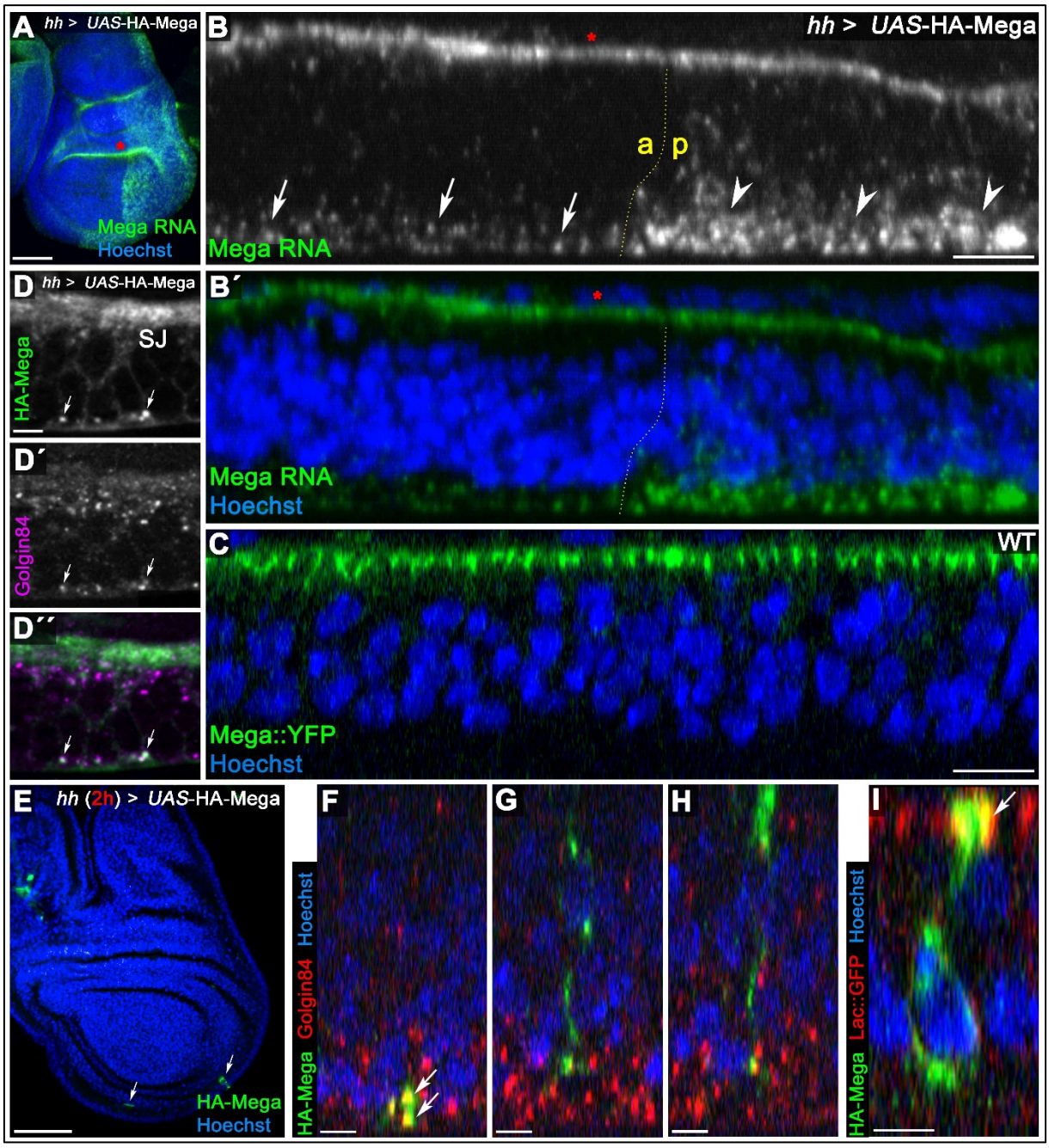

Figure 6. Mega is secreted from Golgi stacks within the basal cytoplasm. (**A**) Fluorescence *in situ* hybridization (FISH) signal from a Mega RNA probe after posterior overexpression of UAS-HA-Mega. Note the strong posterior signal, indicating probe specificity. Unspecific signal between peripodial membrane and disc proper is visible in the epithelial fold of the hinge region (red asterisks in **A** and **B**). (**B**) Mega RNA is detected primarily in the basal cytoplasm of both the wildtype and the UAS-HA-Mega overexpressing posterior compartment (arrows and arrowheads, respectively). Note the higher abundance of fluorescence signal in the posterior compartment with a subcellular localization comparable to endogenous Mega RNA within the anterior tissue. (**C**) In stark contrast to basally localized mRNA, Mega protein (Mega::YFP) localizes within the SJ at the apical pole of the cells. (**D**) Overexpressed Mega colocalizes with the Golgi resident protein Golgin84 in vesicular structures within the basal cytoplasm (arrows), consistent with basal secretion of Mega. Note the high abundance of Golgi stacks in proximity to the SJ but lack of overlap with HA-Mega in this apical region. (**E-I**) A short expression of HA-Mega for 2h

yields discs that contain single cells with detectable HA-Mega expression (arrows). (**F**) Some cells stain for HA-Mega exclusively in basal, punctate spots which overlap with Golgin84 (arrows). This is in line with initial appearance of HA-Mega at the basal cell pole during secretion from local Golgi stacks. (**G-H**) Intracellular spreading of HA-Mega along the apicobasal axis towards the SJ. (**I**) HA-Mega extensively colocalizes with Lac::GFP at the apical pole, indicating efficient SJ targeting (arrow). Scale bars in (**A, B**) represent 50µm, in (**B**), (**C**): 10µm and in all other panels: 5µm.

The basal subcellular localization of Mega RNA is in strong contrast to that of the protein, which almost exclusively localizes in SJs at the apical pole of the cells (Fig. 6C). Thus, the discrepancy in RNA and protein localization may explain the necessity for a transcytosis route from the basodistal membrane to the SJ. We reasoned that the Mega mRNA is translated basally, which may result in its initial targeting to the basodistal membrane following the passage through the Golgi. Consistent with this idea, we found robust colocalization of HA-Mega with the Golgi marker Golgin84 (Riedel et al., 2016) at the basal pole of the cells (Fig. 6D, arrows). In contrast, little colocalization was found in the apical region in proximity to the SJ. This is surprising, since the majority of Golgi stacks appeared to reside apically (Fig. 6D´). To further study the early biosynthetic trafficking of Mega, we induced a short *hh*Gal4-driven expression of UAS-HA-Mega for 2h. Only single cells within the posterior compartment showed detectable expression of HA-Mega (Fig. 6E, arrows). Strikingly, we occasionally detected cells containing exclusively basal vesicular HA-signal that overlapped with Golgin84 (Fig. 6F, arrows). Other cells showed extensive spreading of HA-Mega along the apicobasal axis and colocalization with Lac::GFP at the apical membrane, indicating integration into the SJ (Fig. 6G-I, arrow). These data are consistent with the first appearance of HA-Mega post biosynthesis in basal Golgi stacks, followed by transport to the basodistal membrane and subsequent transcytosis towards the SJ.

Together, the results suggest that basal subcellular localization of Mega mRNA supports its local translation and subsequent secretion of Mega protein from basal Golgi stacks. Thus, the transient basodistal membrane pool of Mega is a consequence of this locally restricted secretion and represents newly synthesized protein that has not yet entered the transcytosis pathway required for anterograde delivery to the SJ.

2.3 Discussion

Here, we describe a novel role of the ESCRT and Retromer machineries in regulating SJ maintenance in a proliferating epithelium, the wing disc of *Drosophila*. By studying the intracellular trafficking route of the SJ component Mega, we reveal a transcytosis-like mechanism in a basal to apical direction that delivers Mega to the junctional region and requires ESCRT and Retromer functions.

While transcytosis of SJ components has been shown to occur during the initial establishment of the SJ in the embryo (Tiklova et al., 2010), we here reveal that this mechanism is also needed during maintenance of the SJs in a rapidly proliferating epithelium. Our data expose that the Retromer CSC functions downstream of ESCRT to export Mega from the endosome. We propose a novel physiological role for the Retromer CSC in regulating membrane levels of several SJ core components. While our data suggest that Retromer fails to export Mega from aberrant endosomes induced by ESCRT depletion, the exact mechanism behind this remains to be determined.

Requirement for ESCRT function in CSC dependent endosomal retrieval of Mega

Our data reveal a critical requirement for ESCRT in a transport pathway that depends on Retromer mediated transcytosis. Defects in endosomal retrieval upon ESCRT inactivation have been previously described in other systems, such as yeast or mammalian cells and, thus, appear to represent a common feature of the pleiotropic ESCRT deficient phenotype. In yeast, the endosome-to-Golgi retrieval of the sorting receptor Vps10p and its cargo carboxypeptidase Y (CPY) depends on Retromer function (Seaman et al., 1997; Seaman et al., 1998). ESCRT mutant strains accumulate CPY in class E compartments from which retrieval to the Golgi is blocked (Babst et al., 1997; Piper et al., 1995; Raymond et al., 1992). A mammalian Retromer cargo, the mannose 6-phosphate receptor (M6PR), also failed to recycle from endosomes to the Golgi in HeLa cells depleted of TSG101/ESCRT-I function (Doyotte et al., 2005). In this study, the authors suggested that generation of class E compartments occurs at the expense of endosomal tubules (Doyotte et al., 2005). Consistently, the Retromer-associated tubulation factor SNX1 and its yeast homolog Vps5p were found on the rims of mammalian and yeast class E compartments, respectively (Doyotte et al., 2005; Seaman et al., 1998). Together with our finding of CSC accumulation on *Drosophila* class E-like compartments (Fig. 3, Fig. S8), this suggests that ESCRT deficient endosomes remain coated with Retromer components but fail to export specific cargo.

While we cannot rule out the possibility of ESCRT components directly cooperating with Retromer to form recycling tubules (note that SNX-BAR, Snx3 and Snx27 are not required for Mega transport; see Fig. S6), we favour an indirect mechanism linking ESCRT and Retromer in this transport pathway. Our analysis of the aberrant endosomal compartments induced upon Shrub depletion revealed that they are enriched in endosomal organisers such as Rab5 and Rab7, which could potentially interfere with Retromer dependent export when their activity at the limiting membrane is unrestrained (Fig. S8). While the role of Rab7 in endosomal recruitment of the CSC is well established, the necessity for Rab7 GDP/GTP cycling during Retromer dependent carrier generation is still under debate (Jia et al., 2016; Jimenez-Orgaz et al., 2018; Seaman et al., 2009). Rab7 and its GTPase-activating protein (GAP) Tbc1d5 are interaction partners of the CSC and can modulate its capability to retrieve endosomal cargo (Jia et al., 2016; Seaman et al., 2009). For example, interfering with Rab7-GTP hydrolysis by Tbc1d5 depletion yielded defects in Retromer dependent transport in HeLa cells (Jia et al., 2016). Strikingly, under these conditions, Retromer cargo was trapped in CSC coated endosomes, paralleling our observation of Mega subcellular localization upon ESCRT depletion (Jia et al., 2016). Similarly, by exposing the interplay between the CSC component Vps29, Tbc1d5 and Rab7 in adult *Drosophila* brains, the authors of a recent study reported the capability of endosomal Rab7 to interfere with Retromer CSC function *in vivo* (Ye et al., 2020). While the exact mechanism rendering Retromer dysfunctional at *Drosophila* class E compartments remains to be determined, our data support the mounting pool of evidence that ESCRT is required for multiple endosomal retrieval pathways. It is therefore likely that aspects of the pleiotropic ESCRT phenotype in metazoans stem from defective export of proteins from the endosomal system. For example, in *Drosophila*, leaky SJ could support ESCRT mediated neoplastic transformation by permitting diffusion of signalling molecules within the imaginal disc tissue.

Transcytosis as a means to provide biosynthetic delivery of SJ components

We here found that the biosynthetic delivery of Mega depends on a transcytosis-like mechanism from the basodistal to the apical plasma membrane. This long-distance transport required sequential action of endocytic (Clathrin, Dynamin, Rab5) and endosomal (ESCRT, Retromer CSC) machineries. Importantly, the finding that overexpressed HA-Mega is unable to reach the SJ in absence of Retromer and ESCRT function (Fig. 5) is in agreement with biosynthetic delivery of Mega relying on endosomal function. Therefore, although we cannot exclude the

possibility that Mega transiently passes the Golgi after endocytosis at the basodistal membrane, we favor the unconventional transcytosis model. Strikingly, while Retromer-dependent endosomal recycling has been extensively documented, only one mammalian cell culture study implicated Retromer in transcytosis from one membrane domain to another (Verges et al., 2004). Thus, SJ delivery of Mega in imaginal discs represents a novel physiological role of Retromer to study this process *in vivo*. The finding that CSC mediated anterograde transport of Mega is independent of Retromer associated sorting nexins (Fig. S6) indicates that this transcytosis pathway is distinct from many established CSC dependent routes and suggests that it may require unknown cofactors (or does not require endosomal tubulation).

Our analysis of *Vps35* clones in pupal wings or leg imaginal discs revealed that in these tissues, clones completely devoid of the SJ core component NrxIV frequently occur (Fig. S3, B′ and D′). Similarly, *shrub* mutant clones in the pupal notum were entirely lacking junctional ATPα (Roland Le Borgne, personal communication, July 2020). This is in contrast to surface levels of SJ components in *Vps35* mutant wing discs, which were consistently reduced by about 50% (Fig. 2H). This provokes the hypothesis that a parallel endosomal export pathway for SJ components may exist in wing discs that could partially compensate for loss of Retromer. However, we think this is unlikely since overexpressed HA-Mega fails to reach the SJ not only upon Shrub but also upon Vps26 depletion (Fig. 5E-J). One has to keep in mind that this experiment specifically monitors delivery of newly synthesized HA-Mega while the *Vps35* clonal analysis assesses the impact of Retromer loss of function on pre-existing SJ. Thus, in a clonal situation, a ‘thinning out’ of junctions is expected with consecutive rounds of cell division, which could explain incomplete phenotypic expressivity in wing disc *Vps35* clones. Nevertheless, it remains to be determined why in leg discs and pupal wings, SJ appear to be more sensitive towards CSC loss (Fig. S3). Pupal wing cells remodel their junctions to support a highly ordered hexagonal cell packing which may require a higher turnover of SJ components (Classen et al., 2005). Hence, distinct SJ kinetics in individual tissues may account for the varying phenotypic expressivity.

Paralleling our findings described here, a previous study showed that embryonic SJ formation depends on endocytosis and subsequent redistribution of junction components from the lateral membrane to the SJ (Tiklova et al., 2010). Thus, transcytosis of SJ components appears to serve as a universal mechanism in *Drosophila*. While we did not assess the roles of ESCRT and Retromer CSC in initial SJ formation, it is conceivable that they are already required for transporting SJ components during embryogenesis. Consistently, *shrub* mutant embryos

display a defective epithelial barrier function, suggesting they fail to form functional SJ (Dong et al., 2014).

The reason for SJ maintenance to rely on such an elaborate trafficking of its components remains to be determined. It has been suggested that SJ components form stable complexes prior to integration into the junction. A possible reason is that essential post-translational modifications of certain SJ components required for complex formation may occur exclusively at the basodistal membrane or during the passage through the endosomal system. However, the finding that Mega mRNA predominantly localizes in the basal cytoplasm (Fig. 6) provides the foundation for a more trivial hypothesis. It is widely accepted that apical and basolateral cargos undergo motif-based sorting leading to secretion towards the respective membrane domains (Stoops and Caplan, 2014). Accordingly, basal translation and exocytosis of Mega (induced by a putative basal/basolateral sorting signal) may lead to its targeting towards the basodistal membrane, despite the fact that the SJ reside apically in wing disc cells. Thus, transcytosis may serve as an adaptation for redistribution of cargos to their destined membrane domain when they are initially secreted to a different one due to early sorting signals. In wing imaginal discs, a similar transcytosis route (albeit with an apical to basal direction) has been described for the signalling molecule Wingless, which is translated apically, transiently presented at the apical membrane and finally transcytosed towards the basal membrane where it is secreted (Yamazaki et al., 2016). Thus, distinct transcytosis pathways in the wing disc epithelium provide a mechanism for targeting certain proteins to their site of action, especially when the protein is translated far away from its terminal destination.

A novel Retromer function in transport of SJ proteins

In this study, we unravel a novel physiological Retromer function in regulating surface levels of a Claudin and other structural SJ components (e.g. Nrg, ATPα, Lac, NrxIV, Cont) in several *Drosophila* tissues (Fig. 2, S3). Presently, we do not know how the SJ components are selected for this Retromer dependent pathway and whether it requires physical interaction with CSC components. Since SJ proteins may traverse the endosomal system in complex, the vast number of different components brings about a plethora of possible interaction sites. Importantly, a mass-spectrometry based study of the Mega interactome did not detect any Retromer- or associated factors but confidently found SJ core components as well as Clathrin (Jaspers et al., 2012). While the interaction mode of CSC and SJ proteins remains to be determined, our data

reflect the assumption that SJ core components represent novel putative Retromer cargos in *Drosophila*.

Strikingly, among the proteins affected by Retromer loss of function, many possess mammalian homologs (e.g. NrxIV/CNTNAP2, ATPα/ATP1A1, Nrg/NRCAM). This suggests they could represent a novel set of conserved Retromer cargos. Indeed, several lines of evidence suggest that ESCRT/Retromer mediated transport of SJ components may be evolutionary conserved from *Drosophila* to mammals. Depletion of ESCRT-I component TSG101 in mammalian epithelial cells led to a reduction of trans-epithelial resistance (TER), indicating defects in TJ mediated barrier function (Dukes et al., 2011). Additionally, Claudin-1, an essential TJ component, continuously underwent endocytosis and recycling back to the plasma membrane in several mammalian cell lines in a process requiring ESCRT function (Dukes et al., 2011).

Importantly, the mechanism behind reduced recycling and entrapment of Claudin-1 in ubiquitin-positive aberrant endosomes upon interference with ESCRT function remained elusive (Dukes et al., 2011). Thus, it is unknown how the export of Claudin-1 from the endosomal system in mammalian cells is achieved (Dukes et al., 2011).

By revealing an ESCRT dependent function of the Retromer CSC in Claudin endosomal export in *Drosophila*, our data may provide an explanation for a possibly conserved trafficking pathway of Claudins. In support of this, Claudin-1 and Claudin-4 membrane levels were significantly reduced in a mass spectrometry-based surface proteome study of Vps35 depleted human cells (Steinberg et al., 2013). Furthermore, the TJ protein Zonula occludens-2 (ZO-2) was strongly enriched in a Vps26 interactome, suggesting that a presumptive Retromer function in TJ maintenance in mammalian cells may not be limited to Claudins, similar to our findings in *Drosophila* presented here (Steinberg et al., 2013).

It remains to be determined whether a physiological role of Retromer in mammalian TJ maintenance occurs also *in vivo*. An increasing amount of tools, such as conditional *Vps35* knockout mice, will enable analysis of this putatively conserved Retromer function in mammalian systems and reveal any possible implications in development and / or disease (de Groot et al., 2013).

2.4 Materials and Methods

Drosophila Stocks and Genetics

A complete list of all stocks used in this study is found in Table 1 below. Flies were raised on standard cornmeal/molasses/yeast diet and kept at room temperature. Crossings were raised on 25°C, except for experiments containing the temperature sensitive *tubGal80ts* (McGuire et al., 2004). Those flies were kept at 18°C (permissive temperature) to inhibit Gal4/UAS-mediated expression (Brand and Perrimon, 1993) and shifted to 29°C (restrictive temperature) for specific time spans to activate UAS-based expression. Flp/FRT system (Xu and Rubin, 1993) induced clones were either generated by expression of Ubx-FLP or using hs-FLP with a 70 min heatshock at 37°C in the first instar larval stage (24-48h after egg laying).

Table 1. Flystocks

Flystock	Source / Reference / a gift from	Stockcenter Identifier (BL: Bloomington Drosophila Stock Center V: Vienna Drosophila Resource Center)
hhGal4		BL67046
tubGal80^{ts}		BL7108
UAS-p35		BL5072
UAS-shrub-RNAi	(Sweeney et al., 2006)	
Lac::GFP	Christian Klämbt	
Ubx-Flp		BL42730
hsFlp		BL8862
FRT42D 2xGFP		BL5625
FRT42D ubi-nls-RFP		BL35496
FRT42D Vps35^{MH20}		BL67202
ATPα::GFP		BL6834
NrxIV::GFP	Christian Klämbt	
Nrg::GFP		BL6844
hsFlp FRT19A ubi-nls-RFP		BL31418
Vps26^{B} FRT19A / Fm7c		BL57140
Vps35::RFP		BL66527
UAS-TSG101-RNAi		BL35710

UAS-Vps4-RNAi		V103383
Vps26-EGFP		BL67153
UAS-Chc-RNAi		V103383
UAS-Shi^{K44}		BL5811
UAS-Rab5-RNAi		V34096
UAS-HA-Mega (II) and (III)	generated for this study	
tubP-HA-Mega (II)	generated for this study	
UAS-HA-Mega^{K2R}	generated for this study	
UAS-Vps35-RNAi		BL22180
UAS-Vps26-RNAi		BL38937
enGal4		BL30564
Mega::YFP	Reinhard Schuh	
FasIII::GFP		BL59809
Vari::Dendra		
UAS-Vps39-RNAi		BL42605
Rbcn-3A-RNAi		V108547
Rab7-RNAi		V40337
Hrs^{D28} Stam^{2L2896} FRT40A / CyO	(Tognon et al., 2014)	BL56816
UAS-Hrs-RNAi		V20933
Rab7$^{GAL4-KO}$	(Chan et al., 2011)	
FRT82B ubi-nls-RFP		BL30555
Dmon1^{Mut4}	(Yousefian et al., 2013)	
FRT40A 2xGFP		BL5189
Snx27^{25} FRT19A	(Strutt et al., 2019)	
FRT42 Fam21^{KO}	(Strutt et al., 2019)	
Snx1$^{\Delta 2}$ FRT40A	(Zhang et al., 2011)	
Snx6^{1} FRT40A	(Zhang et al., 2011)	
FRT82 Snx3^{EY05688}	(Harterink et al., 2011)	

Generation of Transgenic Flies

For generation of *UAS* and *tubP* expressed HA-tagged Mega constructs, the clone LD14222 from Drosophila Genomics Resource Center (DGRC) was used as cDNA source. The HA-tag

followed by a 3xGlycin linker was fused to the N-terminus of the Mega open reading frame by PCR using the following primers:

fw-NotI-ATG-HA-3xGly-Mega

GGCGGCCGCATGTACCCATACGACGTTCCAGACTACGCTGGCGGGGGCCGCGAA CTTAACAAGCAGCAG

rev-Mega-XhoI

CTGCACTCGAGTTATATGTAGCCCTGCAGGC

The generated PCR fragment was restriction digested with NotI and XhoI enzymes (New England Biolabs) and subsequently cloned into pUAST-attB and pTUB vectors. The tubulinP-based plasmid derived from a pCaSpeR4-tubulin-QF#7 vector (addgene) with SV40 polyA 3´ UTR. The UAS-HA-Mega^{K2R} construct was designed analogous to UAS-HA-Mega with all intracellular lysines exchanged to arginines. The cDNA for this construct was synthesized by BaseClear B.V. Generation of transgenic flies was performed by attB/attP specific genomic integration into the landing sites 51C (for 2nd chromosome) and 86Fb (for 3rd chromosome) (Bischof et al., 2007). Injection of embryos was either performed in house or by BestGene Inc.

Immunohistochemistry (IHC)

A complete list of all antibodies used in this study is found in Table 2 below. Late L3 larvae or pupae were dissected in phosphate-buffered saline (PBS, pH 7.4) on ice and immediately fixed for 30 min in 4% paraformaldehyde in PBS. Following three 10 min wash steps in PBT (0.3% Triton X-100 in PBS), tissue was blocked with 5% normal goat serum (NGS, Jackson ImmunoResearch) in PBT and subsequently incubated with primary antibodies in 5% NGS in PBT for 2h. After three 15 min wash steps with PBT, discs were incubated with fluorochrome-conjugated antibodies (Alexa-488, -568, -647 from Thermo Fisher Scientific) for 2h in 5% NGS in PBT. For nuclear staining, Hoechst 33258 (Sigma Aldrich) was used at a concentration of 1:10.000. Discs or pupae were mounted in Vectashield (Vector Laboratories) and imaged with a Zeiss AxioImager Z1 wide field microscope equipped with a Zeiss Apotome. For SJ length measurements, ROIs were manually assigned with Fiji and the total length of electron dense SJ within ROIs was measured to yield a SJ length / ROI length ratio. Statistical analysis was performed with GraphPad Prism 7.0d.

Table 2. Antibodies / Reagents used for IHC

Antibody / Reagent	Source / Reference/ a gift from	Identifier	Concentration used for IHC
Shrub (rb)	Thomas Klein		1:125
Mega (m)	Reinhard Schuh (Jaspers et al., 2012)		1:50
E-cad (rat)	Developmental Studies Hybridoma Bank (DSHB)	5D3	1:50
Rab7 (m)	DSHB	Rab7	1:100
Dlg (m)	DSHB	4F3	1:500
Cora (m)	DSHB	C566.9	1:100
Vps26 (gp)	Hugo Bellen		1:1500
Chc (m)	Matthias Behr		1:50
Golgin84 (m)	DSHB	12-1	1:100
Lgl (gp)	Andreas Wodarz		1:500
Cont (gp)	Manzoor A. Bhat		1:2000
Notch (m)	DSHB	C458.2H	1:100
Hrs (gp)	Hugo Bellen		1:500
FK2 (Ubiquitin)	Enzo Life Sciences	BML-PW8810	1:100
Crb (rat)	Elisabeth Knust	Crb 2.8 rat	1:500
HA (rb)	Cell Signalling Technology	C29F4	1:1600
Rab5 (rb)	Abcam	ab31261	1:250
Fmi (m)	DSHB	#74	1:10
Hoechst 33258	Sigma Aldrich		1:10.000

Live Imaging

Late L3 instar larvae were dissected in PBS and immediately mounted on coverslips in Schneider´s Drosophila Medium (Pan Biotech). Double sided tape containing a punchhole was used both as a spacer to avoid tissue damage during mounting and as a short term imaging chamber that restricted wing disc movement. Imaging was performed with a Zeiss LSM 880 laser scanning microscope equipped with an Airyscan detector. For time series, frames were acquired in 1-4s intervals and line switching was used for dual channel acquisition.

Fluorescence Recovery After Photobleaching (FRAP)

Wing discs were mounted as described above (see Live Imaging). Photobleaching and imaging were performed on a Zeiss LSM 880 confocal microscope using a Gallium arsenide phosphide (GaAsP) detector and 40x objective with a numeric aperture of 1.2. A 15x digital zoom was applied to yield a detection area of 14.17x14.17 micron, equivalent to 512x512 pixels. In the focal plane of the junctions, a bicellular SJ ROI (0.83x0.83 microns) was bleached with 100% excitation laser intensity and 10 repeats. The laser dwell time for each pixel was 4.1µs. After bleaching, the tissue was imaged in 2min intervals for 30min and any potential drifting (x-, y-, z-axis) was corrected manually. Images were merged into a time series with Fiji and the mean gray values within the ROI were plotted against time / min (Fig. 1J). Statistical analysis was performed with Microsoft Excel and GraphPad Prism 7.0d.

Vesicle Tracking

The Fiji plugin TrackMate (Tinevez et al., 2017) was used on bleach corrected (exponential fit) time series obtained by live imaging to analyze movement of vesicles positive for either Vps26-EGFP or Vps35::RFP. A Dog detector with estimated blob diameter of 2 micron and threshold 1 were used as a fixed setup. Tracks were analyzed by the simple LAP tracker with following parameters: Linking max distance: 2. Gap closing distance: 2. Gap closing max frame gap: 20. Mean velocity was used as the parameter for comparing vesicles within wildtype and Shrub depleted tissue. Statistical analysis was performed with GraphPad Prism 7.0d.

Transmission Electron Microscopy (TEM)

Wing discs were dissected in 0.1M phosphate buffer (0.1M PO_4) on ice and immediately fixed with 2.5% glutaraldehyde in 0.1M PO_4 for 1h. Following five 5min washsteps with 0.1M PO_4, tissue was postfixed with osmium tetroxide (2% in 0.1M PO_4) for 1h on ice. After three 5min washsteps with 0.1M PO_4 and further washsteps with ddH_2O, the specimens were gently dehydrated with ethanol in concentrations ranging from 50%-100%. Acetone was used as an intermediate solvent to support Epoxy Embedding Medium (Epon, Sigma Aldrich) infiltration into the tissue. Specimens were stored over night in 100% Epon and subsequently embedded and sectioned. Semi-thin sections were stained with Richardson blue. Ultra-thin sections were contrasted with 2% uranyl acetate and lead citrate prior to imaging. Sections were analyzed with an EM 902 (Zeiss) microscope at 80 KV.

Fluorescence *in situ* Hybridization (FISH)

For generation of Mega RNA antisense probe, the Mega/Pickel cDNA containing LD14222 clone from DGRC was linearized by EcoRI digestion following T7 polymerase dependent *in vitro* transcription and digoxigenin (DIG) labelling. RNA probes were purified with a NucleoSpin Gel and PCR clean-up kit before using in the hybridization reaction. For FISH, late L3 larvae were dissected in PBS on ice and fixed for 20 minutes in 3.7% formaldehyde in PBS. Specimens were handled according to standard protocols. Briefly, larval tissue was incubated with RNA probes in formamide based hybridization buffer at 65°C over night. To detect probes, HRP-conjugated anti-DIG antibodies (Perkin Elmer) were used, followed by a tyramide signal amplification reaction (TSA plus Cyanine 3 Fluorescence Kit, Perkin Elmer). Wing discs were mounted in Vectashield (Vector Laboratories) and imaged with a Zeiss AxioImager Z1 wide field microscope equipped with a Zeiss Apotome.

Dye Penetration Assay

Late L3 larvae were dissected in PBS and briefly rinsed (30 seconds) in PBS containing 10kDa Texas-dsRed labelled Dextran (Molecular Probes D-1828) in a concentration of 1mg/ml. Following two quick wash steps in PBS, imaginal discs were dissected from the carcasses and immediately mounted in Vectashield (Vector Laboratories) on microscope slides. To avoid tissue damage due to compression, double-sided tape was used as a spacer between slide and cover slip. Images were acquired on a Zeiss AxioImager Z1 wide field microscope immediately after mounting (within a timeframe of 5 minutes).

2.5 Acknowledgements

We thank Jessica Hausmann, Stefan Kölzer and Sylvia Tannebaum for excellent technical support. We would like to thank Reinhard Schuh, Fen-Biao Gao, Christian Klämbt, David Strutt, Peter J. Cullen, Xinhua Lin, Konrad Basler, Hugo Bellen, Matthias Behr, Andreas Wodarz, Manzoor A. Bhat and Elisabeth Knust for kindly sharing fly stocks and reagents. We thank the Center for Advanced Imaging (CAi) at the Heinrich-Heine-University for technical support with microscopy and access to imaging equipment. The Bloomington Drosophila Stock Center, Vienna Drosophila Resource Center, Drosophila Genomics Resource Center and the Developmental Studies Hybridoma Bank supplied flystocks, plasmid DNA and antibodies.

2.6 Additional Information

Accompanying the graphs and statistical analyses of Fig.1, Fig. 2, Fig. 3 and Fig. S5 are following source data files, containing raw data:

Fig. 1D source data, quantification SJ density hhGal4 48h p35 shrub-RNAi ant/post

Fig. 1J source data, FRAP Lac-GFP hhGal4 48h p35 shrub-RNAi ant/post

Fig. 2H source data, membrane signal quantification WT/*Vps35* mutant clones

Fig. 3F source data, TrackMate raw data of Vps35-RFP vesicle tracking, hhGal4 48h p35 shrub-RNAi ant/post

Fig. S5 source data, quantification SJ density hhGal4 72h vps26-RNAi ant/post

2.7 Funding

The work of the TK lab was funded by the Deutsche Forschungsgemeinschaft (DFG).

2.8 Competing Interests

The authors declare no competing or financial interests.

2.9 References

Babatz, F., E. Naffin, and C. Klambt. 2018. The Drosophila Blood-Brain Barrier Adapts to Cell Growth by Unfolding of Pre-existing Septate Junctions. *Dev Cell*. 47:697-710 e693.

Babst, M., D.J. Katzmann, E.J. Estepa-Sabal, T. Meerloo, and S.D. Emr. 2002a. Escrt-III: an endosome-associated heterooligomeric protein complex required for mvb sorting. *Dev Cell*. 3:271-282.

Babst, M., D.J. Katzmann, W.B. Snyder, B. Wendland, and S.D. Emr. 2002b. Endosome-associated complex, ESCRT-II, recruits transport machinery for protein sorting at the multivesicular body. *Dev Cell*. 3:283-289.

Babst, M., T.K. Sato, L.M. Banta, and S.D. Emr. 1997. Endosomal transport function in yeast requires a novel AAA-type ATPase, Vps4p. *EMBO J*. 16:1820-1831.

Babst, M., B. Wendland, E.J. Estepa, and S.D. Emr. 1998. The Vps4p AAA ATPase regulates membrane association of a Vps protein complex required for normal endosome function. *EMBO J*. 17:2982-2993.

Bachmann, A., M. Draga, F. Grawe, and E. Knust. 2008. On the role of the MAGUK proteins encoded by Drosophila varicose during embryonic and postembryonic development. *BMC Dev Biol*. 8:55.

Baumgartner, S., J.T. Littleton, K. Broadie, M.A. Bhat, R. Harbecke, J.A. Lengyel, R. Chiquet-Ehrismann, A. Prokop, and H.J. Bellen. 1996. A Drosophila neurexin is required for septate junction and blood-nerve barrier formation and function. *Cell*. 87:1059-1068.

Behr, M., D. Riedel, and R. Schuh. 2003. The claudin-like megatrachea is essential in septate junctions for the epithelial barrier function in Drosophila. *Dev Cell*. 5:611-620.

Bilodeau, P.S., J.L. Urbanowski, S.C. Winistorfer, and R.C. Piper. 2002. The Vps27p Hse1p complex binds ubiquitin and mediates endosomal protein sorting. *Nat Cell Biol*. 4:534-539.

Bischof, J., R.K. Maeda, M. Hediger, F. Karch, and K. Basler. 2007. An optimized transgenesis system for Drosophila using germ-line-specific phiC31 integrases. *Proc Natl Acad Sci U S A*. 104:3312-3317.

Brancolini, C., D. Lazarevic, J. Rodriguez, and C. Schneider. 1997. Dismantling cell-cell contacts during apoptosis is coupled to a caspase-dependent proteolytic cleavage of beta-catenin. *J Cell Biol*. 139:759-771.

Brand, A.H., and N. Perrimon. 1993. Targeted gene expression as a means of altering cell fates and generating dominant phenotypes. *Development*. 118:401-415.

Carlton, J., M. Bujny, B.J. Peter, V.M. Oorschot, A. Rutherford, H. Mellor, J. Klumperman, H.T. McMahon, and P.J. Cullen. 2004. Sorting nexin-1 mediates tubular endosome-to-TGN transport through coincidence sensing of high- curvature membranes and 3-phosphoinositides. *Curr Biol*. 14:1791-1800.

Chan, C.C., S. Scoggin, D. Wang, S. Cherry, T. Dembo, B. Greenberg, E.J. Jin, C. Kuey, A. Lopez, S.Q. Mehta, T.J. Perkins, M. Brankatschk, A. Rothenfluh, M. Buszczak, and P.R. Hiesinger. 2011. Systematic discovery of Rab GTPases with synaptic functions in Drosophila. *Curr Biol*. 21:1704-1715.

Classen, A.K., K.I. Anderson, E. Marois, and S. Eaton. 2005. Hexagonal packing of Drosophila wing epithelial cells by the planar cell polarity pathway. *Dev Cell*. 9:805-817.

Cullen, P.J. 2008. Endosomal sorting and signalling: an emerging role for sorting nexins. *Nat Rev Mol Cell Biol*. 9:574-582.

Cullen, P.J., and F. Steinberg. 2018. To degrade or not to degrade: mechanisms and significance of endocytic recycling. *Nat Rev Mol Cell Biol*. 19:679-696.

Daniel, E., M. Daude, I. Kolotuev, K. Charish, V. Auld, and R. Le Borgne. 2018. Coordination of Septate Junctions Assembly and Completion of Cytokinesis in Proliferative Epithelial Tissues. *Curr Biol*. 28:1380-1391 e1384.

de Groot, R.E., H.F. Farin, M. Macurkova, J.H. van Es, H.C. Clevers, and H.C. Korswagen. 2013. Retromer dependent recycling of the Wnt secretion factor Wls is dispensable for stem cell maintenance in the mammalian intestinal epithelium. *PLoS One*. 8:e76971.

Dong, B., E. Hannezo, and S. Hayashi. 2014. Balance between apical membrane growth and luminal matrix resistance determines epithelial tubule shape. *Cell Rep*. 7:941-950.

Doyotte, A., M.R. Russell, C.R. Hopkins, and P.G. Woodman. 2005. Depletion of TSG101 forms a mammalian "Class E" compartment: a multicisternal early endosome with multiple sorting defects. *J Cell Sci*. 118:3003-3017.

Dukes, J.D., L. Fish, J.D. Richardson, E. Blaikley, S. Burns, C.J. Caunt, A.D. Chalmers, and P. Whitley. 2011. Functional ESCRT machinery is required for constitutive recycling of claudin-1 and maintenance of polarity in vertebrate epithelial cells. *Mol Biol Cell*. 22:3192-3205.

Dunst, S., T. Kazimiers, F. von Zadow, H. Jambor, A. Sagner, B. Brankatschk, A. Mahmoud, S. Spannl, P. Tomancak, S. Eaton, and M. Brankatschk. 2015. Endogenously tagged rab proteins: a resource to study membrane trafficking in Drosophila. *Dev Cell*. 33:351-365.

Franch-Marro, X., F. Wendler, S. Guidato, J. Griffith, A. Baena-Lopez, N. Itasaki, M.M. Maurice, and J.P. Vincent. 2008. Wingless secretion requires endosome-to-Golgi retrieval of Wntless/Evi/Sprinter by the retromer complex. *Nat Cell Biol*. 10:170-177.

Frost, A., V.M. Unger, and P. De Camilli. 2009. The BAR domain superfamily: membrane-molding macromolecules. *Cell*. 137:191-196.

Genova, J.L., and R.G. Fehon. 2003. Neuroglian, Gliotactin, and the Na+/K+ ATPase are essential for septate junction function in Drosophila. *J Cell Biol*. 161:979-989.

Gilula, N.B., D. Branton, and P. Satir. 1970. The septate junction: a structural basis for intercellular coupling. *Proc Natl Acad Sci U S A*. 67:213-220.

Gunzel, D., and A.S. Yu. 2013. Claudins and the modulation of tight junction permeability. *Physiol Rev*. 93:525-569.

Hanson, P.I., R. Roth, Y. Lin, and J.E. Heuser. 2008. Plasma membrane deformation by circular arrays of ESCRT-III protein filaments. *J Cell Biol*. 180:389-402.

Hariharan, I.K., and D. Bilder. 2006. Regulation of imaginal disc growth by tumor-suppressor genes in Drosophila. *Annu Rev Genet*. 40:335-361.

Harterink, M., F. Port, M.J. Lorenowicz, I.J. McGough, M. Silhankova, M.C. Betist, J.R.T. van Weering, R. van Heesbeen, T.C. Middelkoop, K. Basler, P.J. Cullen, and H.C. Korswagen. 2011. A SNX3-dependent retromer pathway mediates retrograde transport of the Wnt sorting receptor Wntless and is required for Wnt secretion. *Nat Cell Biol*. 13:914-923.

Hay, B.A., T. Wolff, and G.M. Rubin. 1994. Expression of baculovirus P35 prevents cell death in Drosophila. *Development*. 120:2121-2129.

Herz, H.M., Z. Chen, H. Scherr, M. Lackey, C. Bolduc, and A. Bergmann. 2006. vps25 mosaics display non-autonomous cell survival and overgrowth, and autonomous apoptosis. *Development*. 133:1871-1880.

Horazdovsky, B.F., B.A. Davies, M.N. Seaman, S.A. McLaughlin, S. Yoon, and S.D. Emr. 1997. A sorting nexin-1 homologue, Vps5p, forms a complex with Vps17p and is required for recycling the vacuolar protein-sorting receptor. *Mol Biol Cell*. 8:1529-1541.

Jaspers, M.H., K. Nolde, M. Behr, S.H. Joo, U. Plessmann, M. Nikolov, H. Urlaub, and R. Schuh. 2012. The claudin Megatrachea protein complex. *J Biol Chem*. 287:36756-36765.

Jia, D., J.S. Zhang, F. Li, J. Wang, Z. Deng, M.A. White, D.G. Osborne, C. Phillips-Krawczak, T.S. Gomez, H. Li, A. Singla, E. Burstein, D.D. Billadeau, and M.K. Rosen. 2016. Structural and mechanistic insights into regulation of the retromer coat by TBC1d5. *Nat Commun*. 7:13305.

Jimenez-Orgaz, A., A. Kvainickas, H. Nagele, J. Denner, S. Eimer, J. Dengjel, and F. Steinberg. 2018. Control of RAB7 activity and localization through the retromer-TBC1D5 complex enables RAB7-dependent mitophagy. *EMBO J*. 37:235-254.

Katzmann, D.J., M. Babst, and S.D. Emr. 2001. Ubiquitin-dependent sorting into the multivesicular body pathway requires the function of a conserved endosomal protein sorting complex, ESCRT-I. *Cell*. 106:145-155.

Koles, K., A.R. Yeh, and A.A. Rodal. 2015. Tissue-specific tagging of endogenous loci in Drosophila melanogaster. *Biol Open*. 5:83-89.

Lamb, R.S., R.E. Ward, L. Schweizer, and R.G. Fehon. 1998. Drosophila coracle, a member of the protein 4.1 superfamily, has essential structural functions in the septate junctions and developmental functions in embryonic and adult epithelial cells. *Mol Biol Cell*. 9:3505-3519.

Lauffer, B.E., C. Melero, P. Temkin, C. Lei, W. Hong, T. Kortemme, and M. von Zastrow. 2010. SNX27 mediates PDZ-directed sorting from endosomes to the plasma membrane. *J Cell Biol*. 190:565-574.

Laval, M., C. Bel, and C. Faivre-Sarrailh. 2008. The lateral mobility of cell adhesion molecules is highly restricted at septate junctions in Drosophila. *BMC Cell Biol*. 9:38.

Llimargas, M., M. Strigini, M. Katidou, D. Karagogeos, and J. Casanova. 2004. Lachesin is a component of a septate junction-based mechanism that controls tube size and epithelial integrity in the Drosophila tracheal system. *Development*. 131:181-190.

Lucas, M., D.C. Gershlick, A. Vidaurrazaga, A.L. Rojas, J.S. Bonifacino, and A. Hierro. 2016. Structural Mechanism for Cargo Recognition by the Retromer Complex. *Cell*. 167:1623-1635 e1614.

McGuire, S.E., Z. Mao, and R.L. Davis. 2004. Spatiotemporal gene expression targeting with the TARGET and gene-switch systems in Drosophila. *Sci STKE*. 2004:pl6.

Moberg, K.H., S. Schelble, S.K. Burdick, and I.K. Hariharan. 2005. Mutations in erupted, the Drosophila ortholog of mammalian tumor susceptibility gene 101, elicit non-cell-autonomous overgrowth. *Dev Cell*. 9:699-710.

Moline, M.M., C. Southern, and A. Bejsovec. 1999. Directionality of wingless protein transport influences epidermal patterning in the Drosophila embryo. *Development*. 126:4375-4384.

Nelson, K.S., M. Furuse, and G.J. Beitel. 2010. The Drosophila Claudin Kune-kune is required for septate junction organization and tracheal tube size control. *Genetics*. 185:831-839.

Nilton, A., K. Oshima, F. Zare, S. Byri, U. Nannmark, K.G. Nyberg, R.G. Fehon, and A.E. Uv. 2010. Crooked, coiled and crimpled are three Ly6-like proteins required for proper localization of septate junction components. *Development*. 137:2427-2437.

Norris, A., P. Tammineni, S. Wang, J. Gerdes, A. Murr, K.Y. Kwan, Q. Cai, and B.D. Grant. 2017. SNX-1 and RME-8 oppose the assembly of HGRS-1/ESCRT-0 degradative microdomains on endosomes. *Proc Natl Acad Sci U S A*. 114:E307-E316.

Nothwehr, S.F., S.A. Ha, and P. Bruinsma. 2000. Sorting of yeast membrane proteins into an endosome-to-Golgi pathway involves direct interaction of their cytosolic domains with Vps35p. *J Cell Biol*. 151:297-310.

Oshima, K., and R.G. Fehon. 2011. Analysis of protein dynamics within the septate junction reveals a highly stable core protein complex that does not include the basolateral polarity protein Discs large. *J Cell Sci*. 124:2861-2871.

Piper, R.C., A.A. Cooper, H. Yang, and T.H. Stevens. 1995. VPS27 controls vacuolar and endocytic traffic through a prevacuolar compartment in Saccharomyces cerevisiae. *J Cell Biol*. 131:603-617.

Pocha, S.M., T. Wassmer, C. Niehage, B. Hoflack, and E. Knust. 2011. Retromer controls epithelial cell polarity by trafficking the apical determinant Crumbs. *Curr Biol*. 21:1111-1117.

Raiborg, C., K.G. Bache, D.J. Gillooly, I.H. Madshus, E. Stang, and H. Stenmark. 2002. Hrs sorts ubiquitinated proteins into clathrin-coated microdomains of early endosomes. *Nat Cell Biol*. 4:394-398.

Raiborg, C., K.G. Bache, A. Mehlum, E. Stang, and H. Stenmark. 2001. Hrs recruits clathrin to early endosomes. *EMBO J*. 20:5008-5021.

Raymond, C.K., I. Howald-Stevenson, C.A. Vater, and T.H. Stevens. 1992. Morphological classification of the yeast vacuolar protein sorting mutants: evidence for a prevacuolar compartment in class E vps mutants. *Mol Biol Cell*. 3:1389-1402.

Riedel, F., A.K. Gillingham, C. Rosa-Ferreira, A. Galindo, and S. Munro. 2016. An antibody toolkit for the study of membrane traffic in Drosophila melanogaster. *Biol Open*. 5:987-992.

Saksena, S., J. Wahlman, D. Teis, A.E. Johnson, and S.D. Emr. 2009. Functional reconstitution of ESCRT-III assembly and disassembly. *Cell*. 136:97-109.

Seaman, M.N., M.E. Harbour, D. Tattersall, E. Read, and N. Bright. 2009. Membrane recruitment of the cargo-selective retromer subcomplex is catalysed by the small GTPase Rab7 and inhibited by the Rab-GAP TBC1D5. *J Cell Sci*. 122:2371-2382.

Seaman, M.N., E.G. Marcusson, J.L. Cereghino, and S.D. Emr. 1997. Endosome to Golgi retrieval of the vacuolar protein sorting receptor, Vps10p, requires the function of the VPS29, VPS30, and VPS35 gene products. *J Cell Biol*. 137:79-92.

Seaman, M.N., J.M. McCaffery, and S.D. Emr. 1998. A membrane coat complex essential for endosome-to-Golgi retrograde transport in yeast. *J Cell Biol*. 142:665-681.

Shih, S.C., D.J. Katzmann, J.D. Schnell, M. Sutanto, S.D. Emr, and L. Hicke. 2002. Epsins and Vps27p/Hrs contain ubiquitin-binding domains that function in receptor endocytosis. *Nat Cell Biol*. 4:389-393.

Steinberg, F., M. Gallon, M. Winfield, E.C. Thomas, A.J. Bell, K.J. Heesom, J.M. Tavare, and P.J. Cullen. 2013. A global analysis of SNX27-retromer assembly and cargo specificity reveals a function in glucose and metal ion transport. *Nat Cell Biol*. 15:461-471.

Steinhusen, U., J. Weiske, V. Badock, R. Tauber, K. Bommert, and O. Huber. 2001. Cleavage and shedding of E-cadherin after induction of apoptosis. *J Biol Chem*. 276:4972-4980.

Stoops, E.H., and M.J. Caplan. 2014. Trafficking to the apical and basolateral membranes in polarized epithelial cells. *J Am Soc Nephrol*. 25:1375-1386.

Strutt, H., P.F. Langton, N. Pearson, K.J. McMillan, D. Strutt, and P.J. Cullen. 2019. Retromer Controls Planar Polarity Protein Levels and Asymmetric Localization at Intercellular Junctions. *Curr Biol*. 29:484-491 e486.

Stuffers, S., C. Sem Wegner, H. Stenmark, and A. Brech. 2009. Multivesicular endosome biogenesis in the absence of ESCRTs. *Traffic*. 10:925-937.

Sweeney, N.T., J.E. Brenman, Y.N. Jan, and F.B. Gao. 2006. The coiled-coil protein shrub controls neuronal morphogenesis in Drosophila. *Curr Biol*. 16:1006-1011.

Teis, D., S. Saksena, and S.D. Emr. 2008. Ordered assembly of the ESCRT-III complex on endosomes is required to sequester cargo during MVB formation. *Dev Cell*. 15:578-589.

Tempesta, C., A. Hijazi, B. Moussian, and F. Roch. 2017. Boudin trafficking reveals the dynamic internalisation of specific septate junction components in Drosophila. *PLoS One*. 12:e0185897.

Thompson, B.J., J. Mathieu, H.H. Sung, E. Loeser, P. Rorth, and S.M. Cohen. 2005. Tumor suppressor properties of the ESCRT-II complex component Vps25 in Drosophila. *Dev Cell*. 9:711-720.

Tiklova, K., K.A. Senti, S. Wang, A. Graslund, and C. Samakovlis. 2010. Epithelial septate junction assembly relies on melanotransferrin iron binding and endocytosis in Drosophila. *Nat Cell Biol*. 12:1071-1077.

Tinevez, J.Y., N. Perry, J. Schindelin, G.M. Hoopes, G.D. Reynolds, E. Laplantine, S.Y. Bednarek, S.L. Shorte, and K.W. Eliceiri. 2017. TrackMate: An open and extensible platform for single-particle tracking. *Methods*. 115:80-90.

Tognon, E., N. Wollscheid, K. Cortese, C. Tacchetti, and T. Vaccari. 2014. ESCRT-0 is not required for ectopic Notch activation and tumor suppression in Drosophila. *PLoS One*. 9:e93987.

Vaccari, T., and D. Bilder. 2005. The Drosophila tumor suppressor vps25 prevents nonautonomous overproliferation by regulating notch trafficking. *Dev Cell*. 9:687-698.

Vaccari, T., T.E. Rusten, L. Menut, I.P. Nezis, A. Brech, H. Stenmark, and D. Bilder. 2009. Comparative analysis of ESCRT-I, ESCRT-II and ESCRT-III function in Drosophila by efficient isolation of ESCRT mutants. *J Cell Sci*. 122:2413-2423.

Verges, M., F. Luton, C. Gruber, F. Tiemann, L.G. Reinders, L. Huang, A.L. Burlingame, C.R. Haft, and K.E. Mostov. 2004. The mammalian retromer regulates transcytosis of the polymeric immunoglobulin receptor. *Nat Cell Biol*. 6:763-769.

Wang, S., K.L. Tan, M.A. Agosto, B. Xiong, S. Yamamoto, H. Sandoval, M. Jaiswal, V. Bayat, K. Zhang, W.L. Charng, G. David, L. Duraine, K. Venkatachalam, T.G. Wensel, and H.J. Bellen. 2014. The retromer complex is required for rhodopsin recycling and its loss leads to photoreceptor degeneration. *PLoS Biol*. 12:e1001847.

Wollert, T., C. Wunder, J. Lippincott-Schwartz, and J.H. Hurley. 2009. Membrane scission by the ESCRT-III complex. *Nature*. 458:172-177.

Woods, D.F., and P.J. Bryant. 1991. The discs-large tumor suppressor gene of Drosophila encodes a guanylate kinase homolog localized at septate junctions. *Cell*. 66:451-464.

Woods, D.F., C. Hough, D. Peel, G. Callaini, and P.J. Bryant. 1996. Dlg protein is required for junction structure, cell polarity, and proliferation control in Drosophila epithelia. *J Cell Biol*. 134:1469-1482.

Wu, V.M., J. Schulte, A. Hirschi, U. Tepass, and G.J. Beitel. 2004. Sinuous is a Drosophila claudin required for septate junction organization and epithelial tube size control. *J Cell Biol*. 164:313-323.

Wu, V.M., M.H. Yu, R. Paik, S. Banerjee, Z. Liang, S.M. Paul, M.A. Bhat, and G.J. Beitel. 2007. Drosophila Varicose, a member of a new subgroup of basolateral MAGUKs, is required for septate junctions and tracheal morphogenesis. *Development*. 134:999-1009.

Xu, T., and G.M. Rubin. 1993. Analysis of genetic mosaics in developing and adult Drosophila tissues. *Development*. 117:1223-1237.

Yamazaki, Y., L. Palmer, C. Alexandre, S. Kakugawa, K. Beckett, I. Gaugue, R.H. Palmer, and J.P. Vincent. 2016. Godzilla-dependent transcytosis promotes Wingless signalling in Drosophila wing imaginal discs. *Nat Cell Biol*. 18:451-457.

Yan, Y., N. Denef, and T. Schupbach. 2009. The vacuolar proton pump, V-ATPase, is required for notch signaling and endosomal trafficking in Drosophila. *Dev Cell*. 17:387-402.

Ye, H., S.A. Ojelade, D. Li-Kroeger, Z. Zuo, L. Wang, Y. Li, J.Y. Gu, U. Tepass, A.A. Rodal, H.J. Bellen, and J.M. Shulman. 2020. Retromer subunit, VPS29, regulates synaptic transmission and is required for endolysosomal function in the aging brain. *Elife*. 9.

Yousefian, J., T. Troost, F. Grawe, T. Sasamura, M. Fortini, and T. Klein. 2013. Dmon1 controls recruitment of Rab7 to maturing endosomes in Drosophila. *J Cell Sci*. 126:1583-1594.

Zhang, P., Y. Wu, T.Y. Belenkaya, and X. Lin. 2011. SNX3 controls Wingless/Wnt secretion through regulating retromer-dependent recycling of Wntless. *Cell Res*. 21:1677-1690.

2.10 Supplementary Information

The ESCRT Machinery regulates Retromer dependent Transcytosis of Septate Junction Components in *Drosophila*

Hendrik Pannen[1], Tim Rapp[1] and Thomas Klein[1*]

[1]Institute of Genetics, Heinrich-Heine-Universität Düsseldorf, Düsseldorf, Germany

[*]Author for correspondence (Thomas.klein@hhu.de)

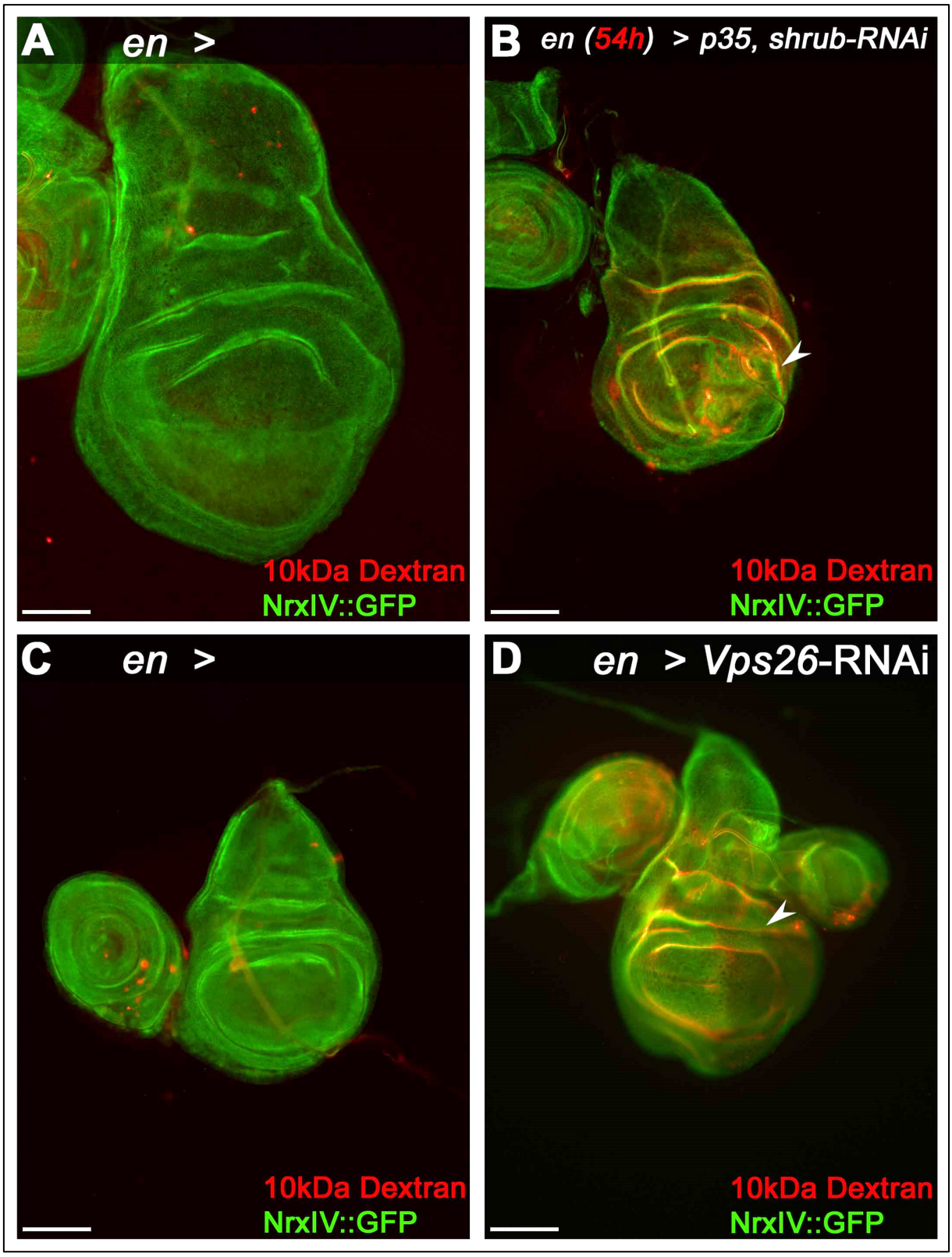

Figure S1. Epithelial barrier function is compromised in Shrub or Vps26 depleted wing disc tissue. (**A**) Control wing disc expressing *engrailed (en)*-Gal4 and Nrx::IV after incubation with dsRed-labeled 10kDa Dextran. Note the faint red staining indicative of Dextran penetration into the tissue. (**B**) Dextran accumulates in epithelial folds of a wing disc depleted of Shrub in the posterior compartment (arrowhead). (**C**) Control disc without RNAi expression and (**D**) after Vps26 depletion. Note the reduced NrxIV::GFP signal in the Vps26

depleted posterior compartment in (**D**), accompanied by Dextran infiltration of the tissue (arrowhead). Scale bars in all panels represent 100µm.

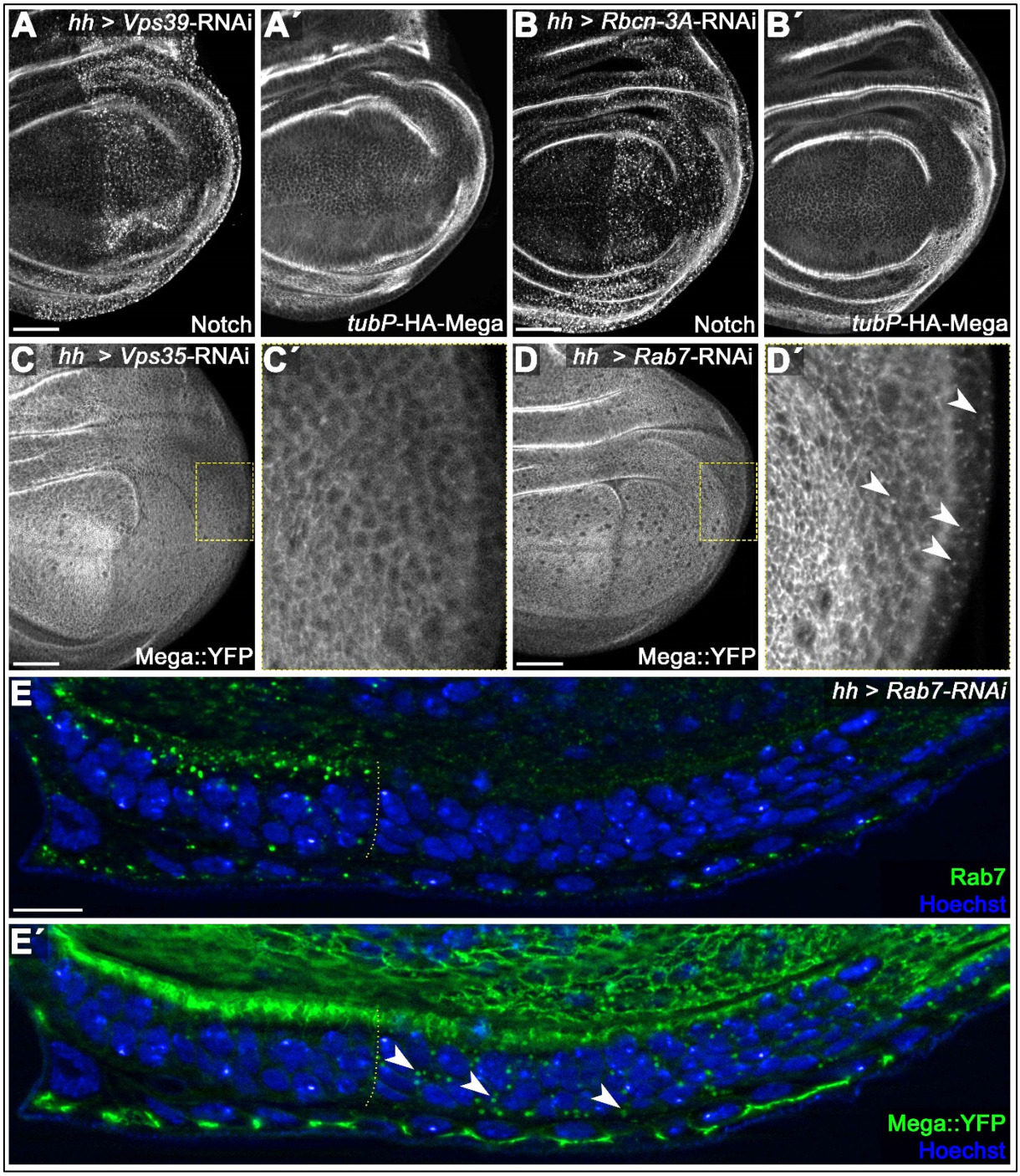

Figure S2. Mega is not target of lysosomal degradation under steady-state conditions. (**A**) Posterior knockdown of the HOPS (homotypic fusion and vacuole protein) complex component Vps39 required for endosome-lysosome fusion. Cargo destined for lysosomal degradation such as the Notch receptor (**A**) accumulates in a punctate pattern upon Vps39 depletion due to failure of endosome-lysosome fusion. (**A´**) In contrast, a *tubulin*-Promotor expressed HA-Mega construct (*tubP*-HA-Mega) that faithfully recapitulates endogenous Mega localization is unaffected by *Vps39*-RNAi expression. This indicates that HA-Mega is not undergoing lysosomal degradation under steady-state condition. (**B**) Similarly, impeding endolysosomal function by expressing an RNAi

against Rabconnectin-3A (Rbcn-3A) accumulates Notch in the posterior Rbcn-3A depleted tissue (**B**), while HA-Mega retains a wildtype localization throughout the disc. Rbcn-3A is a regulator of the vacuolar proton pump (V-ATPase) required for endolysosomal acidification (Yan et al., 2009). (**C**) Depletion of Vps35 reduces Mega::YFP levels within the tissue and little vesicular signal is seen (inset, **C´**). (**D**) In contrast, Mega::YFP levels are only mildly affected by Rab7 depletion but strong vesicular accumulation is seen (arrowheads in **D´**). (**E**) Lateral view of a wing disc expressing *Rab7*-RNAi in the posterior compartment. (**E**) Rab7 depletion is effective. (**E´**) Mega::YFP signal at the SJ is slightly reduced in the posterior compartment and vesicular accumulation is apparent (arrowheads). Rab7 activity is required for both endosome-lysosome fusion as well as for partial recruitment of CSC to endosomes of imaginal discs (see Fig. S5). Thus, Rab7 knockdown simultaneously impedes Retromer trafficking and lysosomal degradation. These data are entirely consistent with Mega being targeted for lysosomal degradation only when Retromer CSC function is compromised. Scale bars in all panels represent 50µm except for (**E)**: 10µm.

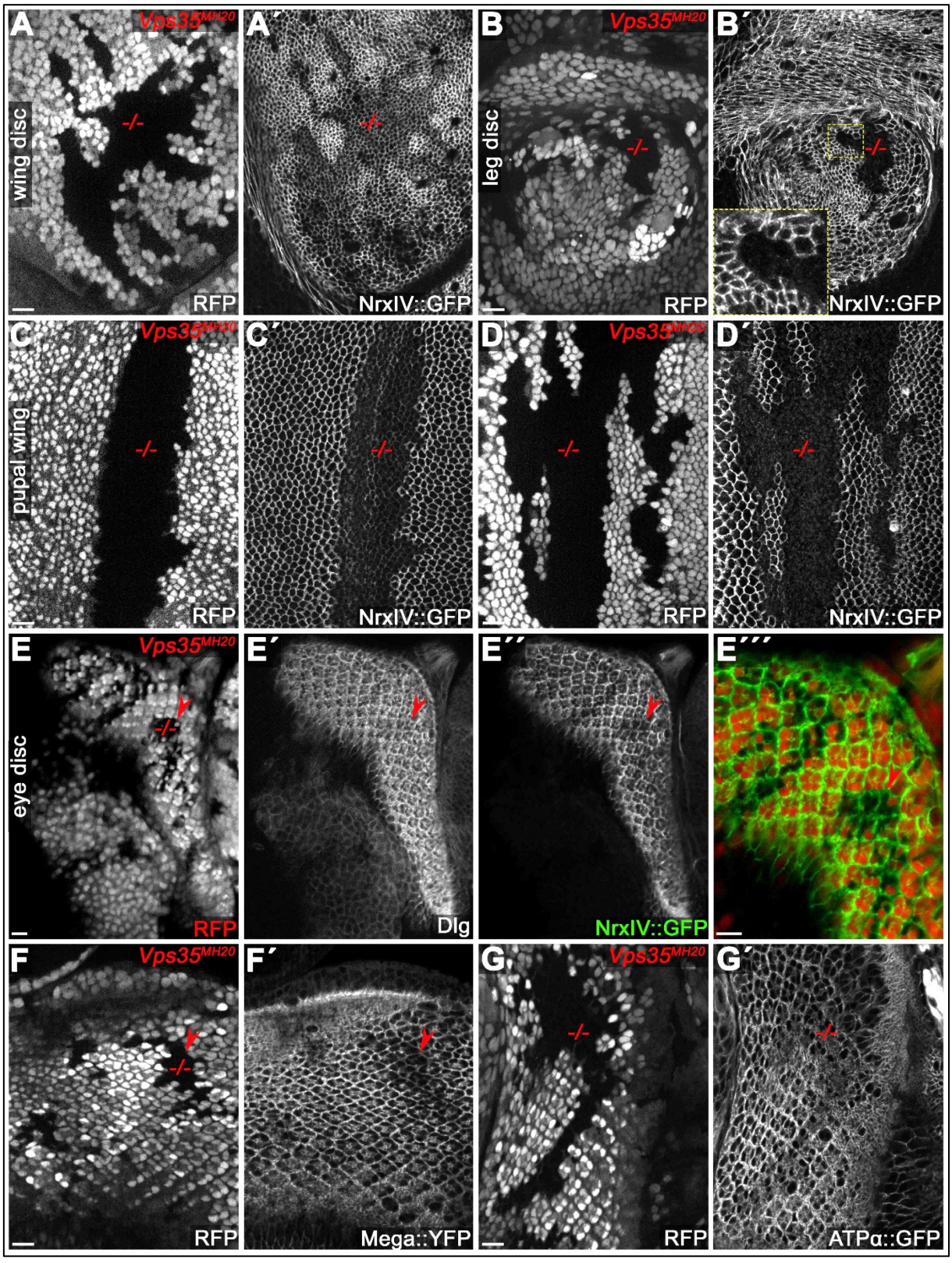

Figure S3. Retromer CSC dependent transport of SJ components is conserved throughout tissues. (**A**) Wing imaginal disc containing *Vps35*^{MH20} clones. Clones in all panels are marked by the absence of RFP. (**A´**) NrxIV::GFP is reduced within the clonal area. (**B**) Leg imaginal disc containing *Vps35*^{MH20} clones showing stronger loss of NrxIV::GFP from the SJ. Note the complete absence of junctional NrxIV::GFP in this clone compared to modestly reduced levels in the wing disc clone (**A´**). (**C-D**) *Vps35*^{MH20} clones in pupal wings. Note

the variable expressivity of the NrxIV::GFP phenotype within the clones, ranging from still detectable junctional levels (**C´**) to complete loss of NrxIV::GFP from the junction (**D´**). (**E-G**) *Vps35*^{MH20} clones in eye imaginal discs. Similar to wing imaginal discs (see Fig. 2), Dlg levels are not affected by *Vps35* loss whereas NrxIV::GFP shows reduced membrane levels (compare arrowheads in **E´** and **E´´**). (**F-G**) Similar to NrxIV::GFP, Mega::YFP (**F´**) as well as ATPα::GFP (**G´**) display reduced membrane levels within *Vps35*^{MH20} clones. Scale bars in all panels represent 10µm.

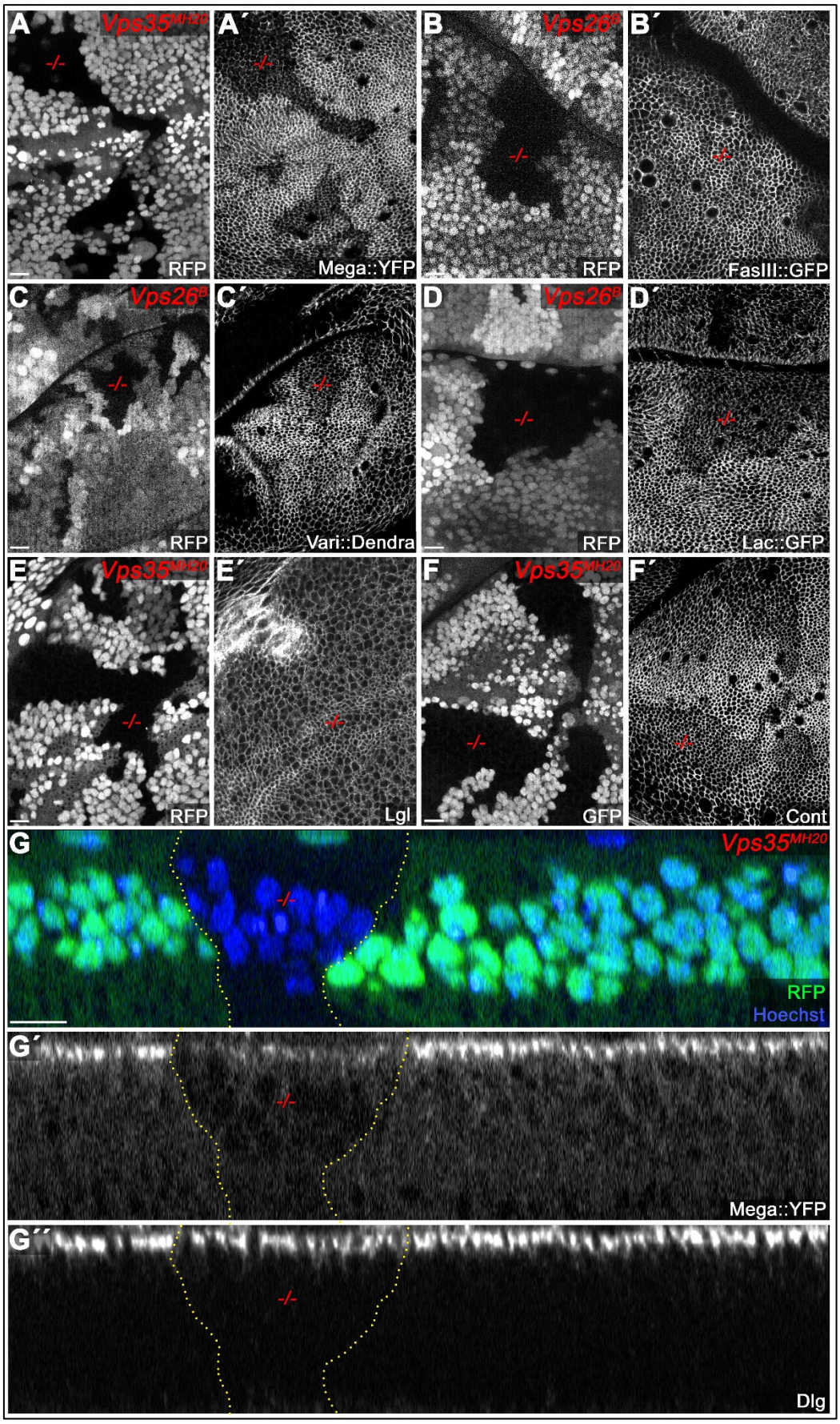

Figure S4. Analysis of further SJ components in Retromer CSC mutant clones. (**A**) Endogenously tagged Mega::YFP recapitulates reduction of Mega membrane levels within *Vps35*^{MH20} tissue detected by antibody

staining (see also Figure 2A). (**B**) FasIII::GFP membrane levels remain wildtype within *Vps26^{B}* mutant clones. (**C-D**) Endogenously tagged Varicose (**C**) and Lachesin (**D**) membrane levels are reduced within *Vps26^{B}* mutant tissue. (**E**) The basolateral cell polarity protein Lethal giant larvae (Lgl) retains a wildtype localization in *Vps35^{MH20}* mutant clones. (**F**) Contactin (Cont) membrane levels are reduced within *Vps35^{MH20}* tissue. (**G**) Optical section of a wing disc containing a *Vps35^{MH20}* mutant clone. (**G´**) Mega::YFP signal at the SJ and throughout the tissue is reduced in the *Vps35^{MH20}* clone. (**G´´**) In contrast to Mega::YFP, apical Dlg signal at the SJ retains wildtype levels in the Retromer mutant clone. Scale bars in all panels represent 10µm.

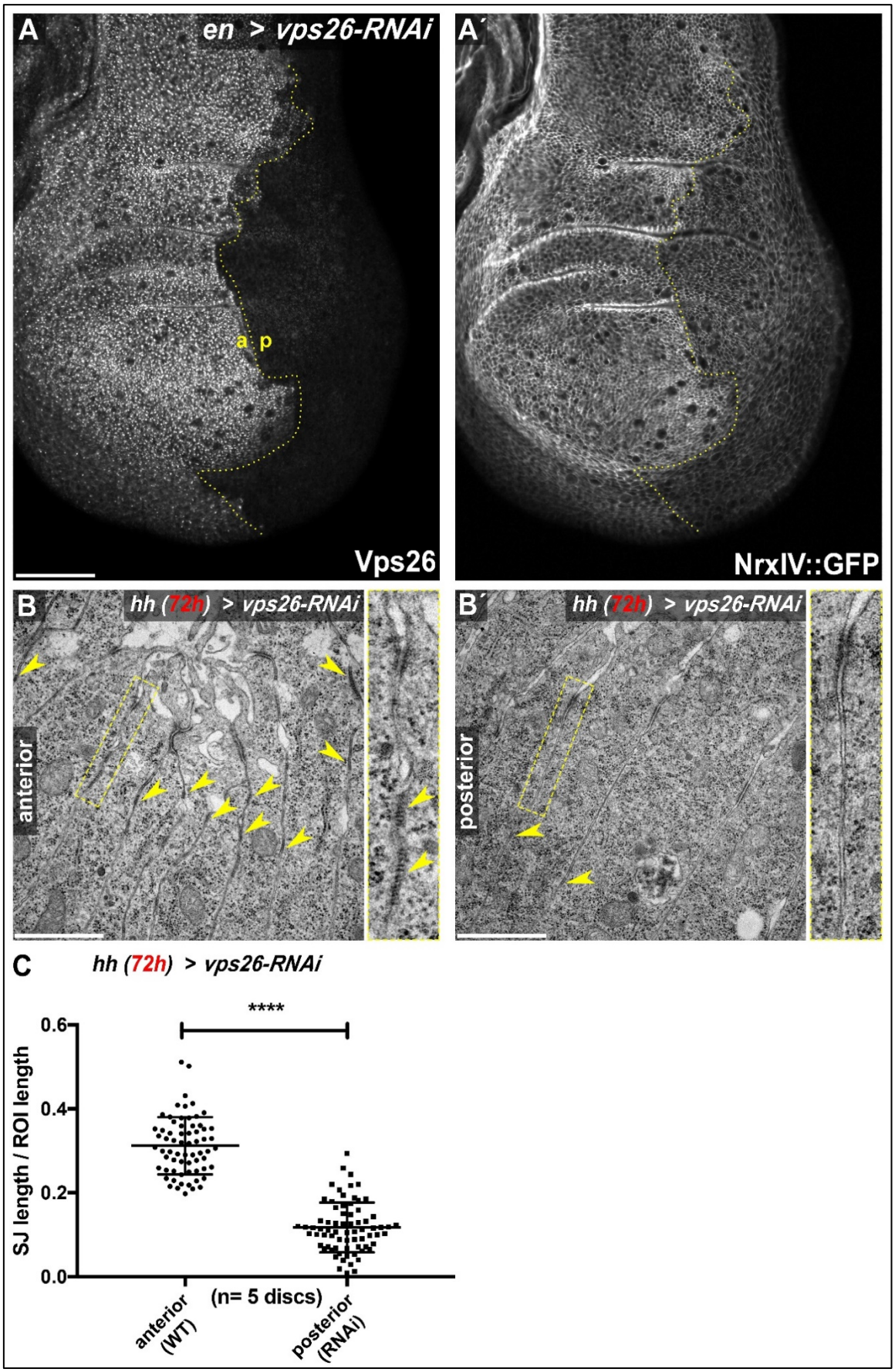

Figure S5. Retromer CSC function is required for SJ integrity. (**A**) RNAi-mediated depletion of Vps26 in the posterior compartment of wing imaginal discs efficiently reduces Vps26 (**A**) and junctional NrxIV::GFP levels

(**A´**). (**B**) TEM analysis of junctions in control (**B**) and Vps26 depleted (**B´**) wing imaginal disc tissue. Expression of *Vps26-RNAi* was restricted to 72h, since continuous *hh*Gal4-driven expression yielded discs with high levels of apoptotic cells, hampering analysis of the junctions. Note the high density of septa in the anterior control compartment compared to the Vps26 depleted posterior compartment (arrowheads in **B** and **B´**, respectively). (**C**) Quantification of electron dense SJ in 2µm ROIs (basal to the AJ) along the juxtaposed membranes. Each data point represents total SJ length within one single ROI. Note that while approximately 30% of ROI length within anterior control compartments is occupied by SJ, the SJ length / ROI length ratio is reduced to about 12% in posterior *Vps26-RNAi* compartments , indicating a reduction of SJ by about 60%. The significance level **** represents a p-value < 0.0001. Scale bar in (**A**) represents 50µm and in (**B**): 0.5µm.

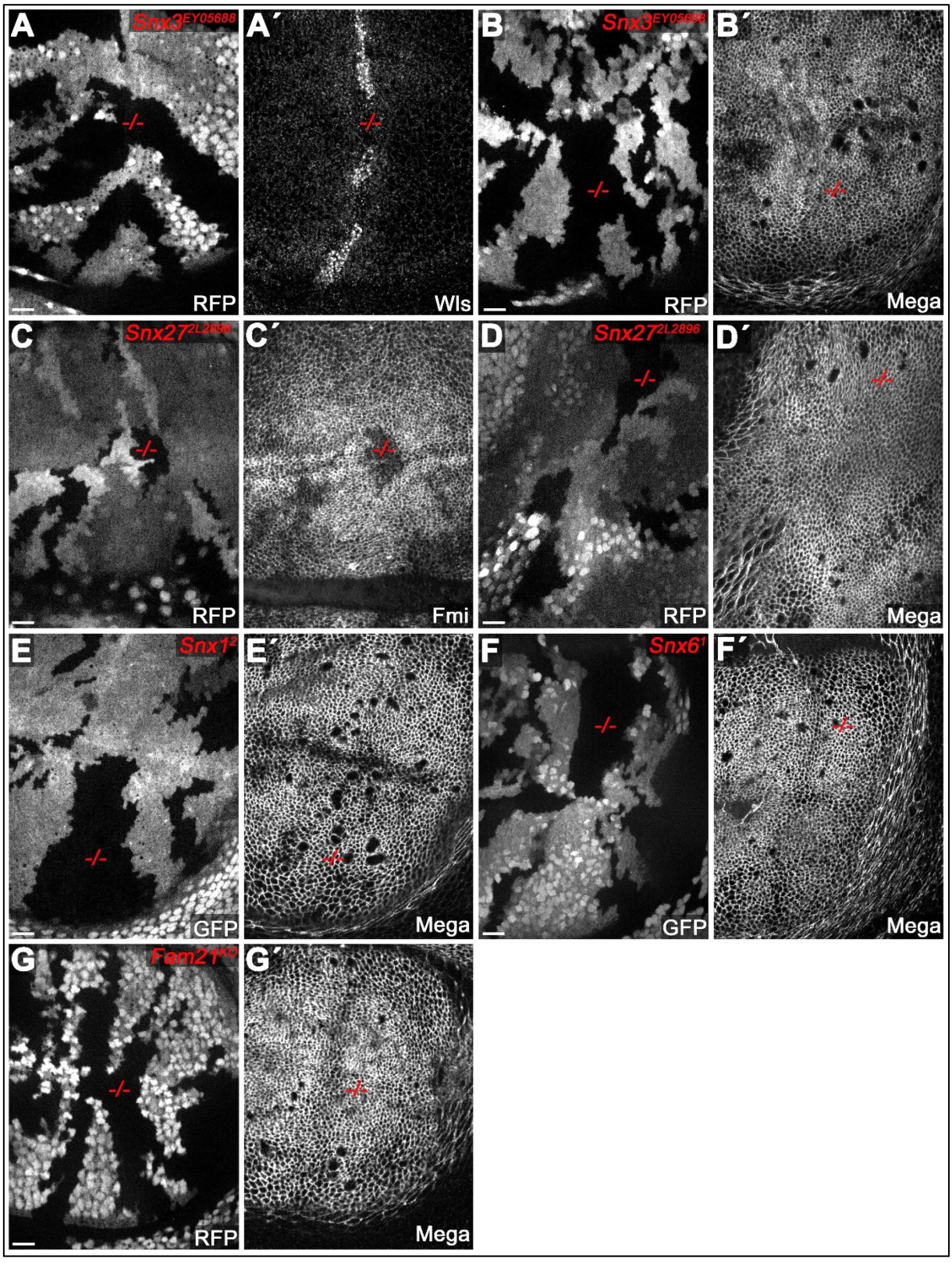

Figure S6. Retromer CSC associated sorting nexins (Snx) are not required for SJ delivery of Mega. (**A-F**) Null mutant clones of Snx family genes in wing imaginal discs, marked by absence of either RFP or GFP. (**A-B**) Null mutant clone of *Snx3* affects levels of the control cargo Wntless (Wls) (Harterink et al., 2011). (**A´**) while Mega retains a wildtype junctional level (**B´**). Mutant clones of *Snx27* affect apical levels of the control cargo Flamingo (Fmi) (Strutt et al., 2019) (**C´**) but not that of Mega (**D´**). Mutant clones of SNX-Bar family genes *Snx1*

(**E**) and *Snx6* (**F**) (Zhang et al., 2011) do not affect junctional levels of Mega. (**G**) Mega membrane levels are wildtype in clones mutant for the WASH (WASP and SCAR Homolog complex) complex component Fam21 (Family with sequence similarity 21) (Strutt et al., 2019). Scale bars in all panels represent 10µm.

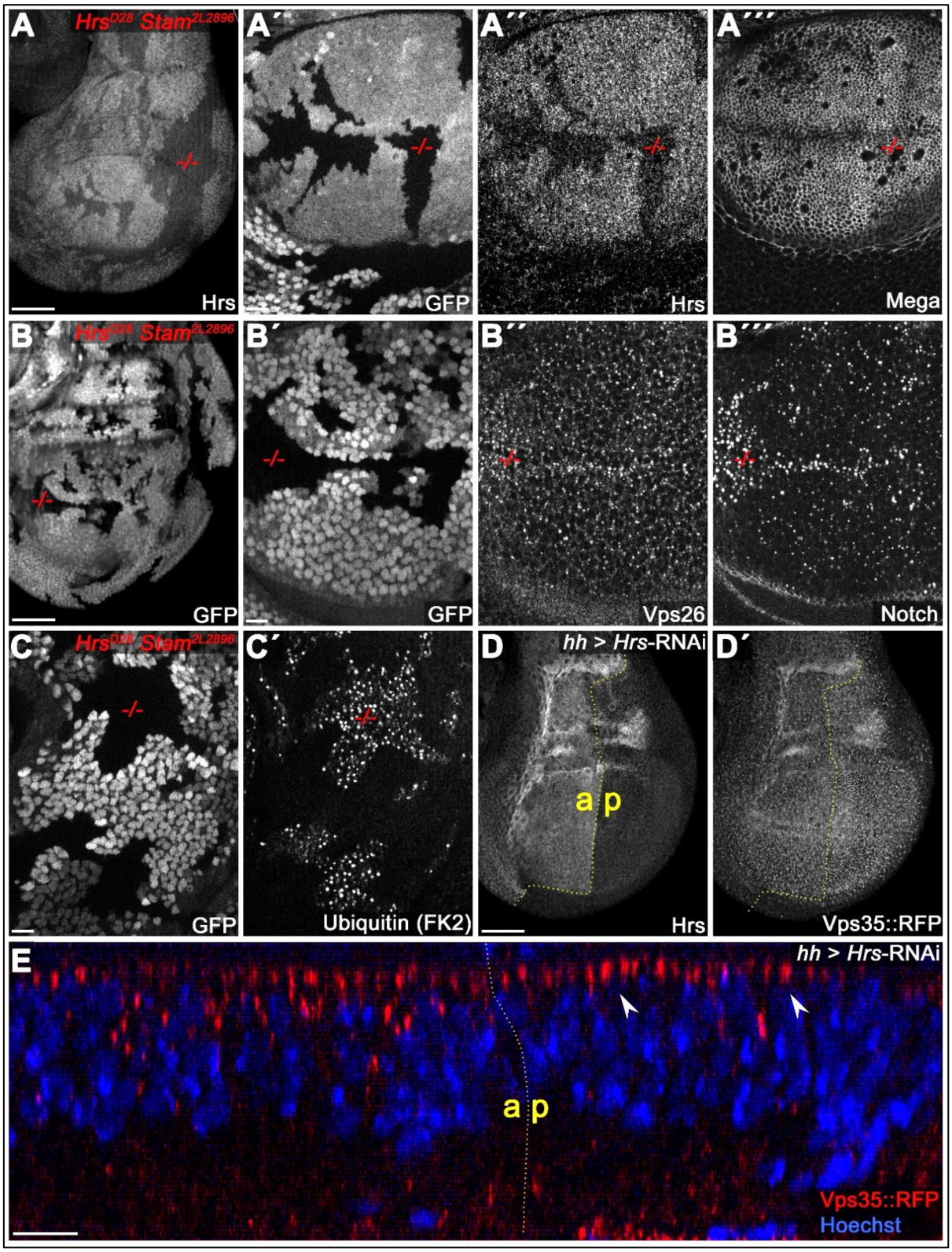

Figure S7. ESCRT-0 is not required for SJ delivery of Mega. (**A**) *Hrs*, *Stam* double mutant clones (marked by the absence of GFP). (**A´´**) Reduction of Hrs within the clonal tissue. (**A´´´**) Mega retains a wildtype membrane

level in *Hrs*, *Stam* tissue. (**B**) Notch accumulates in ESCRT-0 deficient clones (**B´´**) while Vps26 vesicular localization is largely unaffected (**B´**). (**C**) Ubiquitinated cargo fails to degrade in *Hrs*, *Stam* clones. (**D-E**) Knockdown of Hrs in the posterior compartment does not affect Vps35::RFP levels or subcellular localization. Note the intact apical hub in an optical section (arrowheads in **E**). Scale bars in (**A**, **B**, **D**) represent 50µm, in all other panels: 10µm.

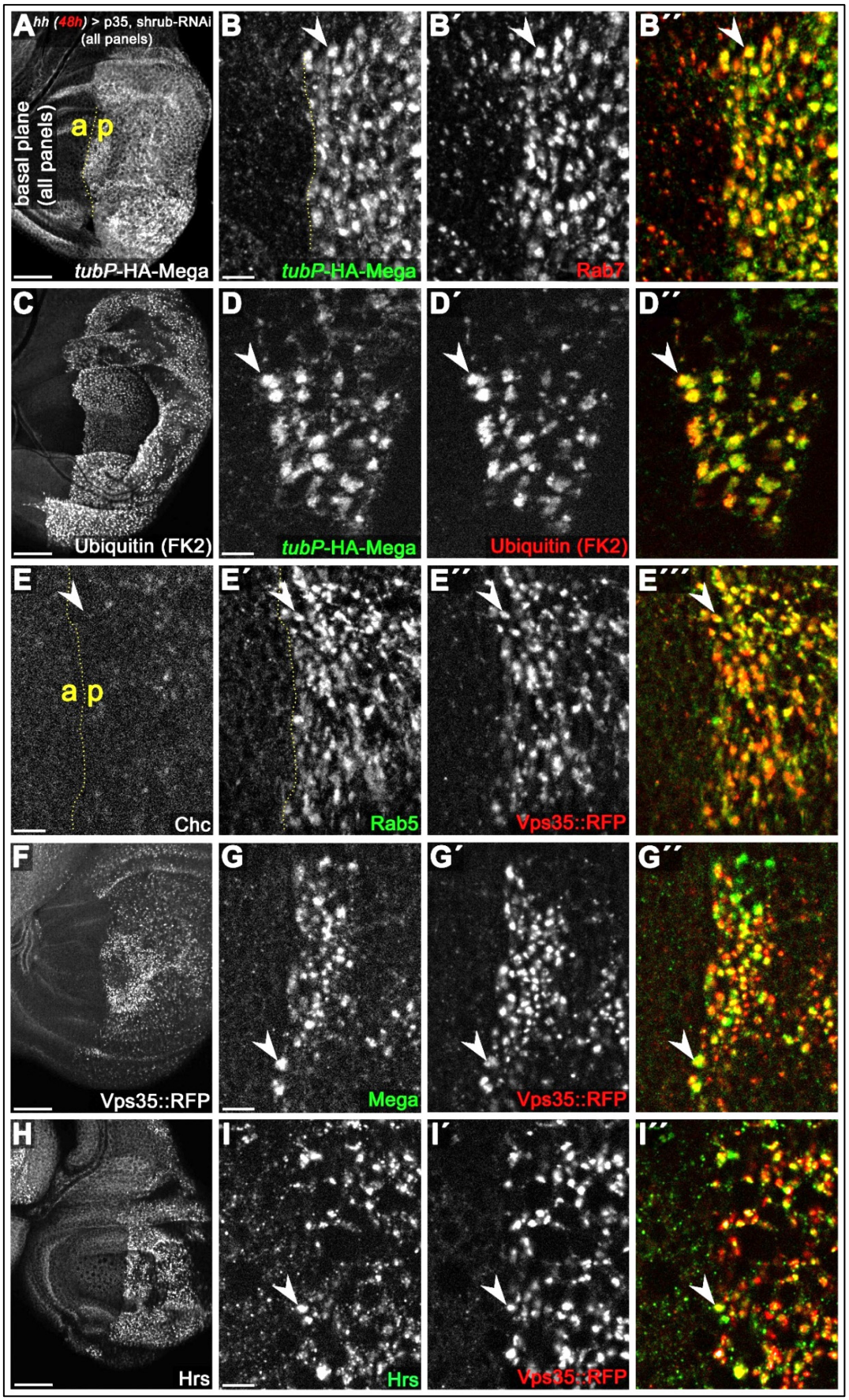

Figure S8. Characterization of basal 'class E like' endosomal compartments induced by Shrub depletion. All panels show basal planes of wing discs expressing *p35, shrub-RNAi* for 48h under control of *hh*Gal4. (**A-B**) In

posterior Shrub depleted compartments, *tubP*-HA-Mega accumulates in basal aberrant endosomes which label positive for Rab7 (arrowheads). (**C-D**) *tubP*-HA-Mega overlaps with ubiquitin at basal aggregates (arrowheads), indicating that these contain large amounts of degradative cargo. (**E**) Basal aggregates are coated with Rab5 and Vps35::RFP but lack clathrin (arrowheads). (**F-G**) Mega and Vps35::RFP largely overlap within basal compartments. (**H-I**) ESCRT-0 component Hrs accumulates on basal aberrant endosomes (arrowheads). Scale bars in (**A**, **C**, **F, H**) represent 50µm, in all other panels: 10µm.

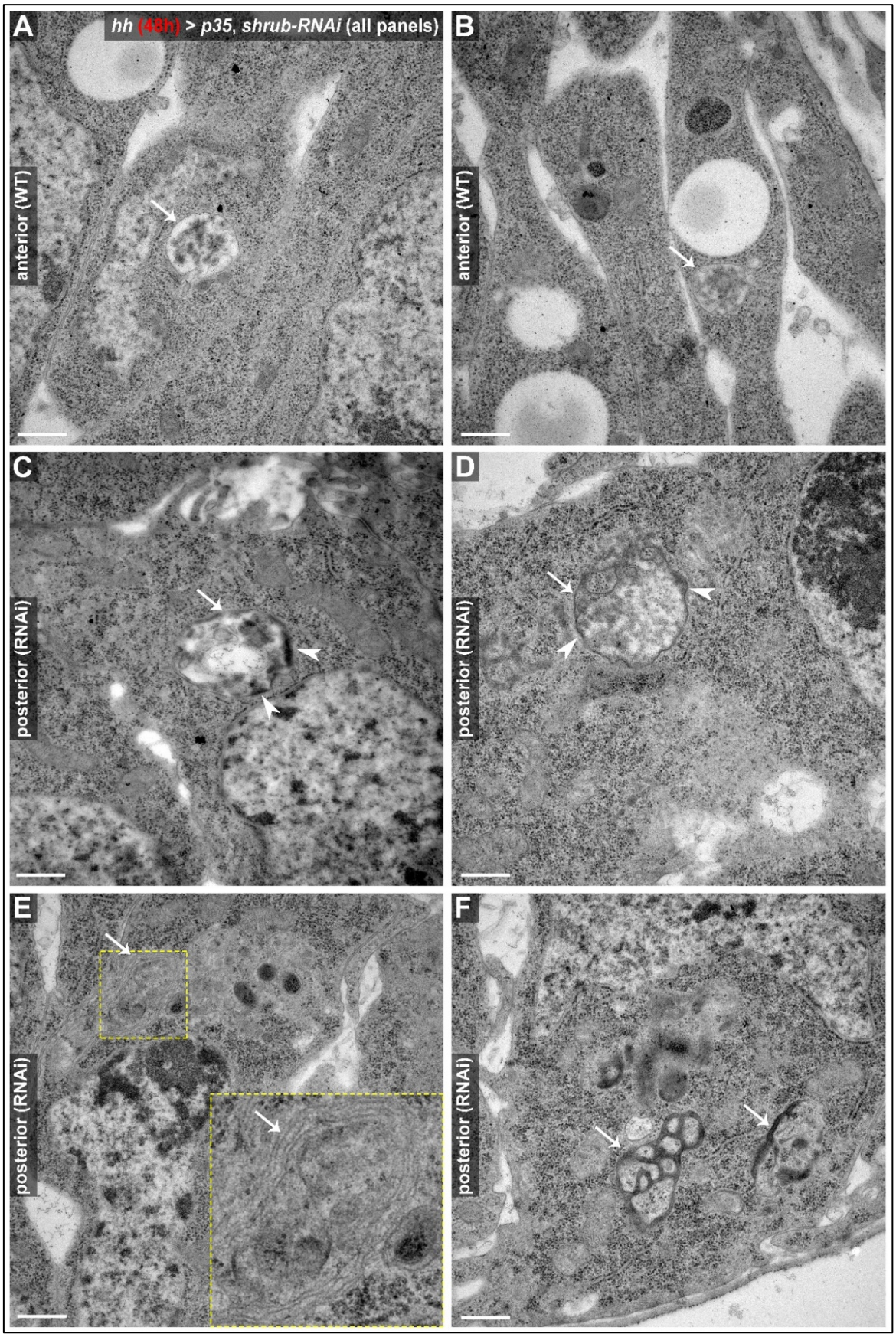

Figure S9. TEM analysis of aberrant endosomal compartments induced by 48h of Shrub depletion. All panels show electron micrographs of wing disc cells in either wildtype anterior control compartments (**A, B**) or

posterior (p35, *shrub*-RNAi) expressing compartments (**C-F**). (**A, B**) In control compartments, endosomes appear as stereotypical, spherical shaped MVBs containing electron dense ILVs (arrows). (**C-D**) In contrast, MVB-like compartments induced by Shrub depletion appear enlarged and irregularly shaped (arrows). Note that the limiting membrane of the endosome is lined with patches of electron-dense material (arrowheads), which could be aggregating endosomal machineries and / or cargo proteins failing to get retrieved or internalized. (**E**) Multicisternal endosomal structure with a stacked membrane morphology (arrow), reminiscent of class E compartments in mammalian cells (Doyotte et al., 2005). (**F**) Aberrant, electron dense endosomal compartments (arrows) in proximity to the basal membrane. These structures likely correlate with the basal endosomal aggregates characterized in Fig. S8 above. Scale bars in all panels represent 0.5µm.

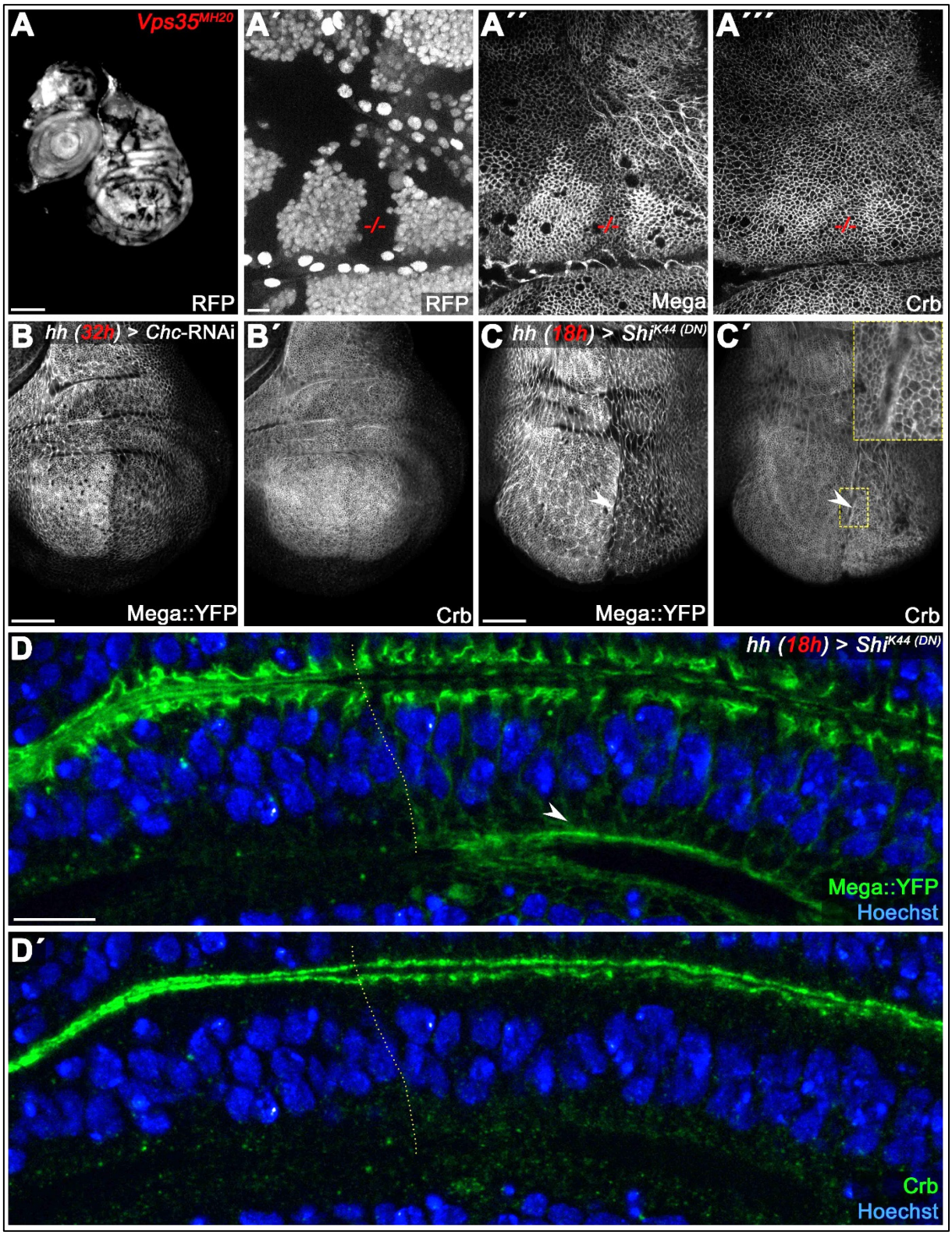

Figure S10. Comparison of Mega phenotypes with the Retromer CSC cargo Crumbs (Pocha et al., 2011). (**A**) *Vps35*^{MH20} clones, marked by the absence of RFP (**A´**), differently affect membrane levels of Mega (**A´´**) and Crb (**A´´´**). Mega appears to be more severely affected by Retromer loss of function. (**B**) Inhibition of clathrin dependent endocytosis by *Chc*-RNAi expression in the posterior compartment reduces apical Mega::YFP levels (**B**) while Crb levels are unaffected (**B´**). Similarly, expression of dominant negative Dynamin (Shi^{K44}) reduces Mega::YFP levels (arrowhead in **C**), while Crb seems to accumulate slightly at the apical membrane (arrowhead

in **C´**). This is consistent with Crb entering the endosomal system via apical internalization. (**D**) Optical section of a wing disc expressing Shi^{K44} for 18h in the posterior compartment reveals Mega::YFP accumulation at the basal pole of the cells (arrowhead in **D**). (**D´**) In contrast, no basal accumulation of Crb is detected. These data are consistent with Mega and Crb utilizing dissimilar Retromer dependent transport pathways. Scale bar in (**A**) represents 100µm, in **(B**, **C**): 50µm, in **(A´**, **D**): 10µm.

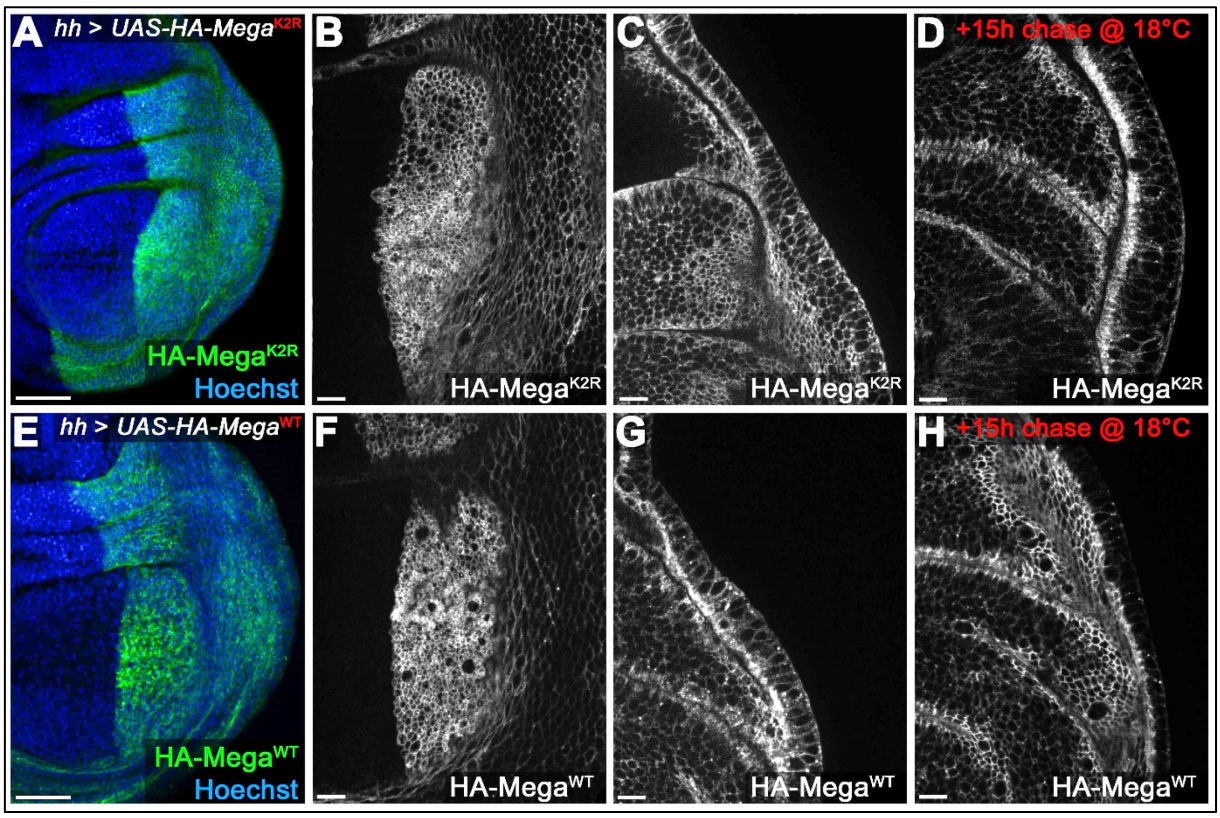

Figure S11. Mega transport towards the SJ is independent of intracellular lysines. (**A-D**) *hh*Gal4 driven posterior expression of an HA-tagged Mega construct in which all intracellular lysines were exchanged with arginines (UAS-HA-Mega^{K2R}). Junctional (**B**) and lateral (**C**) plane of continuously expressed HA-Mega^{K2R} reveals wildtype like membrane localization (compare with **F**, **G**). (**D**) After 15h chase at 18°C to allow intracellular transport of newly synthesized protein, HA-Mega^{K2R} signal is largely confined to the SJ, much like the wildtype (HA-Mega^{WT}) construct (**H**). (**E-H**) Expression of the wildtype control HA-Mega^{WT} construct under identical conditions. The two constructs are largely indistinguishable with HA-Mega^{K2R} retaining slightly more lateral and basal membrane signal after the 15h chase (compare **D** with **H**). The data are consistent with Mega transport to the SJ being independent of lysines (which should mediate direct interactions of cargo proteins with ESCRT components via ubiquitination). Scale bars in (**A**, **E**) represent 50µm, in all other panels: 10µm.

2.11 Author contributions to the manuscript

Hendrik Pannen	Devised, performed and analyzed all experiments except where noted. Designed the figures and wrote the original draft.
Tim Rapp	Performed and analyzed experiments displayed in Fig. 1J and Fig. 2E-F
Thomas Klein	Study supervision, manuscript correction and proofreading

3 Additional Experimental Data

While the above manuscript outlines the complex functions of the endosomal system in transporting SJ components, it does not provide a comprehensive explanation of the mechanisms involved. To gain further insight into regulation of SJ integrity by ESCRT and Retromer, several additional experiments were conducted. These are displayed in the section below. Experimental procedures were performed according to the materials and methods section of the above manuscript.

3.1 Comparative trafficking analysis of the Claudins Mega and Kune

ESCRT and Retromer dependent biosynthetic delivery of Mega to the SJ represents a novel trafficking route of this *Drosophila* claudin. However, besides Mega, the claudins Sinu and Kune are also involved in SJ formation and integrity (Nelson et al., 2010; Wu et al., 2004). Importantly, the latter was proposed to hold a more central role in SJ formation during embryogenesis, as it regulates both intracellular levels and junctional localization of the SJ core component Cora, while Mega was only required for its junctional localization (Nelson et al., 2010). These data suggest that albeit sharing a similar topology, *Drosophila* claudins differ significantly in their physiological functions, akin to mammalian claudins. To test whether Mega and Kune also have distinct functions during SJ maintenance in the proliferating wing disc, RNAi constructs targeting either Mega or Kune were expressed in posterior compartments using *hh*Gal4. Lac::GFP was used as a marker for SJ integrity. Continuous expression of Mega-RNAi (VDRC#50306) effectively depletes Mega levels in the posterior compartment (Fig. A1, A). In contrast, Lac::GFP junctional levels do not appear to differ between the wildtype anterior and the Mega depleted posterior compartment (Fig. A1, A´). However, in a lateral view of the epithelial layer, Lac::GFP is spreading along the basolateral membrane in the posterior compartment (arrowhead in Fig. A1, B´). This phenotype, albeit much weaker, is reminiscent of Lac::GFP subcellular localization upon Shrub depletion (see manuscript Fig.1) and suggests that SJ integrity is partially compromised in wing discs depleted of Mega.

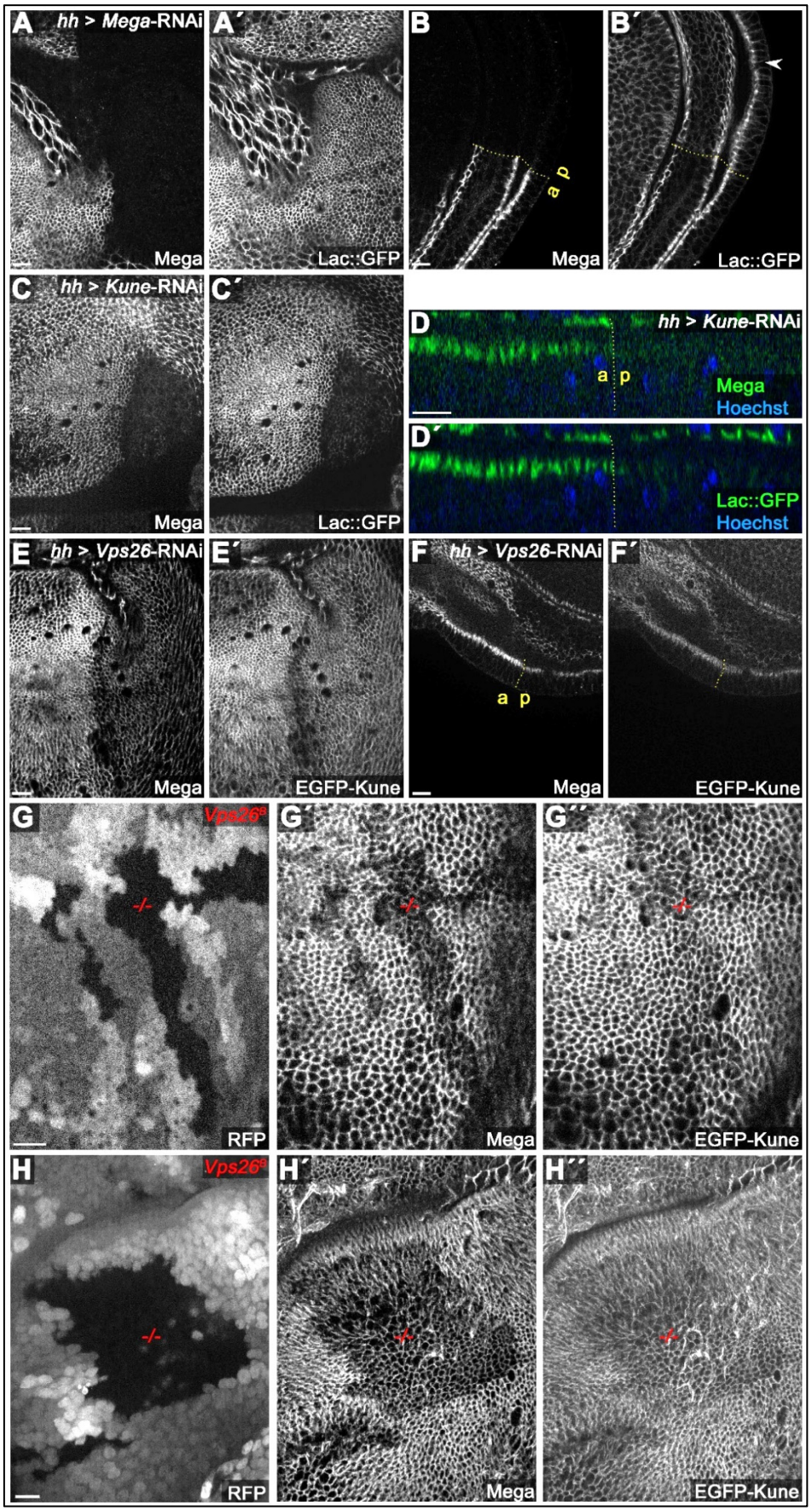

Figure A1. Comparative analysis of Mega and Kune functions and transport in wing imaginal discs. (**A**) RNAi-mediated knockdown of Mega efficiently depletes Mega protein (**A**) while Lac::GFP retains a wildtype like

junctional localization within the posterior RNAi expressing compartment (**A´**). (**B**) Lateral plane view reveals that a subset of Lac::GFP is spreading towards the lateral and basodistal membrane in Mega depleted tissue (arrowhead in **B´**). This is consistent with Mega being required for SJ fence function in wing imaginal discs. (**C-D**) In contrast, depletion of Kune by RNAi reduces overall levels of SJ components Mega and Lac::GFP in the posterior RNAi expressing compartment. (**D**) Optical section of *Kune*-RNAi expressing wing disc showing junctional depletion of Mega and Lac::GFP. (**E**) Vps26 knockdown differently affects Mega and a genomic EGFP-tagged Kune construct (EGFP-Kune). Mega membrane levels in the Vps26 depleted posterior compartment (**E**) show stronger reduction compared to EGFP-Kune levels (**E´**). (**F**) Lateral plane showing differences in junctional level reduction between Mega (**F**) and EGFP-Kune (**F´**) at the expression boundary of *Vps26*-RNAi. (**G-H**) $vps26^{B}$ mutant clones differently affect membrane levels of Mega and EGFP-Kune. Clones are marked by the absence of RFP. Note the relatively mild effect on junctional EGFP-Kune levels (**G´´** and **H´´**) compared to Mega, which shows a more pronounced reduction at the apical membrane within *Vps26* clones (**G´** and **H´**). Scale bars in all panels represent 10µm.

Upon expression of RNAi targeting Kune (BL#38295), junctional levels of Mega as well as Lac::GFP were reduced compared to the control compartment (Fig. A1, C-D). This indicates that similarly to its role during SJ formation, Kune, but not Mega, regulates membrane levels of SJ components in wing imaginal discs.

To gain insight into intracellular transport / junctional delivery of Kune, RNAi targeting the CSC component Vps26 (BL#38937) was expressed in posterior compartments. As expected, this led to solid reduction of Mega at the SJ level (Fig. A1, E). In contrast, an EGFP-tagged genomic Kune construct (Tempesta et al., 2017) showed only slight reduction at the junctional membrane of the RNAi-expressing posterior compartment (Fig. A1, E´). This is also visible in lateral views of the a/p compartment boundary, where the posterior reduction of junctional Mega is apparent, in contrast to relatively unaffected EGFP-Kune levels (Fig. A1, F).

In null mutant *vps26* clones, junctional Mega and EGFP-Kune show a similar phenotype; with apparent reduction of Mega within the clones and only slight effects on EGFP-Kune levels (Fig. A1, G-H). Together, these results suggest that EGFP-Kune delivery to the SJ does not rely on Retromer to a similar extent as Mega. Nevertheless, further investigation is needed to confirm this hypothesis. For example, assessing the SJ delivery of a UAS-driven Kune construct in Shrub or Retromer depleted cells may broaden understanding of the anterograde transport of Kune. Nevertheless, these initial data reveal that distinct functions of Kune and Mega are also at work during SJ maintenance in wing imaginal discs.

3.2 Requirement for Rab7 activity in Retromer dependent junctional delivery of Mega

The Retromer CSC is an effector of the endosomal GTPase Rab7 and requires the latter for its recruitment to the endosomal membrane in mammalian cells (Priya et al., 2015; Rojas et al., 2008; Seaman et al., 2009). To study the role of Rab7 in CSC recruitment and apical delivery of Mega in *Drosophila* wing imaginal discs, null mutant Rab7 clones were generated in wing discs (*Rab7* $^{Gal4\text{-}KO}$, (Chan et al., 2011)) and their effects on CSC and Mega subcellular localization were assessed. *Rab7*$^{Gal4\text{-}KO}$ clones grew well in the wing disc tissue and effectively abolished Rab7 expression while having no effect on junctional E-cad (Fig. A2, A). Vps26 staining revealed that its apical hub localization is partially abolished (Fig. A2, B´´). This suggests that similarly to mammalian cells, *Drosophila* imaginal disc cells also require Rab7 for efficient membrane recruitment of the CSC. Nevertheless, a subset of Vps26 still localizes in a vesicular pattern at the apical hub, suggesting that a fraction of the *Drosophila* CSC is still able to coat endosomal membranes in absence of Rab7 (Fig. A2, B´´). Consistent with partially diminished levels of Vps26 within the apical hub, junctional levels of Mega were reduced in *Rab7*$^{Gal4\text{-}KO}$ clones (Fig. A2, B´´´). This is in line with inefficient CSC dependent SJ delivery of Mega when Rab7 activity is lacking. However, reduction of junctional Mega levels appeared to be weaker when compared to CSC mutant clones (compare with manuscript figure 2A). Although lacking quantification to confirm this notion, it suggests that Rab7 deficiency likely represents a hypomorphic Retromer CSC mutant phenotype with respect to apical delivery of Mega. The data also suggest that the Vps26 fraction remaining associated with the apical hub in *Rab7*$^{Gal4\text{-}KO}$ clones is able to transport Mega towards the SJ.

Next, subcellular localization of Vps35::RFP was analyzed in wing discs partially depleted of Rab7. Expression of Rab7-RNAi (VDRC#40337) driven by *hh*Gal4 efficiently depleted Rab7 expression in the posterior compartment (Fig. A2, C). Surprisingly, despite the strong reduction of Rab7, apical Vps35::RFP levels appeared not to differ between the wildtype anterior and the Rab7 depleted posterior compartment (Fig. A2, C´). Vps35::RFP still localizes at the apical hub of Rab7 depleted wing disc cells, as seen in an optical section of the wing disc tissue (Fig. A2, D). These results provoke the hypothesis that Vps35, but not Vps26, may localize to the endosomal membrane independently of Rab7 in wing imaginal discs. However, it is also possible that a tiny amount of Rab7 is sufficient for complete recruitment of the CSC to the apical hub of wing disc cells. Thus, despite seemingly diminished levels of Rab7 upon RNAi expression (Fig. A2, C), RNAi mediated depletion of Rab7 may not be efficient to induce

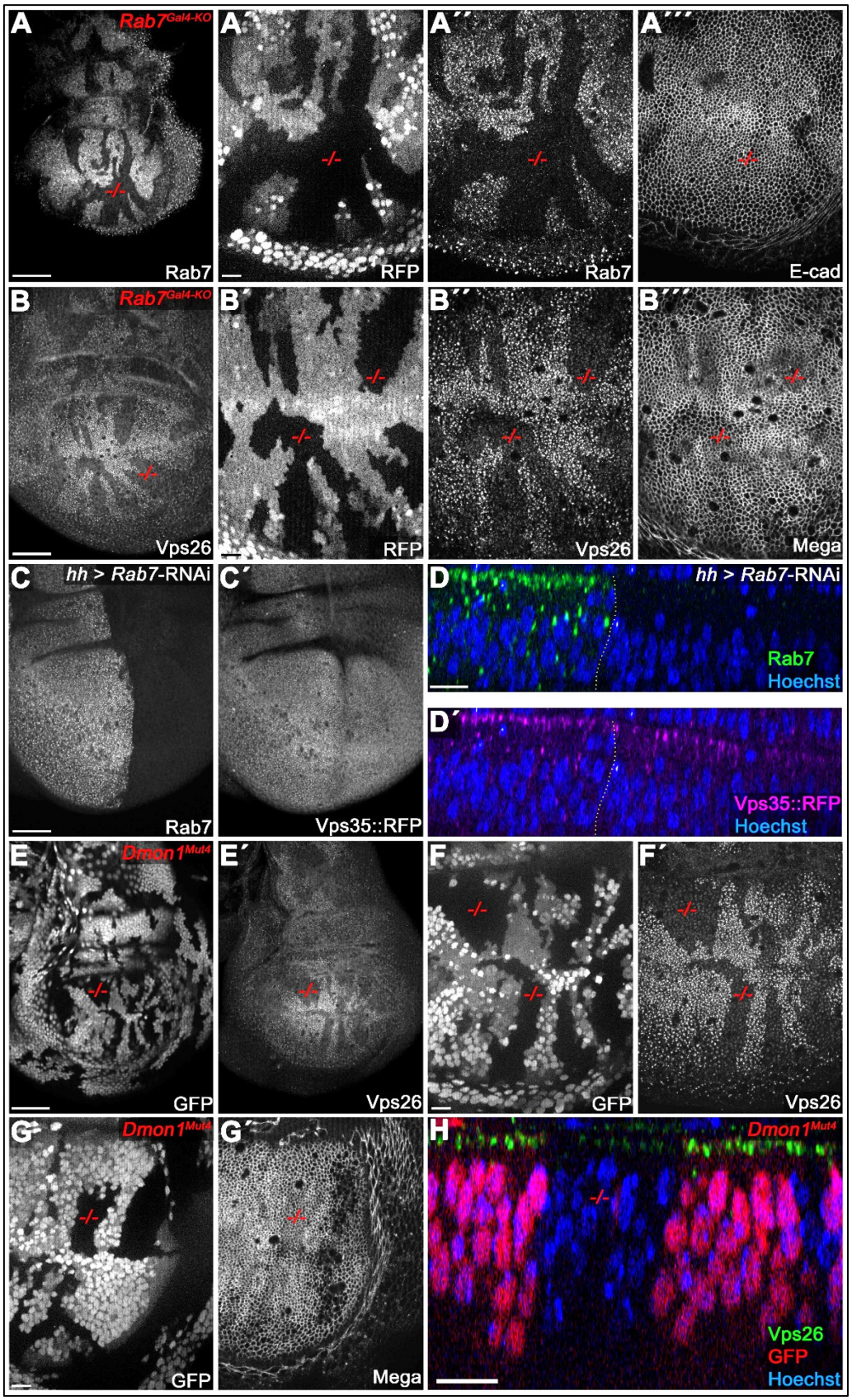

Figure A2. Analysis of Rab7 function in Retromer dependent SJ delivery of Mega. (**A**) Rab7 mutant clones, marked by the absence of RFP (**A´**), are devoid of Rab7 (**A´´**) and show wildtype localization of E-cad (**A´´´**). (**B**) Vps26 (**B´´**) and Mega (**B´´´**) show reduced apical levels within *Rab7*$^{Gal4\text{-}KO}$ clones. Note the relatively mild effect

on Mega compared to Vps26. (**C-D**) RNAi mediated knockdown of Rab7 efficiently depletes Rab7 (**C**) but does not affect Vps35::RFP levels (**C´**). (**D**) Optical section reveals intact apical hub localization of Vps35::RFP in Rab7 depleted tissue. (**E-H**) Null mutant clones of the Rab7 GEF Mon1 affect Vps26 and Mega apical levels in a similar fashion to *Rab7* clones. Note the reduced but not fully abolished vesicular localization of Vps26 (**F´**). (**G´**) Mega junctional levels are slightly reduced in $Dmon1^{Mut4}$ clones. (**H**) Optical section of $Dmon1^{Mut4}$ clones reveals reduced Vps26 levels throughout the tissue. Scale bars in (**A**, **B**, **C, E**) represent 50µm, in all other panels: 10µm.

impaired CSC endosomal recruitment. Nevertheless, it remains to be determined whether Vps35::RFP apical hub levels differ from that of Vps26 in a Rab7 null mutant situation.

Drosophila Mon1 (Dmon1) is a Rab7 guanine nucleotide exchange factor (GEF) and required for endosomal recruitment of Rab7 in wing discs (Yousefian et al., 2013). Therefore, Dmon1 is a major regulator of endosomal maturation by regulating the membrane association of Rab7. Since Rab7 function is required for efficient apical hub localization of Vps26 (Fig. A2, B´´), a similar requirement for Dmon1 in CSC recruitment is expected. Indeed, in Dmon1 null mutant clones ($Dmon1^{Mut4}$, (Yousefian et al., 2013)), apical hub levels of Vps26 were reduced to a similar extent as in $Rab7^{Gal4\text{-}KO}$ clones (compare Fig. A2, F´ with B´´). Consistently, junctional Mega levels were only mildly reduced in $Dmon1^{Mut4}$ clones (Fig. A2, G´). An optical section of a wing disc containing $Dmon1^{Mut4}$ clones reveals that while apical hub levels of Vps26 are reduced, no accumulation of Vps26 in the cytoplasm is detected (Fig. A2, H). Thus, Dmon1 may potentially regulate expression levels or stability of the CSC. However, this hypothesis needs to be addressed with biochemical experiments in the future (e.g. assessing the protein levels of Vps26 in wildtype and Dmon1 deficient wing discs by western blotting).

Together, the above data indicate that Rab7 and its GEF Dmon1 are partially required for apical hub localization of the CSC component Vps26 and for junctional delivery of Mega.

3.3 The function of Vps34/PI3K in transport of Mega

A feature of endosomal maturation is the generation of the endosome specific lipid PI(3)P by the PI3-Kinase complex with its catalytic subunit Vps34 (Marat and Haucke, 2016). PI(3)P is recognized by several protein domains found in endosomal machineries such as the FYVE and GLUE domains of ESCRT components or the Phox homology (PX) domain of SNX-BAR proteins (Bravo et al., 2001; Dumas et al., 2001; Mao et al., 2000; Teo et al., 2006). Thus, PI(3)P function is potentially involved in both degradative as well as recycling routes within the

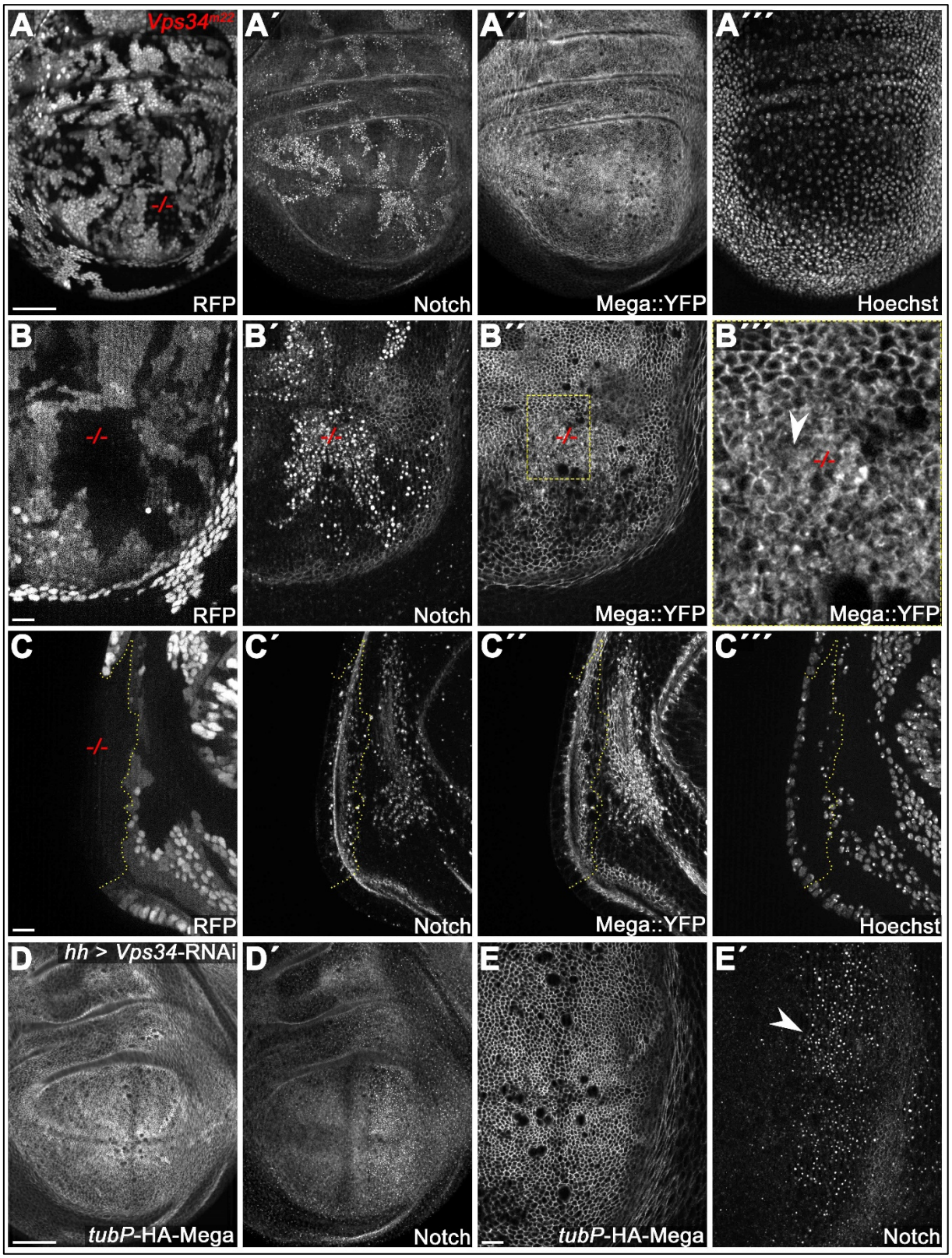

Figure A3. Potential role of the PI3-Kinase Vps34 in transport of Mega. (**A**) Null mutant clones of *Vps34* (marked by the absence of RFP) were generated in wing discs. Within the clones, strong Notch accumulation is seen (**A´**) while Mega::YFP overall levels are not affected (**A´´**). (**B**) At higher magnification, Notch accumulation within the clone is evident as punctate structures (**B´**), while junctional Mega::YFP levels do not seem altered (**B´´**). However, Mega::YFP localization appears blurred within the clone with the junctional honeycomb-like

pattern being frequently abolished (arrowhead in **B´´´**). (**C**) Lateral plane of a clone shows Notch accumulation in vesicular structures (**C´**) and unaltered junctional levels of Mega::YFP (**C´´**) within *Vps34* mutant tissue. (**D-E**) RNAi-mediated depletion of Vps34 accumulates Notch in apically localized vesicular structures (arrowhead in **E´**), while *tubP*-HA-Mega membrane levels remain wildtype (**E**). Scale bars in (**A**, **D**) represent 50µm, in all other panels: 10µm.

endosomal system. Consistently, Vps34 dependent generation of PI(3)P was required in yeast and mammalian cells for membrane association of SNX-BAR proteins and Retromer dependent endosomal retrieval (Burda et al., 2002; Cozier et al., 2002; Verges et al., 2007). Importantly, while mammalian SNX1 and SNX2 recruitment to the endosomal membrane required Vps34 function, endosomal localization of the CSC was shown to be independent of Vps34 (Verges et al., 2007).

The endosomal functions of Vps34 in Retromer dependent recycling prompted an investigation into its potential involvement in trafficking of Mega. $Vps34^{m22}$ null mutant clones (Juhasz et al., 2008) were induced in wing discs to analyze the impact of PI(3)K deficiency on Mega intracellular transport. These clones grew well in the wing disc tissue and strongly accumulated Notch on large vesicular structures, indicating that endosomal cargo flux was impaired (Fig. A3, A-B). In contrast, Mega::YFP did not show an apparent accumulation and, importantly, no obvious reduction in junctional levels was observed (Fig. A3, B´´). Nevertheless, Mega::YFP junctional localization within $Vps34^{m22}$ clones appeared blurred, with the membrane localization / honeycomb pattern being partially disrupted (Fig. A3, arrowhead in B´´´). The overall wildtype levels of Mega::YFP at the junctional membrane of $Vps34^{m22}$ mutant cells is also evident in a lateral view of a large clone at the fringe of the wing disc pouch (Fig. A3, C). Similar to the null mutant situation, depletion of Vps34 by RNAi (VDRC#100296) in the posterior compartment did not reduce junctional levels of a *tubulin*-Promoter (*tubP*) driven HA-Mega construct while showing robust Notch accumulation (Fig. A3, D).

Together, these results indicate that Vps34 is likely not required for Retromer-dependent junctional delivery of Mega. This notion is consistent with the finding that Mega transport towards the SJ does not require PI(3)P dependent, Retromer associated SNX-BAR proteins (see manuscript Figure S6). Nevertheless, partial disruption of the junctional Mega::YFP pattern within $Vps34^{m22}$ clones permits the hypothesis that PI(3)K function might affect efficient integration of apically localized Mega into the membrane / SJ. However, it remains to be determined whether this phenotype is Mega::YFP specific or just reflects a global disruption of certain cellular properties when PI(3)K function is lost.

3.4 Small-scale RNAi screen to find novel factors implicated in SJ delivery of Mega

The unexpected role of ESCRT and Retromer in junctional delivery of Mega raises the question about the endosomal transport mechanism involved. In order to gain further insight into the processes governing this complex intracellular trafficking, a small-scale RNAi screen was devised (Table 1).

Table 1: Small-scale RNAi screen for factors implicated in trafficking of Mega

RNAi targeting	Identifier (stockcenter) BL: BDSC V: VDRC	Cell death posterior	Tissue scar at a/p boundary	Notch (extra) localization	*tubP*-HA-Mega localization	E-cad localization	Reason to include in screen
Snx1	BL38301	(+)	-		WT		Sorting Nexin Family
Snx3	BL41947	-	-		WT		
Snx3	BL50633	+	+		WT		
Snx6	BL38278	(+)	-		WT		
Snx6	BL76057	(+)	+		WT		
SH3PX1	BL54833	-	+	WT	WT		
SH3PX1	BL27653	-	+	WT	WT		
Snx16	BL38992	-	-		WT		
Snx17	V43798	-	+	WT	WT		
Snx21	BL63610	-	+	WT	WT		
Snx27	BL38225	-	(+)	WT	WT		
Snz	BL39036	-	+	WT	WT		
Wash	BL62866	-	-	WT	WT		Retromer associated factors (Seaman, 2012)
Vps29	V101375	(+)	+	WT	WT		
Vps29	BL38963	-	(+)	WT	WT		
DCTN1-p150	BL27721	++	++		WT	WT	
DCTN-1-DN*	BL51645	++	++		WT	WT	
Dlic	BL66981	+++	++		WT	WT	
Dhc64C	BL36583	-	-		WT	WT	
Rme-8	**V107706**	+++	++	++	+		
Rab9	BL31688	(+)	+	WT	WT		Rab GTPases and associated factors
Rab19	V103653	(+)	(+)	WT	WT		
Rab21	V109991	++	+	WT	WT		
Rab30	V27002	+	+	WT	WT		
Tbc1d15	BL34859	-	+	WT	WT		
Vamp7	BL43543	-	-		WT		SNARE proteins (vesicle fusion)
Ykt6	BL50937	-	(+)		WT	WT	
nSyb	BL31983	-	-		WT	WT	
Syx7	BL29546	+++	++		WT	WT	
Syx18	BL26721	+++	++		WT	WT	
Sec5	BL56556	++	+		WT	WT	Exocyst complex (vesicle tethering)
Sec8	BL57441	++	+		WT	WT	
Sec15	BL27499	+++	++		WT	WT	
Exo84	BL28712	+++	++		WT	WT	
Vps55/ Leprot	BL62369	-	(+)	WT	WT		Involved in basal to apical transcytosis in cell culture (Nelms et al., 2017)

The genes that were targeted in this screen were selected based on their involvement in vesicular trafficking and the availability of RNAi constructs.

In *Drosophila* wing discs, apical to basal transcytosis of the signaling molecule Wingless has been shown to require the action of the SNARE (Soluble N-ethylmaleimide-sensitive-factor attachment receptor) Synaptobrevin (Syb) (Yamazaki et al., 2016). To release transcytosed cargo such as Wingless or Mega at their destined site, fusion of the carrier vesicle with the plasma membrane is required. Since SNARE proteins are crucial regulators of vesicular fusion, their involvement in transcytosis is not surprising (Han et al., 2017). Preceding vesicular fusion, the membranes of endocytic vesicles are often actively brought into close juxtaposition in a process termed tethering, which is mediated either by the Exocyst complex or several other specialized tethering factors (Gillingham and Munro, 2019). Consequently, Exocyst components and SNARE proteins were included in the screen. Additionally, RNAi constructs targeting all members of the *Drosophila* SNX family, Retromer associated proteins and several Rab GTPases were added.

All RNAi constructs were expressed continuously with a *hh*Gal4 driver containing a *tubP*-HA-Mega construct at 29°C and wing discs of late L3 larvae were dissected and stained for HA-Mega and Hoechst / DNA (optionally, Notch / E-cad were stained as well). Since the efficiency of the used RNAi constructs could not be tested with antibody staining of the targeted proteins, the morphology and integrity of the wing disc epithelium in the posterior compartment was analyzed. Specifically, the basal part of the disc proper was monitored for condensated DNA most likely stemming from apoptotic cells (nuclear pyknosis) and the a/p boundary was checked for morphological changes (expression scars). While expression of many RNAi constructs induced either expression scars and / or nuclear pyknosis, indicating that they likely suppress the respective proteins and challenge tissue homeostasis, only one noticeably affected the subcellular localization of HA-Mega. Expression of an RNAi construct targeting the Retromer associated factor Receptor mediated endocytosis 8 (Rme-8) reduced membrane levels of HA-Mega (Fig. A4, A´).

In mammalian cells and in *C. elegans*, Rme-8 is required for trafficking of the Retromer cargos CI-MPR and MIG-14/Wntless, respectively (Girard et al., 2005; Shi et al., 2009). Additionally, Rme-8 has been shown to physically interact with *C. elegans* SNX-1 and the mammalian WASH complex component FAM21, underlining its close association with the Retromer interactome (Freeman et al., 2014; Shi et al., 2009).

Drosophila Rme-8 was previously shown to be required for Notch receptor trafficking and regulation of Notch signaling homeostasis (Gomez-Lamarca et al., 2015). Consistently,

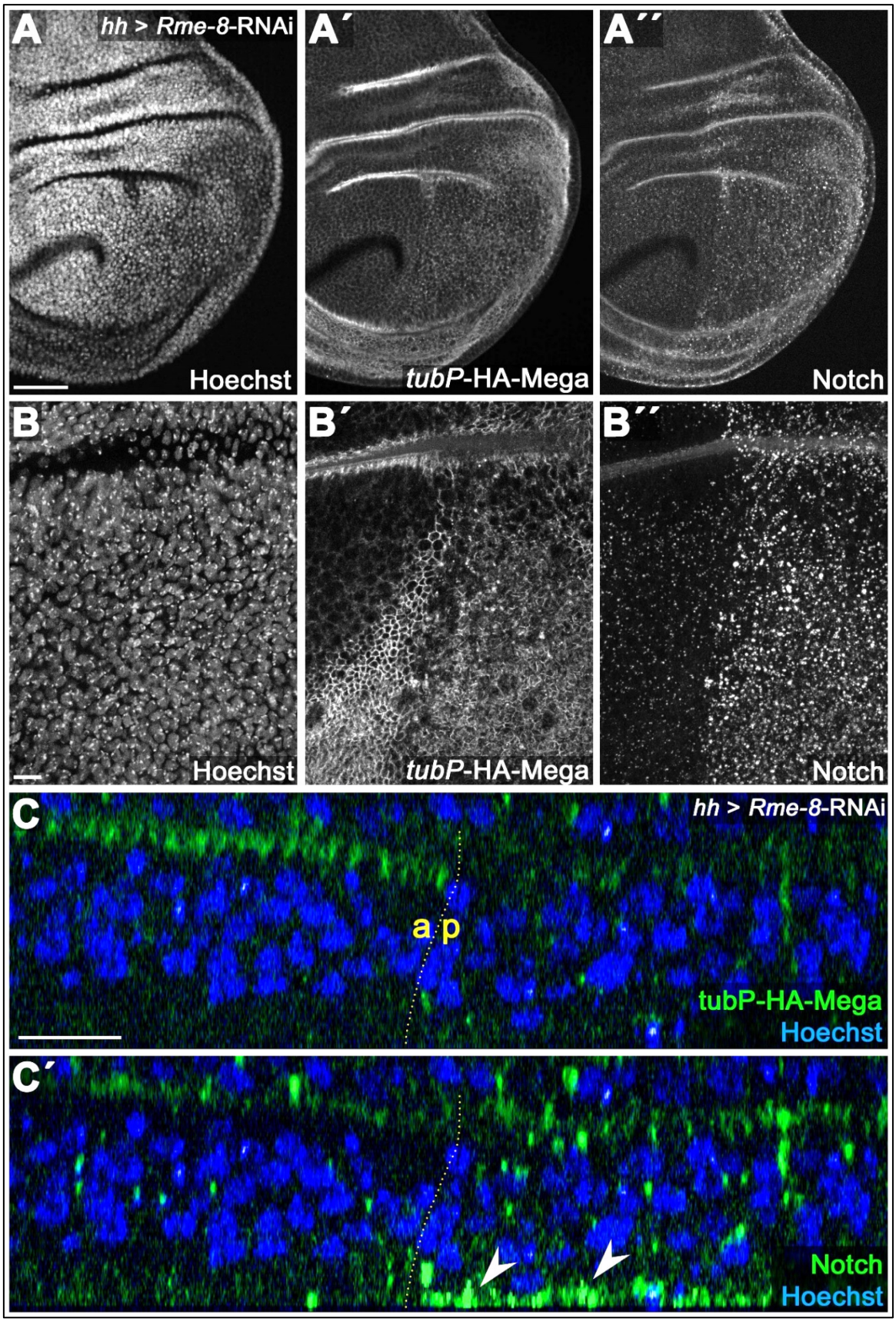

Figure A4. Retromer associated factor Rme8 is required for SJ delivery of Mega. (**A-C**) Knockdown of Rme8 by RNAi in the posterior compartment. In the Rme8 depleted compartment, Notch shows accumulation in a vesicular pattern (**A´´**) while *tubP*-HA-Mega junctional level (visible in the epithelial fold of the hinge region)

appears reduced (**A´**). (**B**) In a higher magnification of the junctional region, the wildtype membrane localization of *tubP*-HA-Mega in the anterior compartment is contrasting the faint membrane signal in the Rme8 depleted posterior compartment (**B´**). (**B´´**) Vesicular accumulation of Notch in the posterior compartment. (**C**) In an optical section of an *Rme8*-RNAi expressing wing disc, the strong reduction of junctional *tubP*-HA-Mega in the posterior compartment is evident (**C**). (**C´**) Notch accumulation in vesicular structures appears to be distributed along the entire apicobasal axis; with a significant basal fraction (arrowheads). Scale bar in (**A**) represents 50µm and in all other panels: 10µm.

vesicular accumulation of Notch was detected upon expression of *Rme-8*-RNAi in the posterior compartment of wing imaginal discs (Fig. A4, B´´). The reduction of junctional HA-Mega is very evident in an optical section of the wing disc at the a/p boundary (Fig. A4, C). This is in contrast to Notch, which does not show reduced levels at the apical membrane but is seen accumulating in vesicular structures throughout the Rme-8 depleted cells (Fig. A4, C´).
Together, the data indicate that junctional delivery of Mega requires the Retromer associated protein Rme-8. Additionally, RNAi lines targeting several endocytic factors such as the Exocyst or the SNAREs Syx7 and Syx18 induced strong nuclear pyknosis and expression scars but did not affect HA-Mega junctional localization, indicating that apical delivery of Mega is likely independent of these proteins.

4 Concluding Remarks

Prior to this work, the knowledge about ESCRT induced neoplasia in *Drosophila* imaginal discs was limited to understanding the cellular signaling pathways that are misregulated upon loss of ESCRT function. The simultaneous disruption of these pathways may cooperate to drive neoplastic tissue transformation, but its impact on junctional integrity remained unexplored.

By outlining a novel role of the ESCRT machinery in maintaining SJ density in wing discs, this work reveals a crucial epithelial structure whose integrity highly depends on ESCRT function. It is important to note that SJ density was already significantly reduced in pre-neoplastic stages (48h of Shrub depletion, see manuscript Fig. 1D). Thus, rather than being a consequence of neoplastic tissue transformation and multilayering, reduction of SJ density is a direct aftermath of ESCRT mediated trafficking defects. This is exemplified by SJ delivery of the Claudin Mega, which critically requires ESCRT function for its integration into the junction (manuscript Fig. 5E).The anterograde trafficking of Mega and other SJ core components to the junctional membrane of wing discs was subsequently shown to require the endocytic recycling complex Retromer, which, just like ESCRT, sorts cargo at maturing endosomes.

Providing the link between ESCRT and Retromer is the finding that upon disruption of ESCRT-I, ESCRT-III or Vps4 function, the Retromer cargo sorting complex loses its apical hub localization and dynamic mobility (manuscript Fig. 3). This leads to the emergence of a mechanistic model, in which ESCRT indirectly regulates delivery of SJ components to the apical membrane by maintaining the integrity and function of Retromer dependent recycling carriers. This indirect transport mechanism is further supported by the finding that HA-Mega^{K2R}, which should be unable to interact with ESCRT components due to a lack of ubiquitinatable lysine residues, integrates into the SJ as efficiently as wildtype HA-Mega (manuscript Fig. S11). Thus, it is unlikely that SJ delivery of Mega requires its packaging into ILV (the canonical ESCRT pathway).

Therefore, ESCRT dependent SJ delivery of Mega can be considered a non-canonical / non-degradative function of the ESCRT machinery.

Another significant finding presented in this work is the intricate trafficking of Mega following its biosynthesis. Although Mega protein almost exclusively localizes at the apical cortex within the SJ, the mRNA of Mega is deposited in the basal cytoplasm, on the opposite pole of the elongated wing disc cells (manuscript Fig. 6). Surprisingly, instead of directly traversing the cell following secretion from the Golgi, Mega protein initially localizes at the basodistal membrane, prior to its internalization into the endosomal system and subsequent transcytosis

towards the apical SJ. The requirement for Mega to traverse the endosomal system underlines the importance of an intact endocytic flux for its integration into the SJ. This flux is abolished in ESCRT deficient situations, as both cargo proteins and endocytic agents (Hrs, Rab5, Rab6, Retromer CSC) are stalled on enlarged aberrant endosomal compartments upon depletion of Shrub (manuscript Fig. S8). This global effect on both degradative as well as recycling routes supports the very central role the ESCRT machinery fulfills in endosomal as well as epithelial homeostasis.

Although still lacking biochemical data on the interaction between the Retromer CSC and SJ components, the data presented here support the view that a subset of SJ core components represents novel *bona fide* Retromer cargos. This expands the physiological roles of the ancient cargo sorting complex with possible implications in humans, since the CSC and several SJ components are conserved throughout species.

While the work presented here outlines a novel function of ESCRT and Retromer in maintenance of a crucial epithelial structure in the wing disc epithelium, new questions emerge on the mechanisms behind this transport function. These include, but are not limited to, the following:

How does ESCRT regulate CSC carrier generation / mobility for SJ component transport?

Why does Mega transiently localize at the basodistal membrane? Is there a specific reason for this intermediate step (e.g. SJ complex assembly)?

How does the CSC select / interact with SJ components within the endosomal system? Does the CSC regulate TJ maintenance in mammalian systems?

What is the physiological relevance of impaired SJ / barrier function during ESCRT mediated neoplasia? Why is multilayering observed despite the relatively high stability of AJ?

Addressing these questions will be important for revealing the exact mechanisms of ESCRT and Retromer dependent transport of SJ components and its implications in epithelial maintenance.

5 Summary

ESCRT mediated formation of intraluminal vesicles at maturing endosomes is a crucial prerequisite to transmembrane protein degradation. Many cellular signaling pathways rely on endosomal degradation of receptors for physiological homeostasis. Consistently, misregulation of signaling pathways induced by ESCRT loss of function causes *Drosophila* imaginal discs to induce apoptosis, overproliferate and grow into disorganized neoplastic tumors. While the signaling events leading to apoptosis and overproliferation in ESCRT deficient imaginal disc tissue are well understood, the processes resulting in apparent loss of cell polarity and multilayering of the epithelium remain obscure. Specifically, whether ESCRT function is required for maintenance of cell-cell junctions is unknown.

To gain insights into neoplastic transformation of ESCRT deficient imaginal disc tissue, transmission electron microscopy was used in this thesis to analyze potential effects of ESCRT depletion on cell junction integrity prior to tissue multilayering. This analysis revealed that the Septate Junction (SJ), but not the Adherens Junction (AJ), is very sensitive towards depletion of the ESCRT-III core component Shrub. Shrub was required to maintain a high density of electron-dense septa in wing imaginal discs and was subsequently shown to function in biosynthetic delivery of the Claudin Megatrachea (Mega) to the SJ. This finding is surprising, since it outlines a novel, non-degradative ESCRT function in the maintenance of a crucial epithelial structure.

Furthermore, it was found that upon depletion of ESCRT function, the cargo selective complex (CSC) of the endosomal recycling machinery Retromer was displaced from dynamic apically localized vesicles and accumulated on aberrant basal endosomes that contained Mega. Basal trapping of Mega and CSC components on endosomes suggested that Retromer might be required for endosomal export of Mega. Indeed, CSC function was found to be necessary not only for transport of Mega but also several other core SJ components to the plasma membrane. Thus, both ESCRT and Retromer functions at the endosome are required for supplying the proliferating wing disc cells with newly synthesized SJ components.

Together, the findings presented in this thesis advance the understanding of the pleiotropic ESCRT deficiency phenotype in *Drosophila* imaginal discs and also unravel novel functions of the ESCRT and Retromer endosomal machineries in maintenance of SJ integrity.

6 Zusammenfassung

ESCRT vermittelte Bildung intraluminaler Vesikel an reifenden Endosomen ist eine Voraussetzung für vollständige Degradation von Transmembranproteinen. Viele Signalwege benötigen für die Regulation der Signalwirkung endosomale Degradation von Rezeptoren oder Liganden. Daher induziert ein Ausfall der ESCRT Funktion in Drosophila Imaginalscheiben durch Fehlregulierung verschiedener Signalwege Apopotose, Überproliferation und neoplastische Transformation des Gewebes. Während die Signalprozesse, welche bei ESCRT Ausfall Apopotose und Überproliferation einleiten gut untersucht sind, so ist es noch unklar, wie es zum Verlust der Zellpolarität und epithelialen Integrität kommt. Insbesondere, ob ESCRT benötigt wird um Zell-Zell-Kontakte (Junctions) aufrechtzuerhalten ist nicht bekannt.
Um Einblicke in die neoplastische Transformation ESCRT defizienten Gewebes zu erlangen, wurde in dieser Arbeit Transmissionselektronenmikroskopie verwendet um potentielle Effekte des ESCRT Ausfalls auf die Integrität der Junctions zu analysieren. Diese Analyse zeigte, dass die Integrität der Septate Junctions (SJ), jedoch nicht die der Adherens Junctions, sensibel auf Reduktion der ESCR-III Kernkomponente Shrub reagierte. Shrub wurde benötigt, um eine hohe Dichte von Septa in Flügelimaginalscheiben aufrechtzuerhalten. Zudem konnte gezeigt werden, dass der Transport des Claudins / der SJ Komponente Megatrachea (Mega) zu der SJ die Funktion von Shrub benötigt. Dieses Ergebnis ist überraschend, da es eine neue, nicht-degradative ESCRT Funktion in der Aufrechterhaltung einer essentiellen epithelialen Struktur darstellt.
Desweiteren konnte gezeigt werden, dass durch Reduktion der ESCRT Aktivität der sogenannte cargo selective complex (CSC) der endosomalen Recyclingmaschinerie Retromer von apikal lokalisierten und dynamischen Vesikeln zu basalen, statischen Endosomen mislokalisiert wurde. Diese CSC positiven Endosomen enthielten zudem Mega, was nahelegt, dass Retromer möglicherweise für den Export Megas aus dem Endosom benötigt wird. Tatsächlich konnte gezeigt werden, dass der Retromer CSC nicht nur den Transport von Mega, sondern auch vieler weiterer SJ Komponenten zu der apikalen Membran reguliert. Demzufolge sind sowohl ESCRT als auch Retromer in Flügelimaginalscheiben notwendig, um das proliferierende Gewebe mit neu synthetisierten SJ Komponenten zu versorgen.
Die hier dargestellten Ergebnisse fördern das Verständnis des pleiotropen ESCRT Phänotyps in Drosophila Imaginalscheiben und stellen zudem neue Funktionen der ESCRT und Retromer endosomalen Maschinerien in der Aufrechterhaltung von SJ vor.

7 References

Assemat, E., E. Bazellieres, E. Pallesi-Pocachard, A. Le Bivic, and D. Massey-Harroche. 2008. Polarity complex proteins. *Biochim Biophys Acta*. 1778:614-630.

Babatz, F., E. Naffin, and C. Klambt. 2018. The Drosophila Blood-Brain Barrier Adapts to Cell Growth by Unfolding of Pre-existing Septate Junctions. *Dev Cell*. 47:697-710 e693.

Babst, M., D.J. Katzmann, W.B. Snyder, B. Wendland, and S.D. Emr. 2002. Endosome-associated complex, ESCRT-II, recruits transport machinery for protein sorting at the multivesicular body. *Dev Cell*. 3:283-289.

Babst, M., B. Wendland, E.J. Estepa, and S.D. Emr. 1998. The Vps4p AAA ATPase regulates membrane association of a Vps protein complex required for normal endosome function. *EMBO J*. 17:2982-2993.

Bachmann, A., M. Draga, F. Grawe, and E. Knust. 2008. On the role of the MAGUK proteins encoded by Drosophila varicose during embryonic and postembryonic development. *BMC Dev Biol*. 8:55.

Baldys, A., and J.R. Raymond. 2009. Critical role of ESCRT machinery in EGFR recycling. *Biochemistry*. 48:9321-9323.

Baumgartner, S., J.T. Littleton, K. Broadie, M.A. Bhat, R. Harbecke, J.A. Lengyel, R. Chiquet-Ehrismann, A. Prokop, and H.J. Bellen. 1996. A Drosophila neurexin is required for septate junction and blood-nerve barrier formation and function. *Cell*. 87:1059-1068.

Beaucher, M., E. Hersperger, A. Page-McCaw, and A. Shearn. 2007. Metastatic ability of Drosophila tumors depends on MMP activity. *Dev Biol*. 303:625-634.

Behr, M., D. Riedel, and R. Schuh. 2003. The claudin-like megatrachea is essential in septate junctions for the epithelial barrier function in Drosophila. *Dev Cell*. 5:611-620.

Beitel, G.J., and M.A. Krasnow. 2000. Genetic control of epithelial tube size in the Drosophila tracheal system. *Development*. 127:3271-3282.

Bilder, D., M. Li, and N. Perrimon. 2000. Cooperative regulation of cell polarity and growth by Drosophila tumor suppressors. *Science*. 289:113-116.

Bilder, D., and N. Perrimon. 2000. Localization of apical epithelial determinants by the basolateral PDZ protein Scribble. *Nature*. 403:676-680.

Bilder, D., M. Schober, and N. Perrimon. 2003. Integrated activity of PDZ protein complexes regulates epithelial polarity. *Nat Cell Biol*. 5:53-58.

Bilodeau, P.S., J.L. Urbanowski, S.C. Winistorfer, and R.C. Piper. 2002. The Vps27p Hse1p complex binds ubiquitin and mediates endosomal protein sorting. *Nat Cell Biol*. 4:534-539.

Bilodeau, P.S., S.C. Winistorfer, W.R. Kearney, A.D. Robertson, and R.C. Piper. 2003. Vps27-Hse1 and ESCRT-I complexes cooperate to increase efficiency of sorting ubiquitinated proteins at the endosome. *J Cell Biol*. 163:237-243.

Boyle, M.E., E.O. Berglund, K.K. Murai, L. Weber, E. Peles, and B. Ranscht. 2001. Contactin orchestrates assembly of the septate-like junctions at the paranode in myelinated peripheral nerve. *Neuron*. 30:385-397.

Bravo, J., D. Karathanassis, C.M. Pacold, M.E. Pacold, C.D. Ellson, K.E. Anderson, P.J. Butler, I. Lavenir, O. Perisic, P.T. Hawkins, L. Stephens, and R.L. Williams. 2001. The crystal structure of the PX domain from p40(phox) bound to phosphatidylinositol 3-phosphate. *Mol Cell*. 8:829-839.

Burda, P., S.M. Padilla, S. Sarkar, and S.D. Emr. 2002. Retromer function in endosome-to-Golgi retrograde transport is regulated by the yeast Vps34 PtdIns 3-kinase. *J Cell Sci*. 115:3889-3900.

Carlton, J.G., A. Caballe, M. Agromayor, M. Kloc, and J. Martin-Serrano. 2012. ESCRT-III governs the Aurora B-mediated abscission checkpoint through CHMP4C. *Science*. 336:220-225.

Chan, C.C., S. Scoggin, D. Wang, S. Cherry, T. Dembo, B. Greenberg, E.J. Jin, C. Kuey, A. Lopez, S.Q. Mehta, T.J. Perkins, M. Brankatschk, A. Rothenfluh, M. Buszczak, and P.R. Hiesinger. 2011. Systematic discovery of Rab GTPases with synaptic functions in Drosophila. *Curr Biol*. 21:1704-1715.

Charles, P., S. Tait, C. Faivre-Sarrailh, G. Barbin, F. Gunn-Moore, N. Denisenko-Nehrbass, A.M. Guennoc, J.A. Girault, P.J. Brophy, and C. Lubetzki. 2002. Neurofascin is a glial receptor for the paranodin/Caspr-contactin axonal complex at the axoglial junction. *Curr Biol*. 12:217-220.

Chen, J., A.C. Sayadian, N. Lowe, H.E. Lovegrove, and D. St Johnston. 2018. An alternative mode of epithelial polarity in the Drosophila midgut. *PLoS Biol*. 16:e3000041.

Christoforidis, S., M. Miaczynska, K. Ashman, M. Wilm, L. Zhao, S.C. Yip, M.D. Waterfield, J.M. Backer, and M. Zerial. 1999. Phosphatidylinositol-3-OH kinases are Rab5 effectors. *Nat Cell Biol*. 1:249-252.

Cozier, G.E., J. Carlton, A.H. McGregor, P.A. Gleeson, R.D. Teasdale, H. Mellor, and P.J. Cullen. 2002. The phox homology (PX) domain-dependent, 3-phosphoinositide-mediated association of sorting nexin-1 with an early sorting endosomal compartment is required for its ability to regulate epidermal growth factor receptor degradation. *J Biol Chem*. 277:48730-48736.

Cullen, P.J., and H.C. Korswagen. 2011. Sorting nexins provide diversity for retromer-dependent trafficking events. *Nat Cell Biol*. 14:29-37.

Cullen, P.J., and F. Steinberg. 2018. To degrade or not to degrade: mechanisms and significance of endocytic recycling. *Nat Rev Mol Cell Biol*. 19:679-696.

Cummins, P.M. 2012. Occludin: one protein, many forms. *Mol Cell Biol*. 32:242-250.

Daniel, E., M. Daude, I. Kolotuev, K. Charish, V. Auld, and R. Le Borgne. 2018. Coordination of Septate Junctions Assembly and Completion of Cytokinesis in Proliferative Epithelial Tissues. *Curr Biol*. 28:1380-1391 e1384.

Denisenko-Nehrbass, N., K. Oguievetskaia, L. Goutebroze, T. Galvez, H. Yamakawa, O. Ohara, M. Carnaud, and J.A. Girault. 2003. Protein 4.1B associates with both Caspr/paranodin and Caspr2 at paranodes and juxtaparanodes of myelinated fibres. *Eur J Neurosci*. 17:411-416.

Djiane, A., H. Shimizu, M. Wilkin, S. Mazleyrat, M.D. Jennings, J. Avis, S. Bray, and M. Baron. 2011. Su(dx) E3 ubiquitin ligase-dependent and -independent functions of polychaetoid, the Drosophila ZO-1 homologue. *J Cell Biol*. 192:189-200.

Dong, B., E. Hannezo, and S. Hayashi. 2014. Balance between apical membrane growth and luminal matrix resistance determines epithelial tubule shape. *Cell Rep*. 7:941-950.

Doyotte, A., M.R. Russell, C.R. Hopkins, and P.G. Woodman. 2005. Depletion of TSG101 forms a mammalian "Class E" compartment: a multicisternal early endosome with multiple sorting defects. *J Cell Sci*. 118:3003-3017.

Dukes, J.D., L. Fish, J.D. Richardson, E. Blaikley, S. Burns, C.J. Caunt, A.D. Chalmers, and P. Whitley. 2011. Functional ESCRT machinery is required for constitutive recycling of claudin-1 and maintenance of polarity in vertebrate epithelial cells. *Mol Biol Cell*. 22:3192-3205.

Dumas, J.J., E. Merithew, E. Sudharshan, D. Rajamani, S. Hayes, D. Lawe, S. Corvera, and D.G. Lambright. 2001. Multivalent endosome targeting by homodimeric EEA1. *Mol Cell*. 8:947-958.

Eichenberger-Glinz, S. 1979. Intercellular junctions during development and in tissue cultures ofDrosophila melanogaster: An electron-microscopic study. *Wilehm Roux Arch Dev Biol*. 186:333-349.

Einheber, S., G. Zanazzi, W. Ching, S. Scherer, T.A. Milner, E. Peles, and J.L. Salzer. 1997. The axonal membrane protein Caspr, a homologue of neurexin IV, is a component of the septate-like paranodal junctions that assemble during myelination. *J Cell Biol*. 139:1495-1506.

Faivre-Sarrailh, C., S. Banerjee, J. Li, M. Hortsch, M. Laval, and M.A. Bhat. 2004. Drosophila contactin, a homolog of vertebrate contactin, is required for septate junction organization and paracellular barrier function. *Development*. 131:4931-4942.

Farquhar, M.G., and G.E. Palade. 1963. Junctional complexes in various epithelia. *J Cell Biol*. 17:375-412.

Fehon, R.G., I.A. Dawson, and S. Artavanis-Tsakonas. 1994. A Drosophila homologue of membrane-skeleton protein 4.1 is associated with septate junctions and is encoded by the coracle gene. *Development*. 120:545-557.

Filshie, B.K., and N.E. Flower. 1977. Junctional structures in hydra. *J Cell Sci*. 23:151-172.

Fjorback, A.W., M. Seaman, C. Gustafsen, A. Mehmedbasic, S. Gokool, C. Wu, D. Militz, V. Schmidt, P. Madsen, J.R. Nyengaard, T.E. Willnow, E.I. Christensen, W.B. Mobley, A. Nykjaer, and O.M. Andersen. 2012. Retromer binds the FANSHY sorting motif in SorLA to regulate amyloid precursor protein sorting and processing. *J Neurosci*. 32:1467-1480.

Freeman, C.L., G. Hesketh, and M.N. Seaman. 2014. RME-8 coordinates the activity of the WASH complex with the function of the retromer SNX dimer to control endosomal tubulation. *J Cell Sci*. 127:2053-2070.

Funke, L., S. Dakoji, and D.S. Bredt. 2005. Membrane-associated guanylate kinases regulate adhesion and plasticity at cell junctions. *Annu Rev Biochem*. 74:219-245.

Furuse, M., K. Furuse, H. Sasaki, and S. Tsukita. 2001. Conversion of zonulae occludentes from tight to leaky strand type by introducing claudin-2 into Madin-Darby canine kidney I cells. *J Cell Biol*. 153:263-272.

Furuse, M., M. Itoh, T. Hirase, A. Nagafuchi, S. Yonemura, S. Tsukita, and S. Tsukita. 1994. Direct association of occludin with ZO-1 and its possible involvement in the localization of occludin at tight junctions. *J Cell Biol*. 127:1617-1626.

Furuse, M., and S. Tsukita. 2006. Claudins in occluding junctions of humans and flies. *Trends Cell Biol*. 16:181-188.

Ganot, P., D. Zoccola, E. Tambutte, C.R. Voolstra, M. Aranda, D. Allemand, and S. Tambutte. 2015. Structural molecular components of septate junctions in cnidarians point to the origin of epithelial junctions in eukaryotes. *Mol Biol Evol*. 32:44-62.

Garrus, J.E., U.K. von Schwedler, O.W. Pornillos, S.G. Morham, K.H. Zavitz, H.E. Wang, D.A. Wettstein, K.M. Stray, M. Cote, R.L. Rich, D.G. Myszka, and W.I. Sundquist. 2001. Tsg101 and the vacuolar protein sorting pathway are essential for HIV-1 budding. *Cell*. 107:55-65.

Genova, J.L., and R.G. Fehon. 2003. Neuroglian, Gliotactin, and the Na+/K+ ATPase are essential for septate junction function in Drosophila. *J Cell Biol*. 161:979-989.

Gillingham, A.K., and S. Munro. 2019. Transport carrier tethering - how vesicles are captured by organelles. *Curr Opin Cell Biol*. 59:140-146.

Girard, M., V. Poupon, F. Blondeau, and P.S. McPherson. 2005. The DnaJ-domain protein RME-8 functions in endosomal trafficking. *J Biol Chem*. 280:40135-40143.

Goldstein, B., and I.G. Macara. 2007. The PAR proteins: fundamental players in animal cell polarization. *Dev Cell*. 13:609-622.

Gomez-Lamarca, M., L.A. Snowdon, E. Seib, T. Klein, and S. Bray. 2015. Rme-8 depletion perturbs Notch recycling and predisposes to pathogenic signaling. *J Cell Biol*. 210:517.

Gomez, T.S., and D.D. Billadeau. 2009. A FAM21-containing WASH complex regulates retromer-dependent sorting. *Dev Cell*. 17:699-711.

Grawe, F., A. Wodarz, B. Lee, E. Knust, and H. Skaer. 1996. The Drosophila genes crumbs and stardust are involved in the biogenesis of adherens junctions. *Development*. 122:951-959.

Green, C.R., and N.E. Flower. 1980. Two new septate junctions in the phylum Coelenterata. *J Cell Sci*. 42:43-59.

Guerra, F., and C. Bucci. 2016. Multiple Roles of the Small GTPase Rab7. *Cells*. 5.

Guizetti, J., L. Schermelleh, J. Mantler, S. Maar, I. Poser, H. Leonhardt, T. Muller-Reichert, and D.W. Gerlich. 2011. Cortical constriction during abscission involves helices of ESCRT-III-dependent filaments. *Science*. 331:1616-1620.

Gunzel, D., and A.S. Yu. 2013. Claudins and the modulation of tight junction permeability. *Physiol Rev*. 93:525-569.

Han, J., K. Pluhackova, and R.A. Bockmann. 2017. The Multifaceted Role of SNARE Proteins in Membrane Fusion. *Front Physiol*. 8:5.

Harterink, M., F. Port, M.J. Lorenowicz, I.J. McGough, M. Silhankova, M.C. Betist, J.R.T. van Weering, R. van Heesbeen, T.C. Middelkoop, K. Basler, P.J. Cullen, and H.C. Korswagen. 2011. A SNX3-dependent retromer pathway mediates retrograde transport of the Wnt sorting receptor Wntless and is required for Wnt secretion. *Nat Cell Biol*. 13:914-923.

Haskins, J., L. Gu, E.S. Wittchen, J. Hibbard, and B.R. Stevenson. 1998. ZO-3, a novel member of the MAGUK protein family found at the tight junction, interacts with ZO-1 and occludin. *J Cell Biol*. 141:199-208.

Hemphala, J., A. Uv, R. Cantera, S. Bray, and C. Samakovlis. 2003. Grainy head controls apical membrane growth and tube elongation in response to Branchless/FGF signalling. *Development*. 130:249-258.

Henne, W.M., N.J. Buchkovich, Y. Zhao, and S.D. Emr. 2012. The endosomal sorting complex ESCRT-II mediates the assembly and architecture of ESCRT-III helices. *Cell*. 151:356-371.

Herz, H.M., Z. Chen, H. Scherr, M. Lackey, C. Bolduc, and A. Bergmann. 2006. vps25 mosaics display non-autonomous cell survival and overgrowth, and autonomous apoptosis. *Development*. 133:1871-1880.

Hierro, A., A.L. Rojas, R. Rojas, N. Murthy, G. Effantin, A.V. Kajava, A.C. Steven, J.S. Bonifacino, and J.H. Hurley. 2007. Functional architecture of the retromer cargo-recognition complex. *Nature*. 449:1063-1067.

Hierro, A., J. Sun, A.S. Rusnak, J. Kim, G. Prag, S.D. Emr, and J.H. Hurley. 2004. Structure of the ESCRT-II endosomal trafficking complex. *Nature*. 431:221-225.

Hijazi, A., W. Masson, B. Auge, L. Waltzer, M. Haenlin, and F. Roch. 2009. boudin is required for septate junction organisation in Drosophila and codes for a diffusible protein of the Ly6 superfamily. *Development*. 136:2199-2209.

Hildebrand, C., S. Remahl, H. Persson, and C. Bjartmar. 1993. Myelinated nerve fibres in the CNS. *Prog Neurobiol*. 40:319-384.

Hofmann, K., and L. Falquet. 2001. A ubiquitin-interacting motif conserved in components of the proteasomal and lysosomal protein degradation systems. *Trends Biochem Sci*. 26:347-350.

Horazdovsky, B.F., B.A. Davies, M.N. Seaman, S.A. McLaughlin, S. Yoon, and S.D. Emr. 1997. A sorting nexin-1 homologue, Vps5p, forms a complex with Vps17p and is required for recycling the vacuolar protein-sorting receptor. *Mol Biol Cell*. 8:1529-1541.

Huotari, J., and A. Helenius. 2011. Endosome maturation. *EMBO J*. 30:3481-3500.

Im, Y.J., T. Wollert, E. Boura, and J.H. Hurley. 2009. Structure and function of the ESCRT-II-III interface in multivesicular body biogenesis. *Dev Cell*. 17:234-243.

Itoh, M., K. Morita, and S. Tsukita. 1999. Characterization of ZO-2 as a MAGUK family member associated with tight as well as adherens junctions with a binding affinity to occludin and alpha catenin. *J Biol Chem*. 274:5981-5986.

Izumi, Y., M. Motoishi, K. Furuse, and M. Furuse. 2016. A tetraspanin regulates septate junction formation in Drosophila midgut. *J Cell Sci*. 129:1155-1164.

Izumi, Y., Y. Yanagihashi, and M. Furuse. 2012. A novel protein complex, Mesh-Ssk, is required for septate junction formation in the Drosophila midgut. *J Cell Sci*. 125:4923-4933.

Jaspers, M.H., K. Nolde, M. Behr, S.H. Joo, U. Plessmann, M. Nikolov, H. Urlaub, and R. Schuh. 2012. The claudin Megatrachea protein complex. *J Biol Chem*. 287:36756-36765.

Juhasz, G., J.H. Hill, Y. Yan, M. Sass, E.H. Baehrecke, J.M. Backer, and T.P. Neufeld. 2008. The class III PI(3)K Vps34 promotes autophagy and endocytosis but not TOR signaling in Drosophila. *J Cell Biol*. 181:655-666.

Katzmann, D.J., M. Babst, and S.D. Emr. 2001. Ubiquitin-dependent sorting into the multivesicular body pathway requires the function of a conserved endosomal protein sorting complex, ESCRT-I. *Cell*. 106:145-155.

Katzmann, D.J., C.J. Stefan, M. Babst, and S.D. Emr. 2003. Vps27 recruits ESCRT machinery to endosomes during MVB sorting. *J Cell Biol*. 162:413-423.

Kendall, A.K., B. Xie, P. Xu, J. Wang, R. Burcham, M.N. Frazier, E. Binshtein, H. Wei, T.R. Graham, T. Nakagawa, and L.P. Jackson. 2020. Mammalian Retromer Is an Adaptable Scaffold for Cargo Sorting from Endosomes. *Structure*. 28:393-405 e394.

Kostelansky, M.S., C. Schluter, Y.Y. Tam, S. Lee, R. Ghirlando, B. Beach, E. Conibear, and J.H. Hurley. 2007. Molecular architecture and functional model of the complete yeast ESCRT-I heterotetramer. *Cell*. 129:485-498.

Kostelansky, M.S., J. Sun, S. Lee, J. Kim, R. Ghirlando, A. Hierro, S.D. Emr, and J.H. Hurley. 2006. Structural and functional organization of the ESCRT-I trafficking complex. *Cell*. 125:113-126.

Krause, G., L. Winkler, S.L. Mueller, R.F. Haseloff, J. Piontek, and I.E. Blasig. 2008. Structure and function of claudins. *Biochim Biophys Acta*. 1778:631-645.

Kvainickas, A., A. Jimenez-Orgaz, H. Nagele, Z. Hu, J. Dengjel, and F. Steinberg. 2017. Cargo-selective SNX-BAR proteins mediate retromer trimer independent retrograde transport. *J Cell Biol*. 216:3677-3693.

Lamb, R.S., R.E. Ward, L. Schweizer, and R.G. Fehon. 1998. Drosophila coracle, a member of the protein 4.1 superfamily, has essential structural functions in the septate junctions and developmental functions in embryonic and adult epithelial cells. *Mol Biol Cell*. 9:3505-3519.

Lata, S., G. Schoehn, A. Jain, R. Pires, J. Piehler, H.G. Gottlinger, and W. Weissenhorn. 2008. Helical structures of ESCRT-III are disassembled by VPS4. *Science*. 321:1354-1357.

Lauffer, B.E., C. Melero, P. Temkin, C. Lei, W. Hong, T. Kortemme, and M. von Zastrow. 2010. SNX27 mediates PDZ-directed sorting from endosomes to the plasma membrane. *J Cell Biol*. 190:565-574.

Le Bivic, A. 2013. Evolution and cell physiology. 4. Why invent yet another protein complex to build junctions in epithelial cells? *Am J Physiol Cell Physiol*. 305:C1193-1201.

Li, L., and S.N. Cohen. 1996. Tsg101: a novel tumor susceptibility gene isolated by controlled homozygous functional knockout of allelic loci in mammalian cells. *Cell*. 85:319-329.

Llimargas, M., M. Strigini, M. Katidou, D. Karagogeos, and J. Casanova. 2004. Lachesin is a component of a septate junction-based mechanism that controls tube size and epithelial integrity in the Drosophila tracheal system. *Development*. 131:181-190.

Loh, C.Y., J.Y. Chai, T.F. Tang, W.F. Wong, G. Sethi, M.K. Shanmugam, P.P. Chong, and C.Y. Looi. 2019. The E-Cadherin and N-Cadherin Switch in Epithelial-to-Mesenchymal Transition: Signaling, Therapeutic Implications, and Challenges. *Cells*. 8.

Lucas, M., D.C. Gershlick, A. Vidaurrazaga, A.L. Rojas, J.S. Bonifacino, and A. Hierro. 2016. Structural Mechanism for Cargo Recognition by the Retromer Complex. *Cell*. 167:1623-1635 e1614.

Luzio, J.P., P.R. Pryor, and N.A. Bright. 2007. Lysosomes: fusion and function. *Nat Rev Mol Cell Biol*. 8:622-632.

Mao, Y., A. Nickitenko, X. Duan, T.E. Lloyd, M.N. Wu, H. Bellen, and F.A. Quiocho. 2000. Crystal structure of the VHS and FYVE tandem domains of Hrs, a protein involved in membrane trafficking and signal transduction. *Cell*. 100:447-456.

Marat, A.L., and V. Haucke. 2016. Phosphatidylinositol 3-phosphates-at the interface between cell signalling and membrane traffic. *EMBO J*. 35:561-579.

McCullough, J., A. Frost, and W.I. Sundquist. 2018. Structures, Functions, and Dynamics of ESCRT-III/Vps4 Membrane Remodeling and Fission Complexes. *Annu Rev Cell Dev Biol*. 34:85-109.

Menegoz, M., P. Gaspar, M. Le Bert, T. Galvez, F. Burgaya, C. Palfrey, P. Ezan, F. Arnos, and J.A. Girault. 1997. Paranodin, a glycoprotein of neuronal paranodal membranes. *Neuron*. 19:319-331.

Mettlen, M., T. Pucadyil, R. Ramachandran, and S.L. Schmid. 2009. Dissecting dynamin's role in clathrin-mediated endocytosis. *Biochem Soc Trans*. 37:1022-1026.

Misra, S., and J.H. Hurley. 1999. Crystal structure of a phosphatidylinositol 3-phosphate-specific membrane-targeting motif, the FYVE domain of Vps27p. *Cell*. 97:657-666.

Moberg, K.H., S. Schelble, S.K. Burdick, and I.K. Hariharan. 2005. Mutations in erupted, the Drosophila ortholog of mammalian tumor susceptibility gene 101, elicit non-cell-autonomous overgrowth. *Dev Cell*. 9:699-710.

Morita, E., and W.I. Sundquist. 2004. Retrovirus budding. *Annu Rev Cell Dev Biol*. 20:395-425.

Moyer, K.E., and J.R. Jacobs. 2008. Varicose: a MAGUK required for the maturation and function of Drosophila septate junctions. *BMC Dev Biol*. 8:99.

Muhammad, A., I. Flores, H. Zhang, R. Yu, A. Staniszewski, E. Planel, M. Herman, L. Ho, R. Kreber, L.S. Honig, B. Ganetzky, K. Duff, O. Arancio, and S.A. Small. 2008. Retromer deficiency observed in Alzheimer's disease causes hippocampal dysfunction, neurodegeneration, and Abeta accumulation. *Proc Natl Acad Sci U S A*. 105:7327-7332.

Muller, H.A., and E. Wieschaus. 1996. armadillo, bazooka, and stardust are critical for early stages in formation of the zonula adherens and maintenance of the polarized blastoderm epithelium in Drosophila. *J Cell Biol*. 134:149-163.

Nelms, B., N.F. Dalomba, and W. Lencer. 2017. A targeted RNAi screen identifies factors affecting diverse stages of receptor-mediated transcytosis. *J Cell Biol*. 216:511-525.

Nelson, K.S., M. Furuse, and G.J. Beitel. 2010. The Drosophila Claudin Kune-kune is required for septate junction organization and tracheal tube size control. *Genetics*. 185:831-839.

Nichols, S.A., B.W. Roberts, D.J. Richter, S.R. Fairclough, and N. King. 2012. Origin of metazoan cadherin diversity and the antiquity of the classical cadherin/beta-catenin complex. *Proc Natl Acad Sci U S A*. 109:13046-13051.

Nilton, A., K. Oshima, F. Zare, S. Byri, U. Nannmark, K.G. Nyberg, R.G. Fehon, and A.E. Uv. 2010. Crooked, coiled and crimpled are three Ly6-like proteins required for proper localization of septate junction components. *Development*. 137:2427-2437.

Nothwehr, S.F., and A.E. Hindes. 1997. The yeast VPS5/GRD2 gene encodes a sorting nexin-1-like protein required for localizing membrane proteins to the late Golgi. *J Cell Sci*. 110 (Pt 9):1063-1072.

Oda, H., and M. Takeichi. 2011. Evolution: structural and functional diversity of cadherin at the adherens junction. *J Cell Biol*. 193:1137-1146.

Oshima, K., and R.G. Fehon. 2011. Analysis of protein dynamics within the septate junction reveals a highly stable core protein complex that does not include the basolateral polarity protein Discs large. *J Cell Sci*. 124:2861-2871.

Paul, S.M., M. Ternet, P.M. Salvaterra, and G.J. Beitel. 2003. The Na+/K+ ATPase is required for septate junction function and epithelial tube-size control in the Drosophila tracheal system. *Development*. 130:4963-4974.

Peles, E., M. Nativ, M. Lustig, M. Grumet, J. Schilling, R. Martinez, G.D. Plowman, and J. Schlessinger. 1997. Identification of a novel contactin-associated transmembrane receptor with multiple domains implicated in protein-protein interactions. *EMBO J*. 16:978-988.

Petri, J., M.H. Syed, S. Rey, and C. Klambt. 2019. Non-Cell-Autonomous Function of the GPI-Anchored Protein Undicht during Septate Junction Assembly. *Cell Rep*. 26:1641-1653 e1644.

Pocha, S.M., and E. Knust. 2013. Complexities of Crumbs function and regulation in tissue morphogenesis. *Curr Biol*. 23:R289-293.

Pocha, S.M., T. Wassmer, C. Niehage, B. Hoflack, and E. Knust. 2011. Retromer controls epithelial cell polarity by trafficking the apical determinant Crumbs. *Curr Biol*. 21:1111-1117.

Priya, A., I.V. Kalaidzidis, Y. Kalaidzidis, D. Lambright, and S. Datta. 2015. Molecular insights into Rab7-mediated endosomal recruitment of core retromer: deciphering the role of Vps26 and Vps35. *Traffic*. 16:68-84.

Raab, M., M. Gentili, H. de Belly, H.R. Thiam, P. Vargas, A.J. Jimenez, F. Lautenschlaeger, R. Voituriez, A.M. Lennon-Dumenil, N. Manel, and M. Piel. 2016. ESCRT III repairs nuclear envelope ruptures during cell migration to limit DNA damage and cell death. *Science*. 352:359-362.

Raiborg, C., K.G. Bache, A. Mehlum, E. Stang, and H. Stenmark. 2001a. Hrs recruits clathrin to early endosomes. *EMBO J*. 20:5008-5021.

Raiborg, C., B. Bremnes, A. Mehlum, D.J. Gillooly, A. D'Arrigo, E. Stang, and H. Stenmark. 2001b. FYVE and coiled-coil domains determine the specific localisation of Hrs to early endosomes. *J Cell Sci*. 114:2255-2263.

Raymond, C.K., I. Howald-Stevenson, C.A. Vater, and T.H. Stevens. 1992. Morphological classification of the yeast vacuolar protein sorting mutants: evidence for a prevacuolar compartment in class E vps mutants. *Mol Biol Cell*. 3:1389-1402.

Rieder, S.E., L.M. Banta, K. Kohrer, J.M. McCaffery, and S.D. Emr. 1996. Multilamellar endosome-like compartment accumulates in the yeast vps28 vacuolar protein sorting mutant. *Mol Biol Cell*. 7:985-999.

Rink, J., E. Ghigo, Y. Kalaidzidis, and M. Zerial. 2005. Rab conversion as a mechanism of progression from early to late endosomes. *Cell*. 122:735-749.

Rojas, R., T. van Vlijmen, G.A. Mardones, Y. Prabhu, A.L. Rojas, S. Mohammed, A.J. Heck, G. Raposo, P. van der Sluijs, and J.S. Bonifacino. 2008. Regulation of retromer recruitment to endosomes by sequential action of Rab5 and Rab7. *J Cell Biol*. 183:513-526.

Rosenbluth, J. 2009. Multiple functions of the paranodal junction of myelinated nerve fibers. *J Neurosci Res*. 87:3250-3258.

Sachse, M., S. Urbe, V. Oorschot, G.J. Strous, and J. Klumperman. 2002. Bilayered clathrin coats on endosomal vacuoles are involved in protein sorting toward lysosomes. *Mol Biol Cell*. 13:1313-1328.

Saksena, S., J. Wahlman, D. Teis, A.E. Johnson, and S.D. Emr. 2009. Functional reconstitution of ESCRT-III assembly and disassembly. *Cell*. 136:97-109.

Schoneberg, J., M.R. Pavlin, S. Yan, M. Righini, I.H. Lee, L.A. Carlson, A.H. Bahrami, D.H. Goldman, X. Ren, G. Hummer, C. Bustamante, and J.H. Hurley. 2018. ATP-dependent force generation and membrane scission by ESCRT-III and Vps4. *Science*. 362:1423-1428.

Scott, A., J. Gaspar, M.D. Stuchell-Brereton, S.L. Alam, J.J. Skalicky, and W.I. Sundquist. 2005. Structure and ESCRT-III protein interactions of the MIT domain of human VPS4A. *Proc Natl Acad Sci U S A*. 102:13813-13818.

Seaman, M.N. 2004. Cargo-selective endosomal sorting for retrieval to the Golgi requires retromer. *J Cell Biol*. 165:111-122.

Seaman, M.N. 2012. The retromer complex - endosomal protein recycling and beyond. *J Cell Sci*. 125:4693-4702.

Seaman, M.N., M.E. Harbour, D. Tattersall, E. Read, and N. Bright. 2009. Membrane recruitment of the cargo-selective retromer subcomplex is catalysed by the small GTPase Rab7 and inhibited by the Rab-GAP TBC1D5. *J Cell Sci*. 122:2371-2382.

Seaman, M.N., E.G. Marcusson, J.L. Cereghino, and S.D. Emr. 1997. Endosome to Golgi retrieval of the vacuolar protein sorting receptor, Vps10p, requires the function of the VPS29, VPS30, and VPS35 gene products. *J Cell Biol*. 137:79-92.

Shi, A., L. Sun, R. Banerjee, M. Tobin, Y. Zhang, and B.D. Grant. 2009. Regulation of endosomal clathrin and retromer-mediated endosome to Golgi retrograde transport by the J-domain protein RME-8. *EMBO J*. 28:3290-3302.

Shih, S.C., D.J. Katzmann, J.D. Schnell, M. Sutanto, S.D. Emr, and L. Hicke. 2002. Epsins and Vps27p/Hrs contain ubiquitin-binding domains that function in receptor endocytosis. *Nat Cell Biol*. 4:389-393.

Simonsen, A., R. Lippe, S. Christoforidis, J.M. Gaullier, A. Brech, J. Callaghan, B.H. Toh, C. Murphy, M. Zerial, and H. Stenmark. 1998. EEA1 links PI(3)K function to Rab5 regulation of endosome fusion. *Nature*. 394:494-498.

Small, S.A., and G.A. Petsko. 2015. Retromer in Alzheimer disease, Parkinson disease and other neurological disorders. *Nat Rev Neurosci*. 16:126-132.

Snow, P.M., A.J. Bieber, and C.S. Goodman. 1989. Fasciclin III: a novel homophilic adhesion molecule in Drosophila. *Cell*. 59:313-323.

Steinberg, F., M. Gallon, M. Winfield, E.C. Thomas, A.J. Bell, K.J. Heesom, J.M. Tavare, and P.J. Cullen. 2013. A global analysis of SNX27-retromer assembly and cargo specificity reveals a function in glucose and metal ion transport. *Nat Cell Biol*. 15:461-471.

Strochlic, T.I., T.G. Setty, A. Sitaram, and C.G. Burd. 2007. Grd19/Snx3p functions as a cargo-specific adapter for retromer-dependent endocytic recycling. *J Cell Biol*. 177:115-125.

Strutt, H., P.F. Langton, N. Pearson, K.J. McMillan, D. Strutt, and P.J. Cullen. 2019. Retromer Controls Planar Polarity Protein Levels and Asymmetric Localization at Intercellular Junctions. *Curr Biol*. 29:484-491 e486.

Suzuki, S.W., Y.S. Chuang, M. Li, M.N.J. Seaman, and S.D. Emr. 2019. A bipartite sorting signal ensures specificity of retromer complex in membrane protein recycling. *J Cell Biol*. 218:2876-2886.

Tait, S., F. Gunn-Moore, J.M. Collinson, J. Huang, C. Lubetzki, L. Pedraza, D.L. Sherman, D.R. Colman, and P.J. Brophy. 2000. An oligodendrocyte cell adhesion molecule at the site of assembly of the paranodal axo-glial junction. *J Cell Biol*. 150:657-666.

Takahashi, H., J.R. Mayers, L. Wang, J.M. Edwardson, and A. Audhya. 2015. Hrs and STAM function synergistically to bind ubiquitin-modified cargoes in vitro. *Biophys J*. 108:76-84.

Tanentzapf, G., and U. Tepass. 2003. Interactions between the crumbs, lethal giant larvae and bazooka pathways in epithelial polarization. *Nat Cell Biol*. 5:46-52.

Teis, D., S. Saksena, and S.D. Emr. 2008. Ordered assembly of the ESCRT-III complex on endosomes is required to sequester cargo during MVB formation. *Dev Cell*. 15:578-589.

Teis, D., S. Saksena, and S.D. Emr. 2009. SnapShot: the ESCRT machinery. *Cell*. 137:182-182 e181.

Teis, D., S. Saksena, B.L. Judson, and S.D. Emr. 2010. ESCRT-II coordinates the assembly of ESCRT-III filaments for cargo sorting and multivesicular body vesicle formation. *EMBO J*. 29:871-883.

Temkin, P., B. Lauffer, S. Jager, P. Cimermancic, N.J. Krogan, and M. von Zastrow. 2011. SNX27 mediates retromer tubule entry and endosome-to-plasma membrane trafficking of signalling receptors. *Nat Cell Biol*. 13:715-721.

Tempesta, C., A. Hijazi, B. Moussian, and F. Roch. 2017. Boudin trafficking reveals the dynamic internalisation of specific septate junction components in Drosophila. *PLoS One*. 12:e0185897.

Teo, H., D.J. Gill, J. Sun, O. Perisic, D.B. Veprintsev, Y. Vallis, S.D. Emr, and R.L. Williams. 2006. ESCRT-I core and ESCRT-II GLUE domain structures reveal role for GLUE in linking to ESCRT-I and membranes. *Cell*. 125:99-111.

Teo, H., O. Perisic, B. Gonzalez, and R.L. Williams. 2004. ESCRT-II, an endosome-associated complex required for protein sorting: crystal structure and interactions with ESCRT-III and membranes. *Dev Cell*. 7:559-569.

Tepass, U. 1996. Crumbs, a component of the apical membrane, is required for zonula adherens formation in primary epithelia of Drosophila. *Dev Biol*. 177:217-225.

Tepass, U., E. Gruszynski-DeFeo, T.A. Haag, L. Omatyar, T. Torok, and V. Hartenstein. 1996. shotgun encodes Drosophila E-cadherin and is preferentially required during cell rearrangement in the neurectoderm and other morphogenetically active epithelia. *Genes Dev*. 10:672-685.

Tepass, U., and V. Hartenstein. 1994. The development of cellular junctions in the Drosophila embryo. *Dev Biol*. 161:563-596.

Thompson, B.J., J. Mathieu, H.H. Sung, E. Loeser, P. Rorth, and S.M. Cohen. 2005. Tumor suppressor properties of the ESCRT-II complex component Vps25 in Drosophila. *Dev Cell*. 9:711-720.

Thompson, B.J., F. Pichaud, and K. Roper. 2013. Sticking together the Crumbs - an unexpected function for an old friend. *Nat Rev Mol Cell Biol*. 14:307-314.

Tiklova, K., K.A. Senti, S. Wang, A. Graslund, and C. Samakovlis. 2010. Epithelial septate junction assembly relies on melanotransferrin iron binding and endocytosis in Drosophila. *Nat Cell Biol*. 12:1071-1077.

Tsukita, S., H. Tanaka, and A. Tamura. 2019. The Claudins: From Tight Junctions to Biological Systems. *Trends Biochem Sci*. 44:141-152.

Vaccari, T., and D. Bilder. 2005. The Drosophila tumor suppressor vps25 prevents nonautonomous overproliferation by regulating notch trafficking. *Dev Cell*. 9:687-698.

Vaccari, T., and D. Bilder. 2009. At the crossroads of polarity, proliferation and apoptosis: the use of Drosophila to unravel the multifaceted role of endocytosis in tumor suppression. *Mol Oncol*. 3:354-365.

van der Bliek, A.M., and E.M. Meyerowitz. 1991. Dynamin-like protein encoded by the Drosophila shibire gene associated with vesicular traffic. *Nature*. 351:411-414.

Verges, M., I. Sebastian, and K.E. Mostov. 2007. Phosphoinositide 3-kinase regulates the role of retromer in transcytosis of the polymeric immunoglobulin receptor. *Exp Cell Res*. 313:707-718.

Vilarino-Guell, C., C. Wider, O.A. Ross, J.C. Dachsel, J.M. Kachergus, S.J. Lincoln, A.I. Soto-Ortolaza, S.A. Cobb, G.J. Wilhoite, J.A. Bacon, B. Behrouz, H.L. Melrose, E. Hentati, A. Puschmann, D.M. Evans, E. Conibear, W.W. Wasserman, J.O. Aasly, P.R. Burkhard, R. Djaldetti, J. Ghika, F. Hentati, A. Krygowska-Wajs, T. Lynch, E. Melamed, A. Rajput, A.H. Rajput, A. Solida, R.M. Wu, R.J. Uitti, Z.K. Wszolek, F. Vingerhoets, and M.J. Farrer. 2011. VPS35 mutations in Parkinson disease. *Am J Hum Genet*. 89:162-167.

Volkmer, H., U. Zacharias, U. Norenberg, and F.G. Rathjen. 1998. Dissection of complex molecular interactions of neurofascin with axonin-1, F11, and tenascin-R, which promote attachment and neurite formation of tectal cells. *J Cell Biol*. 142:1083-1093.

Wandinger-Ness, A., and M. Zerial. 2014. Rab proteins and the compartmentalization of the endosomal system. *Cold Spring Harb Perspect Biol*. 6:a022616.

Wang, J., A. Fedoseienko, B. Chen, E. Burstein, D. Jia, and D.D. Billadeau. 2018. Endosomal receptor trafficking: Retromer and beyond. *Traffic*. 19:578-590.

Wang, S., K.L. Tan, M.A. Agosto, B. Xiong, S. Yamamoto, H. Sandoval, M. Jaiswal, V. Bayat, K. Zhang, W.L. Charng, G. David, L. Duraine, K. Venkatachalam, T.G. Wensel, and H.J. Bellen. 2014. The retromer complex is required for rhodopsin recycling and its loss leads to photoreceptor degeneration. *PLoS Biol*. 12:e1001847.

Ward, R.E.t., R.S. Lamb, and R.G. Fehon. 1998. A conserved functional domain of Drosophila coracle is required for localization at the septate junction and has membrane-organizing activity. *J Cell Biol*. 140:1463-1473.

Weber, C.R., G.H. Liang, Y. Wang, S. Das, L. Shen, A.S. Yu, D.J. Nelson, and J.R. Turner. 2015. Claudin-2-dependent paracellular channels are dynamically gated. *Elife*. 4:e09906.

Williams, R.L., and S. Urbe. 2007. The emerging shape of the ESCRT machinery. *Nat Rev Mol Cell Biol*. 8:355-368.

Wodarz, A., U. Hinz, M. Engelbert, and E. Knust. 1995. Expression of crumbs confers apical character on plasma membrane domains of ectodermal epithelia of Drosophila. *Cell*. 82:67-76.

Wood, R.L. 1959. Intercellular attachment in the epithelium of Hydra as revealed by electron microscopy. *J Biophys Biochem Cytol*. 6:343-352.

Woodfield, S.E., H.K. Graves, J.A. Hernandez, and A. Bergmann. 2013. De-regulation of JNK and JAK/STAT signaling in ESCRT-II mutant tissues cooperatively contributes to neoplastic tumorigenesis. *PLoS One*. 8:e56021.

Woods, D.F., and P.J. Bryant. 1991. The discs-large tumor suppressor gene of Drosophila encodes a guanylate kinase homolog localized at septate junctions. *Cell*. 66:451-464.

Woods, D.F., C. Hough, D. Peel, G. Callaini, and P.J. Bryant. 1996. Dlg protein is required for junction structure, cell polarity, and proliferation control in Drosophila epithelia. *J Cell Biol*. 134:1469-1482.

Wu, V.M., J. Schulte, A. Hirschi, U. Tepass, and G.J. Beitel. 2004. Sinuous is a Drosophila claudin required for septate junction organization and epithelial tube size control. *J Cell Biol*. 164:313-323.

Wu, V.M., M.H. Yu, R. Paik, S. Banerjee, Z. Liang, S.M. Paul, M.A. Bhat, and G.J. Beitel. 2007. Drosophila Varicose, a member of a new subgroup of basolateral MAGUKs, is required for septate junctions and tracheal morphogenesis. *Development*. 134:999-1009.

Xu, Y., H. Hortsman, L. Seet, S.H. Wong, and W. Hong. 2001. SNX3 regulates endosomal function through its PX-domain-mediated interaction with PtdIns(3)P. *Nat Cell Biol*. 3:658-666.

Yamada, S., S. Pokutta, F. Drees, W.I. Weis, and W.J. Nelson. 2005. Deconstructing the cadherin-catenin-actin complex. *Cell*. 123:889-901.

Yamazaki, Y., L. Palmer, C. Alexandre, S. Kakugawa, K. Beckett, I. Gaugue, R.H. Palmer, and J.P. Vincent. 2016. Godzilla-dependent transcytosis promotes Wingless signalling in Drosophila wing imaginal discs. *Nat Cell Biol*. 18:451-457.

Yanagihashi, Y., T. Usui, Y. Izumi, S. Yonemura, M. Sumida, S. Tsukita, T. Uemura, and M. Furuse. 2012. Snakeskin, a membrane protein associated with smooth septate junctions, is required for intestinal barrier function in Drosophila. *J Cell Sci*. 125:1980-1990.

Yong, X., L. Zhao, W. Deng, H. Sun, X. Zhou, L. Mao, W. Hu, X. Shen, Q. Sun, D.D. Billadeau, Y. Xue, and D. Jia. 2020. Mechanism of cargo recognition by retromer-linked SNX-BAR proteins. *PLoS Biol*. 18:e3000631.

Yousefian, J., T. Troost, F. Grawe, T. Sasamura, M. Fortini, and T. Klein. 2013. Dmon1 controls recruitment of Rab7 to maturing endosomes in Drosophila. *J Cell Sci*. 126:1583-1594.

Zeitler, J., C.P. Hsu, H. Dionne, and D. Bilder. 2004. Domains controlling cell polarity and proliferation in the Drosophila tumor suppressor Scribble. *J Cell Biol*. 167:1137-1146.

Zhang, P., Y. Wu, T.Y. Belenkaya, and X. Lin. 2011. SNX3 controls Wingless/Wnt secretion through regulating retromer-dependent recycling of Wntless. *Cell Res*. 21:1677-1690.

Zihni, C., C. Mills, K. Matter, and M.S. Balda. 2016. Tight junctions: from simple barriers to multifunctional molecular gates. *Nat Rev Mol Cell Biol*. 17:564-580.

Zimprich, A., A. Benet-Pages, W. Struhal, E. Graf, S.H. Eck, M.N. Offman, D. Haubenberger, S. Spielberger, E.C. Schulte, P. Lichtner, S.C. Rossle, N. Klopp, E. Wolf, K. Seppi, W. Pirker, S. Presslauer, B. Mollenhauer, R. Katzenschlager, T. Foki, C. Hotzy, E. Reinthaler, A. Harutyunyan, R. Kralovics, A. Peters, F. Zimprich, T. Brucke, W. Poewe, E. Auff, C. Trenkwalder, B. Rost, G. Ransmayr, J. Winkelmann, T. Meitinger, and T.M. Strom. 2011. A mutation in VPS35, encoding a subunit of the retromer complex, causes late-onset Parkinson disease. *Am J Hum Genet*. 89:168-175.

8 List of Abbreviations

a/p	anterior/posterior	**MAGUK**	membrane-associated guanylate kinases
AJ	Adherens Junction	**ME**	maturing endosome
aPKC	atypical Protein Kinase C	**Mega**	Megatrachea
APP	amyloid precursor protein	**Mon1**	Monensin sensitivity 1
ATPα	Na pump α subunit	**MVB**	multivesicular body
BAR	Bin, Amphiphysin, Rvs	**NF155**	Neurofascin-155
Baz	Bazooka	**NGS**	normal goat serum
BDSC	Bloomington Drosophila Stock Center	**NRCAM**	Neuronal Cell Adhesion Molecule
Cdc42	Cell division cycle 42	**Nrg**	Neuroglian
Chc	Clathrin heavy chain	**Nrv2**	Nervana2
CI-MPR	cation-independent mannose 6-phosphate receptor	**NrxIV**	NeurexinIV
CNTNAP/Caspr	Contactin-associated protein-like 2	**PAR**	partitioning defective
Cont	Contactin	**PBS**	phosphate buffered saline
Cora	Coracle	**PBT**	PBS + 0,3% Triton
CPY	Carboxypeptidase Y	**PCR**	polymerase chain reaction
Crb	Crumbs	**PI3K**	phosphoinositide-3-Kinase
CSC	cargo selective complex	**PIP3/PI3P**	phosphatidylinositol 3-phosphate
DGRC	Drosophila Genomics Resource Center	**pSJ**	pleated Septate Junction
Dlg	Discslarge	**PSJ**	Paranodal Septate Junction
DN	dominant negative	**PX**	Phox homology
Dpp	Decapentaplegic	**Rab**	Ras-related in brain
DSHB	Developmental Studies Hybridoma Bank	**RFP**	red fluorescent protein
E-cad	epithelial Cadherin	**Rme-8**	Receptor-mediated endocytosis 8
EEA1	Early Endosome Antigen 1	**ROI**	region of interest
EGFP	enhanced green fluorescent protein	**Scrib**	Scribble
EMT	epithelial to mesenchymal transition	***shg***	*shotgun*
ESCRT	Endosomal Sorting Complex Required for Transport	**Shi**	Shibire
Fam21	Family with sequence similarity 21	**Shrb**	Shrub
FasIII	FasciclinIII	**Sinu**	Sinuous
Flp	Flippase	**SJ**	Septate Junction
FRAP	fluorescence recovery after photobleaching	**SNARE**	soluble N-ethylmaleimide-sensitive-factor attachment receptor
FRT	Flippase recognition target	**SNX**	Sorting Nexin
FYVE	Fab 1, YOTB, Vac 1, EEA1	**sSJ**	smooth Septate Junction
Gal4	galactose 4 transcription factor	**STAM**	Signal transducing adaptor molecule
GAP	GTPase-activating protein	**Syb**	Synaptobrevin
GEF	guanosine triphosphate exchange factor	**Syx**	Syntaxin
GFP	green fluorescent protein	**TEM**	transmission electron microscopy
GLUE	GRAM-like ubiquitin-binding in EAP45	**TER**	transepithelial resistance
GPI	glycosylphosphatidylinositol	**TMP**	transmembrane protein
HA	Hemagglutinin	**TSA**	tyramide signal amplification
Hh	Hedgehog	**TSG101**	tumor susceptibility gene 101
Hrs	Hepatocyte growth factor regulated tyrosine kinase substrate	***tubP***	tubulin promotor
hs	heat shock	**UAS**	upstream activating sequence
IHC	immunohistochemistry	**Ubx**	ultrabithorax
ILV	intraluminal vesicle	**UIM**	ubiquitin interacting motif
JAK/STAT	Januskinase/ signal transducers and activators of transcription	**UTR**	untranslated region
JNK	c-Jun N-terminale Kinase	**VDRC**	Vienna Drosophila Resource Center
K2R	Lysine to Arginine exchange	**Vps**	vacuolar protein sorting
Kune	Kune-Kune	**WASH**	WASP and SCAR homologue
Lac	Lachesin	**Wnt**	Wingless and Int1
Lgl	Lethal (2) giant larvae	**YFP**	yellow fluorescent protein
		ZO	Zonula Occludens

9 Acknowledgements

In this section, I would like to express my gratitude and appreciation for the people that supported me in a multitude of ways during this PhD journey. Of course, limited by space and memory constraints, the following list is definitely incomplete!

First of all, I would like to thank my supervisor Prof. Dr. Thomas Klein for sparking my interest for *Drosophila* science. I am very grateful for all the personal and scientific discussions and his continued support throughout the years.

I thank Jun.-Prof. Dr. Mathias Beller for being part of the thesis committee and co-supervising this work.

I would like to thank all present and former members of the Klein group for the great company, the fun times in the lab and of course the help and support during so many experiments. Specifically, I thank Jessica Hausmann (also known as Hansi) for spending so much time processing and imaging samples for me at the Elmi. I would like to thank Sylvia Tannebaum and Stefan Kölzer for generating transgenic flies that were crucial for many experiments.
I am also grateful to Gisela, Mehmet, Monika and Elke for keeping the lab running and laying the foundation to any experimental work within the group.

Huge thanks go out to my students Tim and Alisa, who lifted a lot of workload off my shoulders and (hopefully) learned a few things along the way as well ;-). I also want to thank all PhD students and Postdocs in the lab for the guidance and for proofreading this thesis.

I would also like to thank the *Drosophila* community for sharing many reagents, which were incredibly helpful and essential for innumerable experiments.

I am grateful to the gentlemen of the Tea Club, led by the man of honour Sir Winston, for the frequent bergamot-flavoured escapes from the lab-life and the friendships (not exclusively revolving around fine teas).

Last but not least, I want to thank my family for always having my back!

10 Eidesstattliche Erklärung

Ich versichere an Eides Statt, dass die Dissertation von mir selbständig und ohne unzulässige fremde Hilfe unter Beachtung der „Grundsätze zur Sicherung guter wissenschaftlicher Praxis an der Heinrich-Heine-Universität Düsseldorf“ erstellt worden ist, dass diese Dissertation noch keiner anderen Fakultät zur Prüfung vorgelegen hat.

Düsseldorf, Oktober 2020 Hendrik Pannen